Stony Brook University

Garcia Center for Polymers at Engineered Interfaces

Sustainable Energy Generation: Nanotechnology for Enhancing Power, Durability, & Upcycling of Ion Exchange Fuel Cells

Miriam Rafailovich

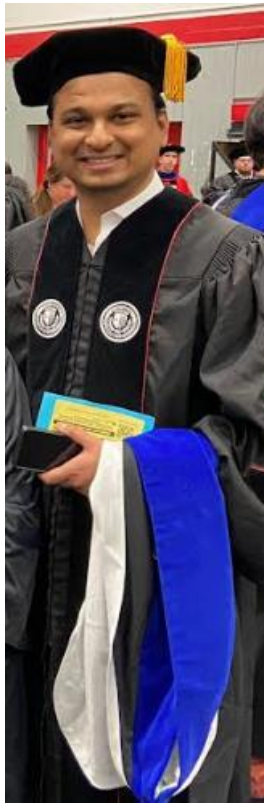

Based on the PhD thesis of Aniket Raut

Materials Science & Chemical Engineering
State University of New York at Stony Brook

Date – 06/06/23

Hydrogen Energy

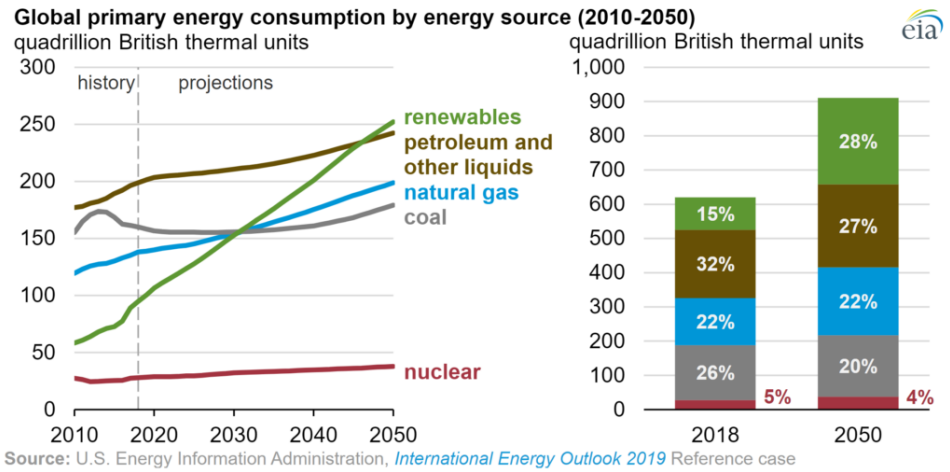

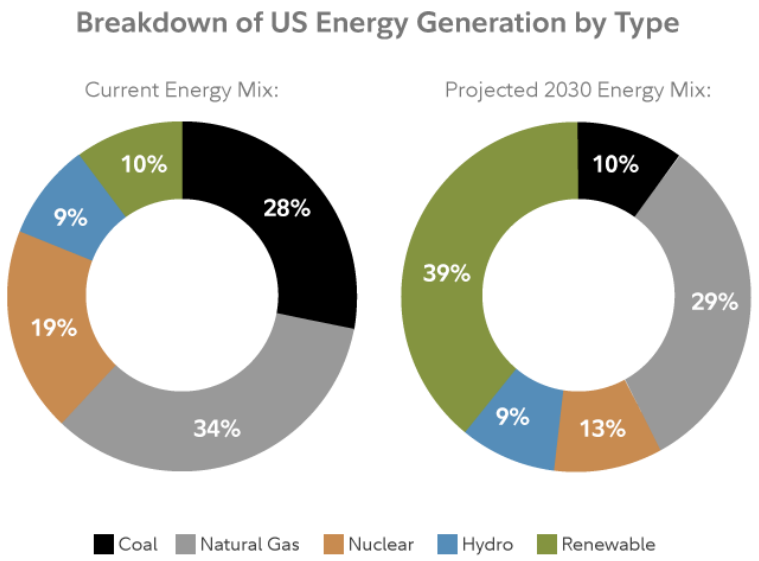

Source: Energy Information Agency (eia.gov), Fidelity Investments, as of Nov. 1, 2019.
Current data from eia.gov and projections from Fidelity.

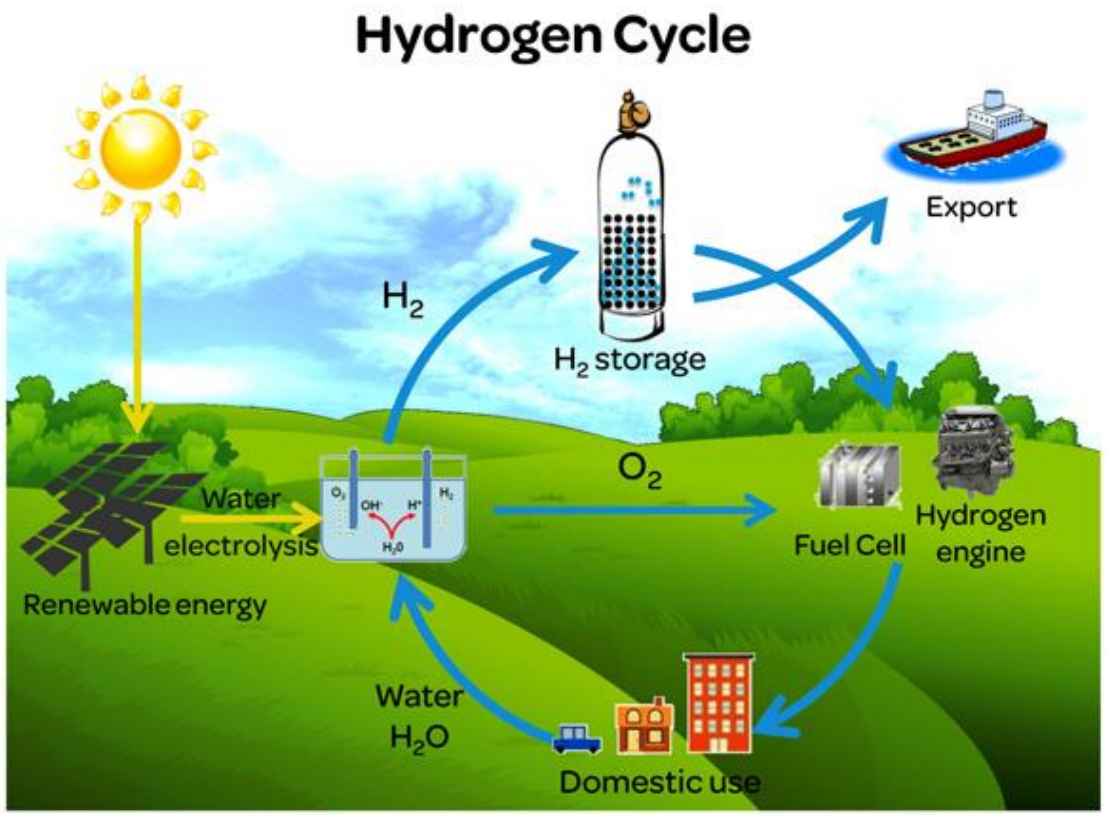

http://www.merlin.unsw.edu.au/energyh/about-hydrogen-energy/

Hydrogen Fuel Cells: who wants them ?

Trains: INNOTRANS, Germany will produce H2 trains to replace Diesel units --reduce urban noise and CO2 footprint. Advantage: trains don't need to stop for refueling.

US Army/GM: Paul Rogers, director of TARDEC, "The Army envisions a high torque vehicle that could be used for "silent watch" patrols with

- no engine noise and
- no significant heat signature from the exhaust. "

Consumer automotive: Honda Clarity Fuel Cell can travel 366 miles on a single tank of H2, Japanese Govt subsidies (up to $28K for H2 vehicles).

Walmart Chooses Fuel Cell Forklift: With the hydrogen fuel cell system, the forklift can be fueled at an indoor fueling station right in the warehouse in a matter of minutes, and its power won't decrease as the forklift uses the hydrogen. The fuel cell and small hydrogen tank is a direct replacement for a typical battery –and, because the fuel cell contains no hazardous materials, disposal is safe and inexpensive.

Renewable to Hydrogen: efficient 24 hour power generation

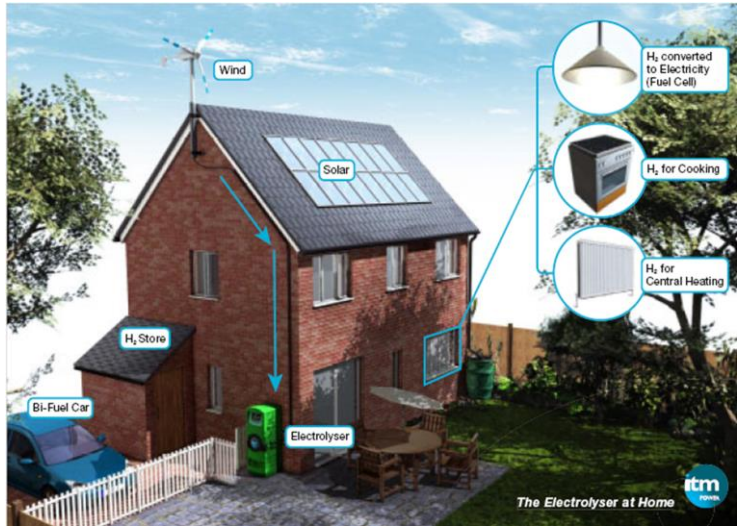

Differences In Energy Efficiency Among Automobile Types

Type	Energy source	Overall energy efficiency
Fuel-cell vehicle	Hydrogen produced from natural gas	40%
Hybrid vehicle	Gasoline refined from crude oil	34%
Electric vehicle	Electricity generated at thermal power station using natural gas	33%
Gasoline vehicle	Gasoline refined from crude oil	19%

Source: Toyota

Highest efficiency for renewable energy storage and power density.

- Consumer market
- Emerging smart grid markets

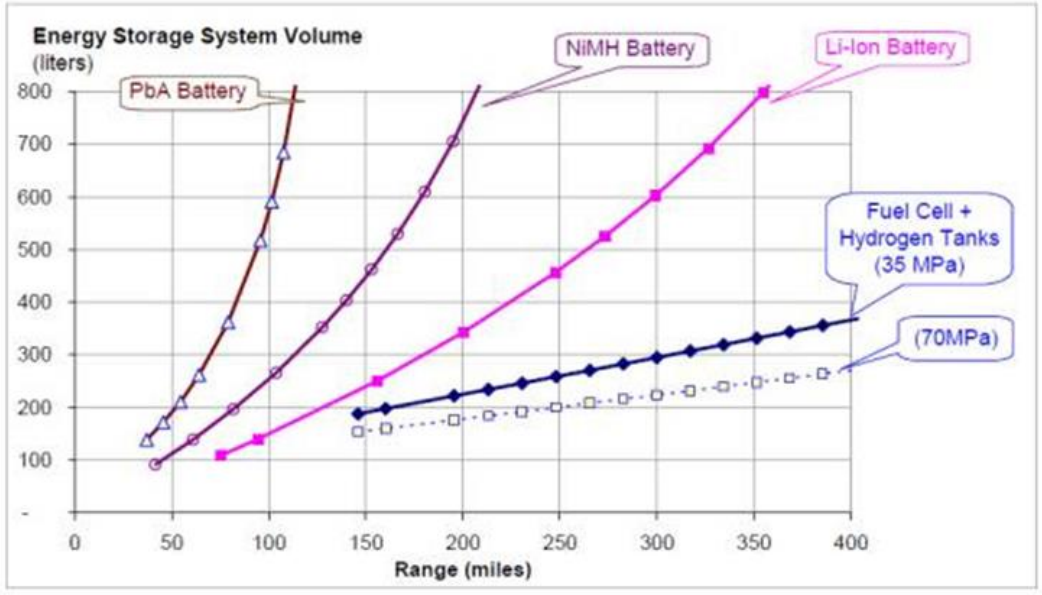

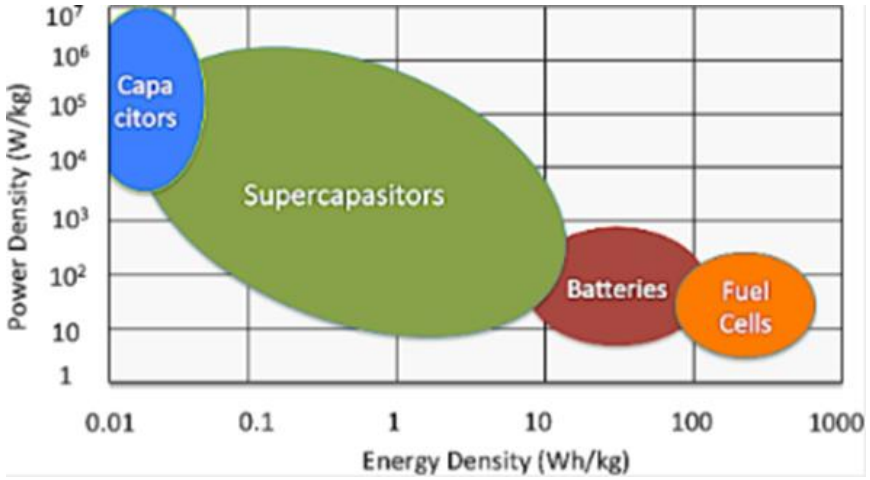

Published online 29 April 2010 | *Nature* **464**, 1262-1264 (2010) | doi:10.1038/4641262a

Box: The hydrogen challenge

From the article:
Hydrogen vehicles: Fuel of the future?

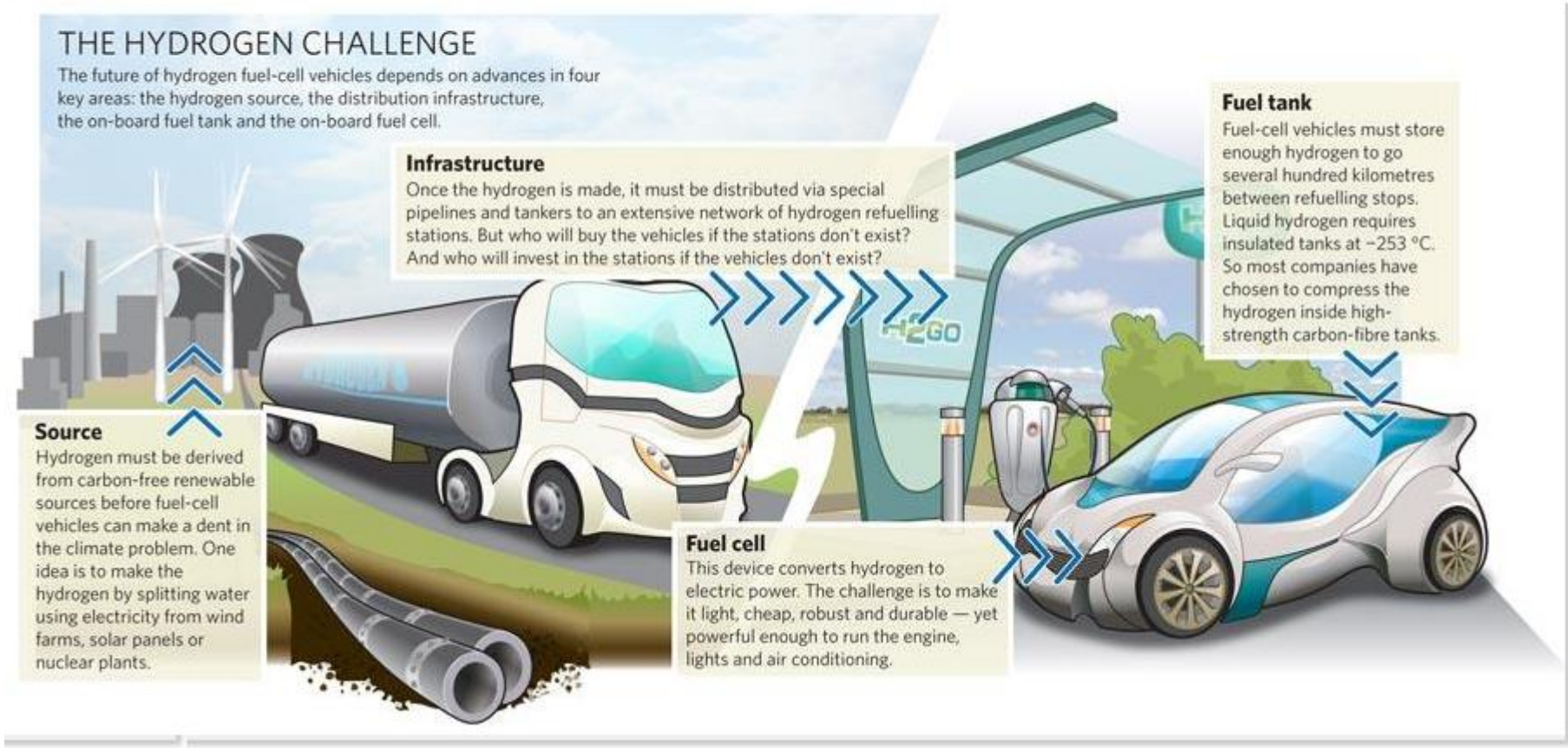

Elon Musk famously dismissed fuel cells as “mind-bogglingly stupid”

Secretly Superior

Most car executives agree fuel cells, not batteries, will be real breakthrou electric mobility

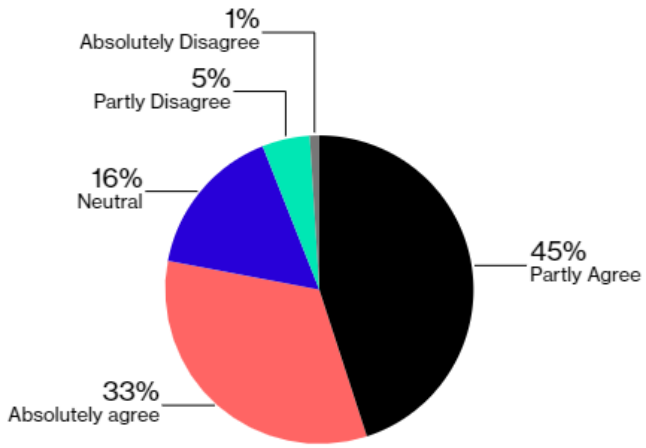

Source: KPMG 2017 Global Automotive Executive Survey

- Immature power distribution network
- The investment tax credit (30%) for investment in fuel cells was not extended, though parallel credits were extended for wind and solar energy, which effectively means fuel cells are about 43% more expensive http://www.fool.com/investing/2016/12/26/why-fuel-cell-stocks-face-an-uphill-battle.aspx

Japan to be 1st country to reach 100 hydrogen filling station milestone

KYODO NEWS - Mar 23, 2018 - 19:34 | All, Lifestyle

Bloomberg

By the 2030s, fossil-fuel cars will be rare as powering vehicles with batteries, hydrogen take off

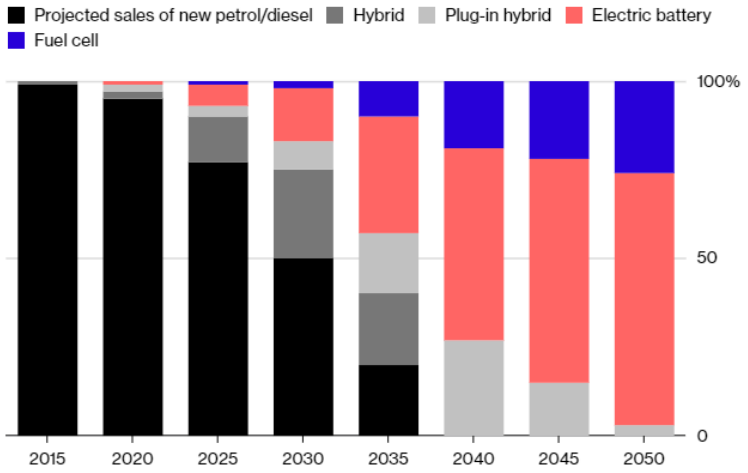

Source: European Climate Foundation

State	HRS Count
California	71
Hawaii	9
Massachussetts	4
Connecticut	3
Michigan	2
Ohio	2
New York	2
Pennsylvania	1
South Carolina	1
Texas	1
Delaware	1
Colorado	1
District of Columbia	1
Rhode Island	1
Washington	1

Compare Fuel Cell Vehicles

Source: EPA.gov

Fuel cell vehicles (FCVs) are now for sale or lease in the United States although availability is limited to areas with an adequate number of hydrogen refueling stations. Fuel economy estimates and other information are provided below.

Cars | SUVs

Problems…
Reduced cost of oil
Reduced govt. subsidies
Public perception
Durability

	2022 Hyundai Nexo			2022 Hyundai Nexo Blue		
						
Fuel Economy						
Mi/Kg	**56** comb	58 city	53 hwy	**60** comb	64 city	56 hwy
MPGE	**57** comb	59 city	54 hwy	**61** comb	65 city	58 hwy
Other Estimates						
Range (miles)	354			380		
Vehicle Characteristics						
Vehicle Class	Small SUV - 2WD			Small SUV - 2WD		
Motor	Interior Permanent Magnet Synchronous (120 kW)			Interior Permanent Magnet Synchronous (120 kW)		
Battery	240 V Lithium Ion			240 V Lithium Ion		
Availability	California only			California only		

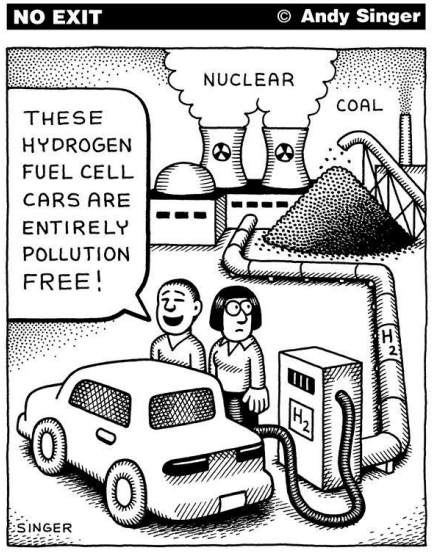

Biden-Harris Administration Announces First-Ever Offshore Wind Lease Sale in the Pacific

California sale opens new opportunities for U.S. floating offshore wind

10/18/2022

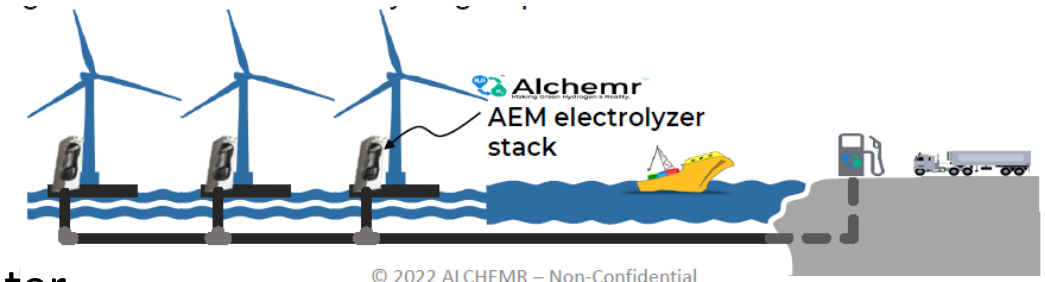

Challenge: Store wind energy as hydrogen produced from sea water
Develop newer technologies: Anionic Fuel Cells and Electrolyzer

hq@cartoonstock.com

Hydrogen Technologies at TECNALIA: the largest center of applied research and technology in Spain

Our Value Proposal for the Hydrogen Value Chain

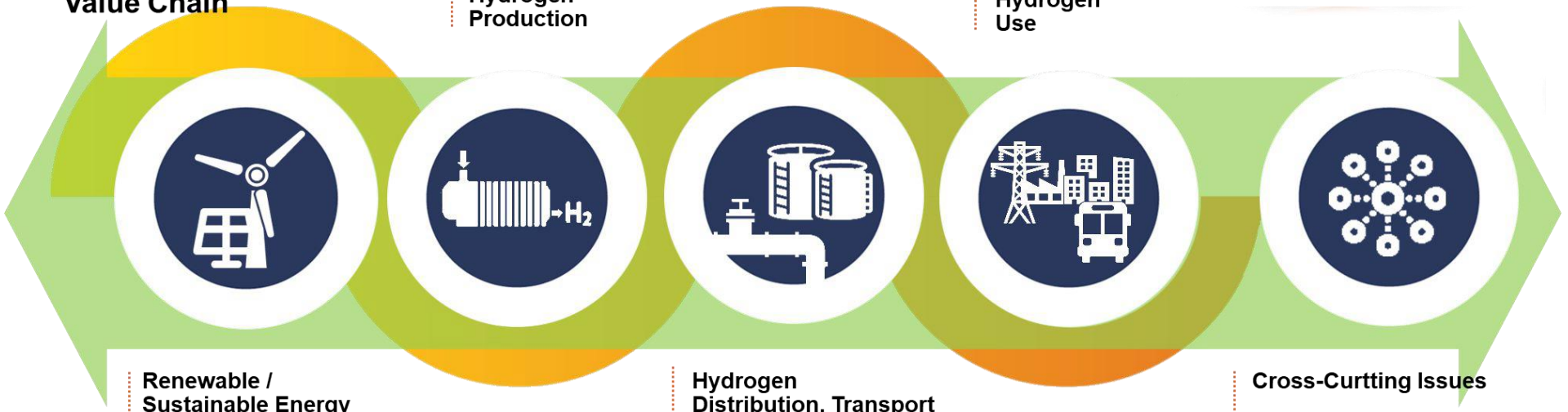

Renewable / Sustainable Energy Generation

- Solar energy
- Wind Energy
- Offshore energy
- …

Hydrogen Production

- Alkaline electrolysis
- PEM electrolysis
- AEM electrolysis
- Photoelectrolysis
- Solid oxide electrolysis
- Reforming / Pirolisis / Gasification

Hydrogen Distribution, Transport and Storage

- Injection in gas grids
- H_2 purification
- Hydrogen storage
- Power to X / Energy carriers
- Materials in contact with H_2

Hydrogen Use

- Integration in Smart Grids
- Use in transport
- Use in industry
- Use in buildings
- Fuel cells

Cross-Curtting Issues

- Materials characterisation
- Surface engineering
- Sensoring
- Power electronics
- Support to digitalization
- Simulation and prototyping
- Support to manufacturing
- Recovery of valuable materials Modelling

https://www.tecnalia.com/en/

Major Challenges to Commercialization: (Meeting DOE 2020 requirements by 2020!!)

1. On board hydrogen storage and distribution
2. Decrease Cost (membrane and catalyst)
3. Increase durability (Reduce Pt fouling)
4. Increase safety (Units operate at 300V)
5. Increase energy density

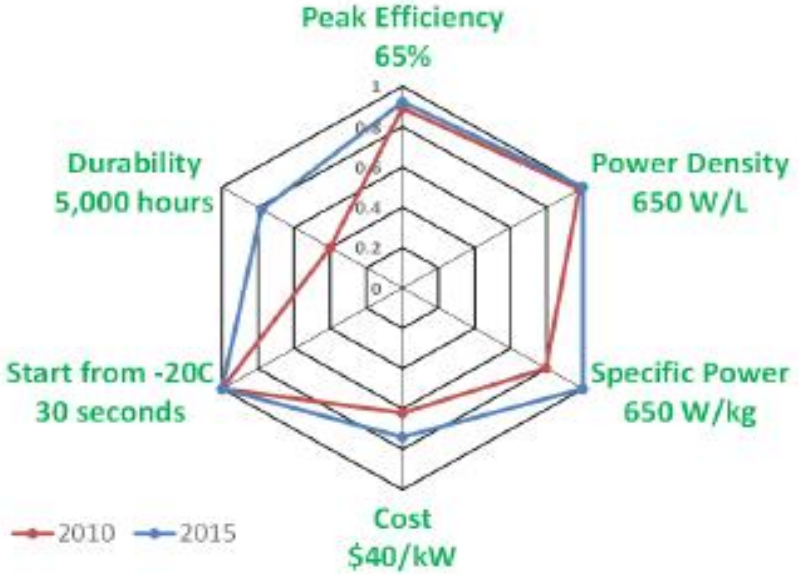

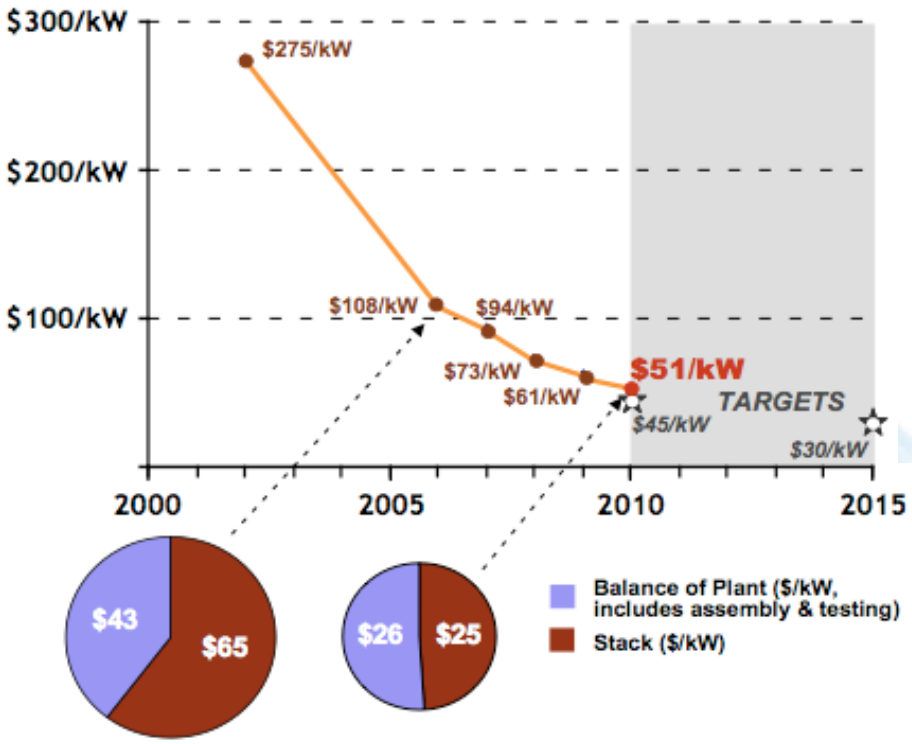

	Units	DOE 2020 Target
Platinum group metal (PGM) total content (both electrodes)	g/kW	<0.125
PGM total loading (both electrodes)	mg/cm^2	<0.125
Loss in catalytic (mass) activity	% loss	<40
Loss in performance at 0.8 A/cm^2	mV	30
Loss in performance at 1.5 A/cm^2	mV	30
Mass activity @ 900 $mV_{iR\text{-}free}$	A/mg_{PGM}	0.44

DOE 2020 requirements

Proton **E**xchange **M**embrane **F**uel **Ce**lls (**PEMFC**), are the type of fuel cells which utilize a polymer membrane (such as Nafion®) to generate power by separating the electrons and positive ions from a hydrogen gas source.
Byproducts: Water (environmentally friendly) and **Carbon Monoxide (CO)**

- Low temperature operation
- Relative high efficiency (40-60%)
- Anode:

$$H_2 + 2Pt \longrightarrow 2Pt\text{-}H$$

$$2Pt\text{-}H \longrightarrow 2Pt + 2H^+ + 2e^-$$

- Cathode:

$$1/2O_2 + Pt \longrightarrow Pt\text{-}O$$

$$Pt\text{-}O + H^+ + 2e^- \longrightarrow Pt + H_2O$$

- Drawbacks:
  - CO Poisoning
  - Expensive Pt catalyst

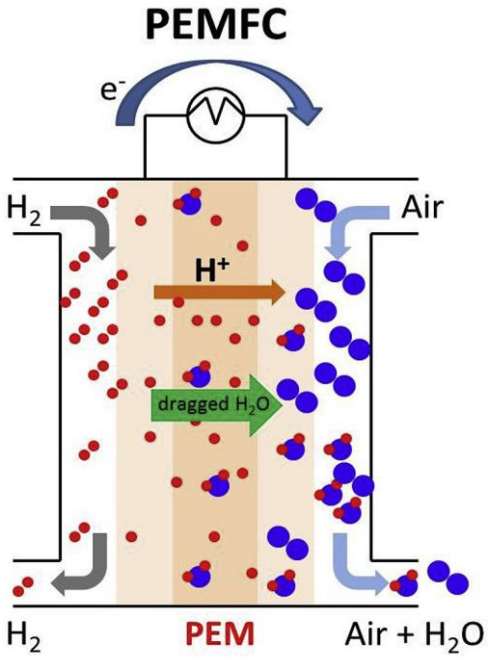

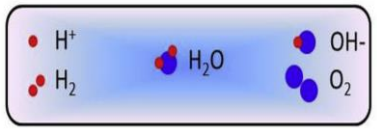

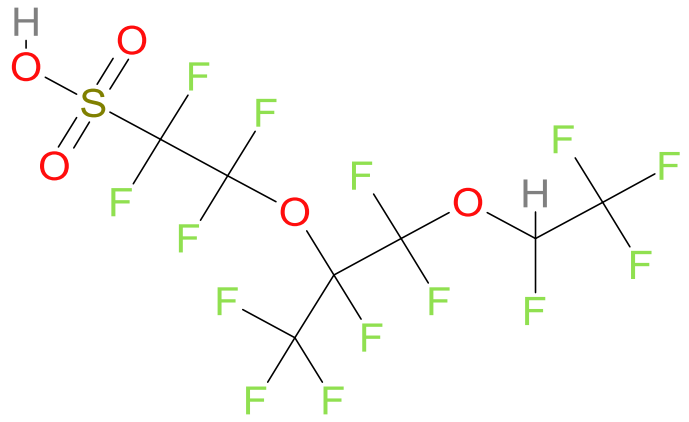

Chemical structure of Nafion membrane containing multiple fluorine groups as the charge carriers

Image source: Dekel, D. R. (2018). "Review of cell performance in anion exchange membrane fuel cells." Journal of power sources **375: 158-169.**

Sources of hydrogen gas

Natural gas reforming
(contains up to 25% CO_2)

$$CH_4 + H_2O \leftrightarrow CO + H_2$$

$$CO + H_2O \rightarrow CO_2 + H_2$$

95% of hydrogen

Water electrolysis
(cost: ~4.5 kWh/Nm3)

$$2H_2O \xrightarrow{\text{Electricity}} 2H_2 + O_2$$

Photocatalytic water splitting
(Expensive catalysts: Pt, Ru, Pd)

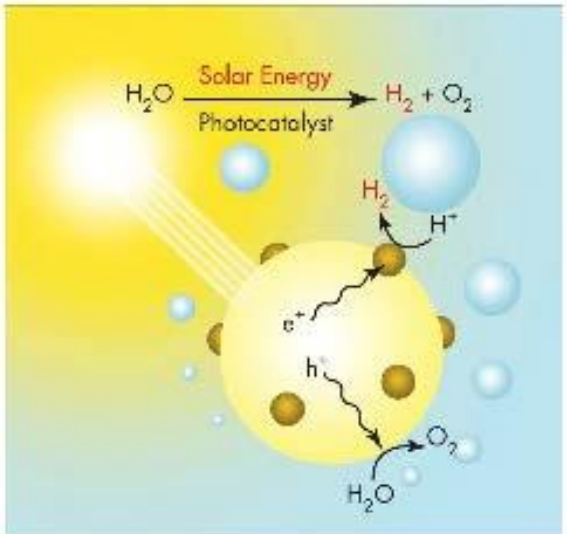

Reversed water gas shift reaction in hydrogen fuel cell

Reformate hydrogen gas contains large amount of CO_2 (up to 25%)

$$CO_2 + H_2 \longleftrightarrow CO + H_2O$$

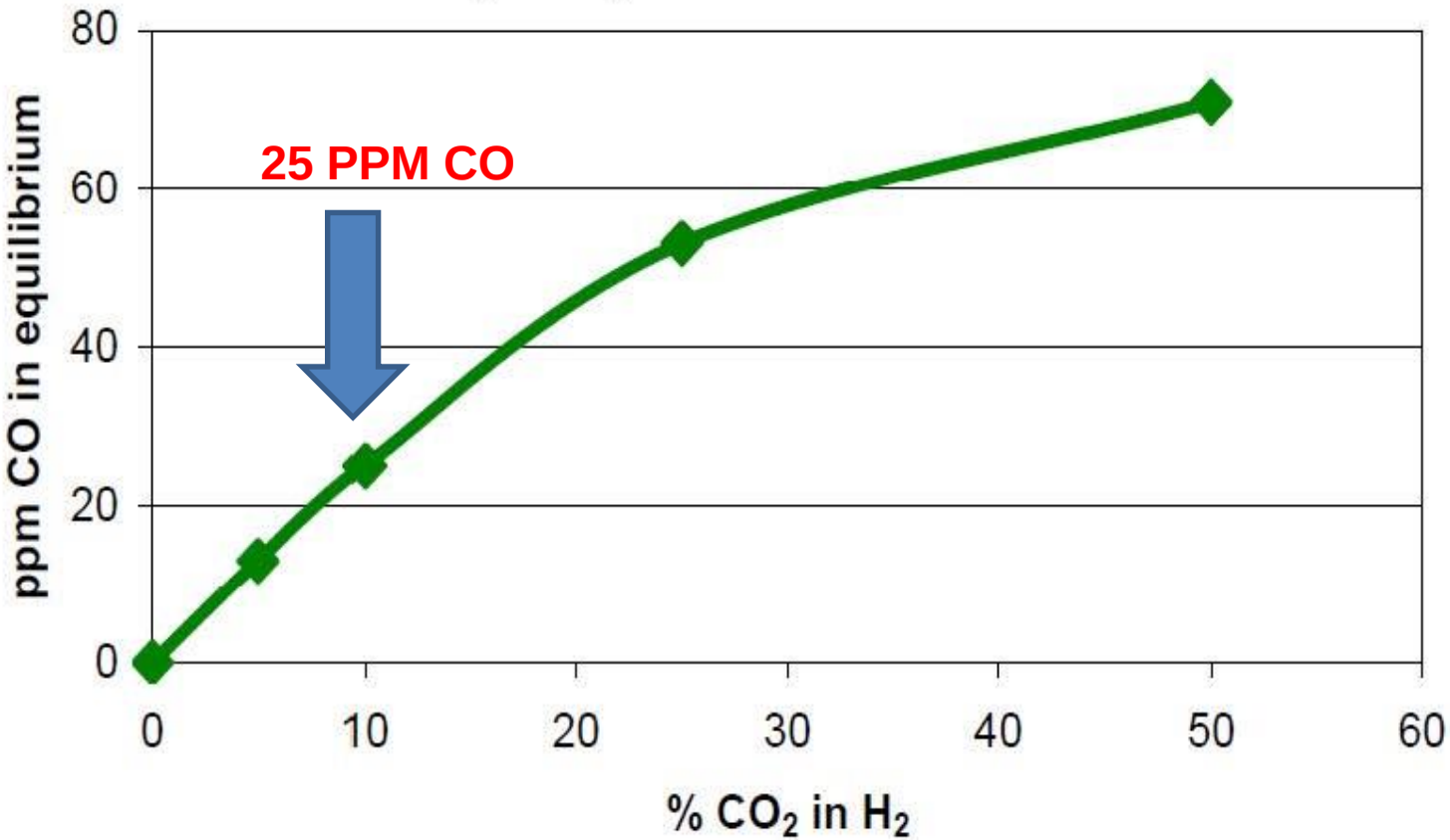

*Janssen, G. J. M., and N. P. Lebedeva. In *Presented at the Conference: Fuel Cells Science and Technology*, vol. 2004, pp. 6-7. 2004.

Carbon Monoxide: Major obstacle to Meeting Department of Energy 2020 Standards

- Generated by the cell when operating in ambient conditions.
- Poisons platinum catalyst which reduces PEMFC lifetime, and power density by more than 50%.
- Requires high temperature operation (T>80C).
- Requires expensive pure hydrogen gas stream. (Syngas/reformate H2 gas contains approx. 20% CO2)

Atmospheric (50 PPM)

Syngas H2 Source (100 PPM)

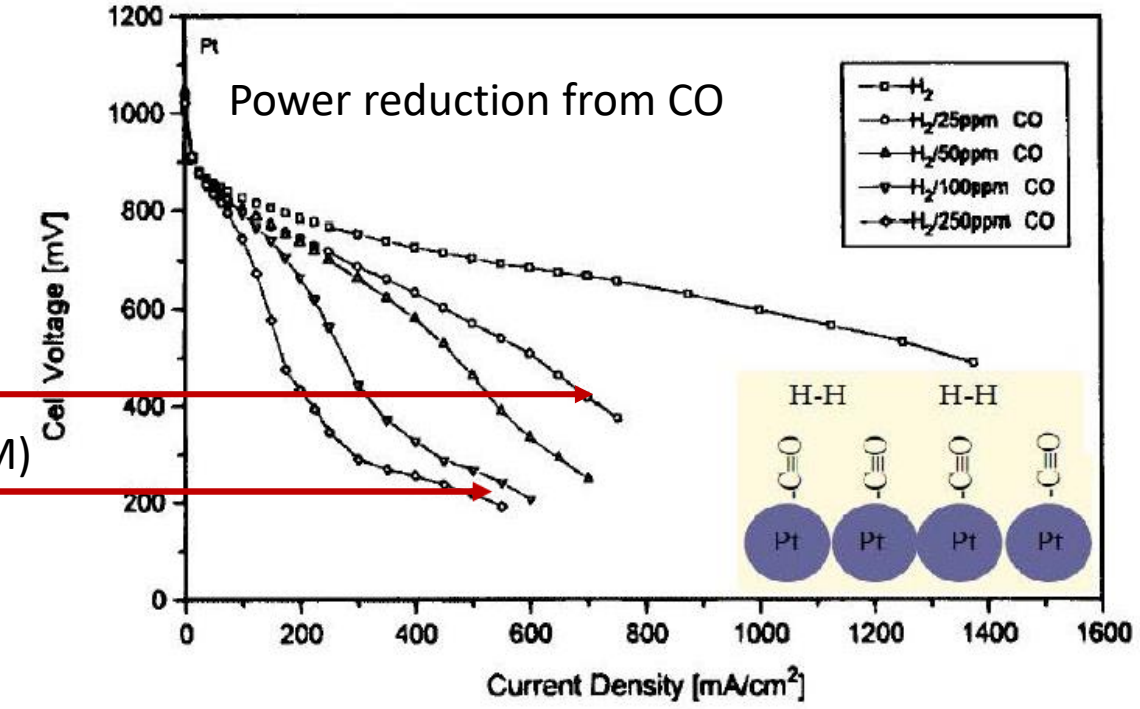

schuk, J. J., and Xianguo Li. *International Journal of Energy Research* 25, no. 8 (200

Alkaline Exchange Membrane Fuel Cell (AEMFC)

- Usage of non-platinum-group metals
- Less expensive metal catalysts
- Anode:

$$2H_2 + 4OH^- \longrightarrow 4H_2O + 4e^-$$

- Cathode:

$$O_2 + 2H_2O + 4e^- \longrightarrow 4OH^-$$

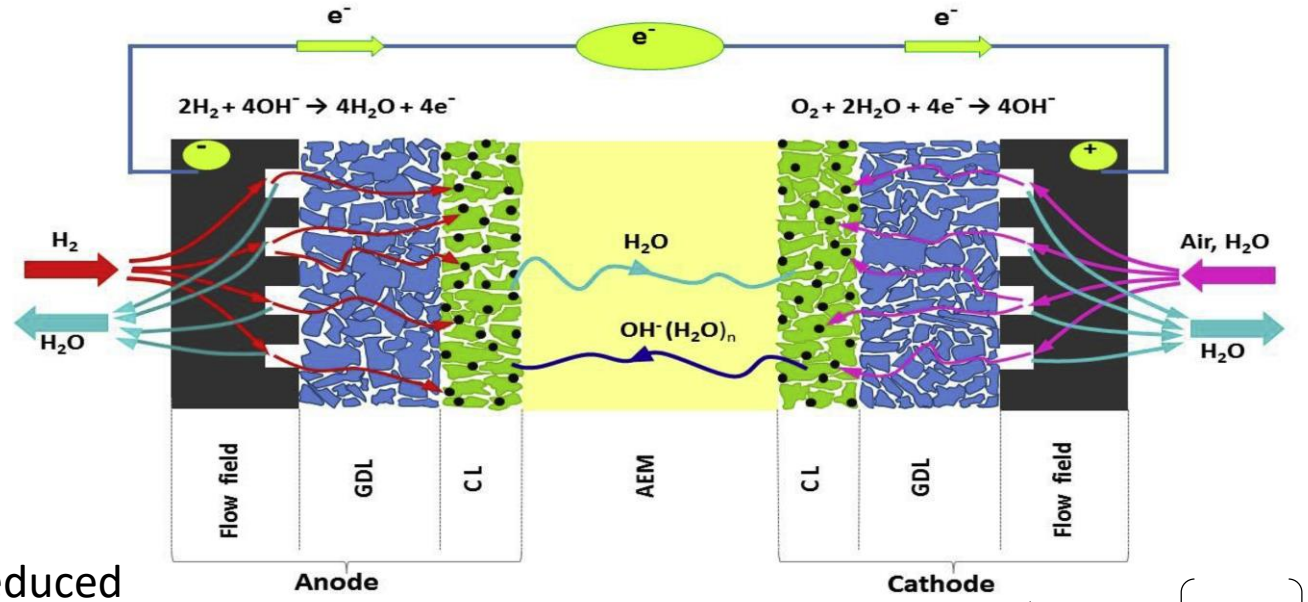

- ORR potential vs SHE at standard conditions is reduced (0.401 V in alkaline vs 1.229 V in acid). Only Pt, and PGM have a high enough O2 adsorption free energy to bind to the surface and allow the ORR to occur.
- The lower potential lowers free energy of adsorption for oxygen and permits the usage of many non Platinum group metals such as Ni, Co, Fe group metal.
- Easier to use under saline conditions—Seawater elelctrolysis.

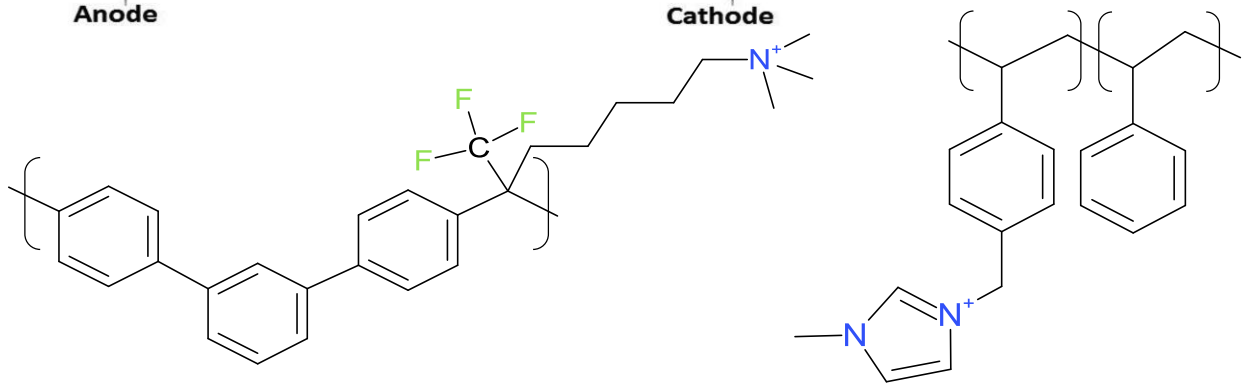

Chemical structure of mTPN1-TMA membrane and Sustainion membrane

Image source: Dekel, D. R. (2018). "Review of cell performance in anion exchange membrane fuel cells." Journal of power sources **375: 158-169.**

Anion Exchange Membrane Fuel Cell

tecnalia

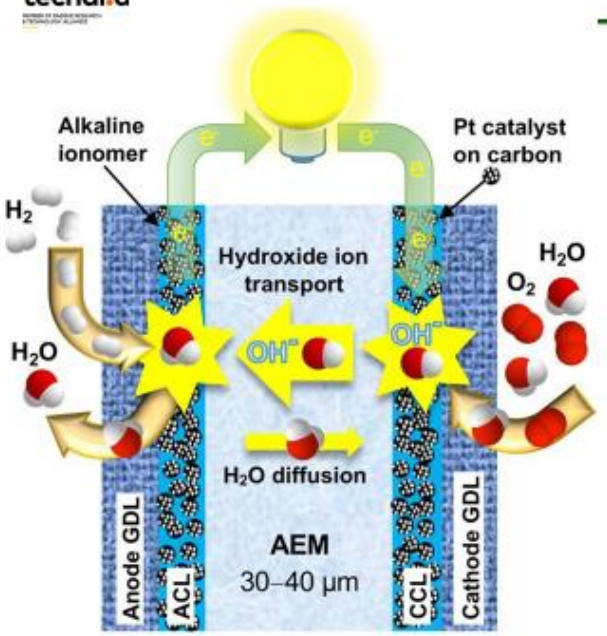

Anode (ox): $2\ H_2 + 4\ OH^- \rightarrow 4\ H_2O + 4e^-$ (Raney Ni Catalyst)

Cathode (red): $O_2 + 2\ H_2O + 4e^- \rightarrow 4\ OH^-$ (Ag Catalyst)

Overall: $O_2 + 2H_2 \rightarrow 2H_2O$

Image: APEFC Schematic
Lu et. al.; 2008. *Proc. Natl. Acad. Sci.* 2008. 105, 52; 20611-20614.

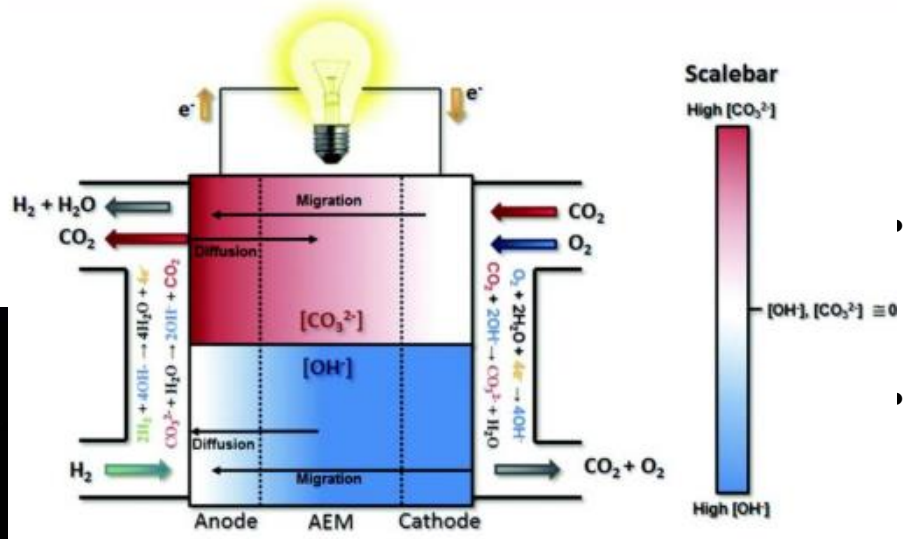

https://www.ncbi.nlm.nih.gov/core/lw/2.0/html/tileshop_pmc/tileshop_pmc_inline.html?title=Click%20on%20image%20to%20zoom&p=PMC3&id=8955432_poly

Image: Shuttle AMFC Cell Stack
Fray, D.; 2011. "DoITPoMS: Fuel Cells."
University of Cambridge.
http://www.doitpoms.ac.uk/tlplib/fuel-cells/printall.php

AEMFCs used by NASA subs and submarines in UK

tecnalia

Challenges of PEM and alkaline FC

Air

From Air (Cathode): $O_2 + 2\ H_2O + 4e^- \rightarrow 4\ OH^-$

$CO_2 + OH^- \rightarrow HCO_3^-$

Membrane Crossover: $[HCO_3^-] > [OH^-]$

To Air (Anode): $2\ HCO_3^- \rightarrow 2\ OH^- + 2\ CO_2$

$H_2 + 2\ OH^- \rightarrow 2e^- + 2H_2O$

CO_2 Poisoning
Ph Change, Reduced Operation,
Precipitation of Carbonates

- HCO3- competes with OH-, and migrates faster reducing the power output.
- HCO3- produces only 2 electrons, vs OH- which produces 4 electrons when reduced to H2O.
- Difficult to maintain high PH

Gold as a Novel Catalyst in the 21st Century: Preparation, Working Mechanism and Applications

Gold Bulletin 2004 • 37/1–2

Masatake Haruta
Research Institute for Green Technology, AIST
16-1 Onogawa, Tsukuba 305-8569, Japan
E mail:m.haruta@aist.go.jp

Our Focus: The Membrane

- Enable lower temperature operation—last longer
- Tolerate CO impurities—cheaper gas sources
- Increase efficiency of ion transport
- **Modifications should NOT interfere with other components**

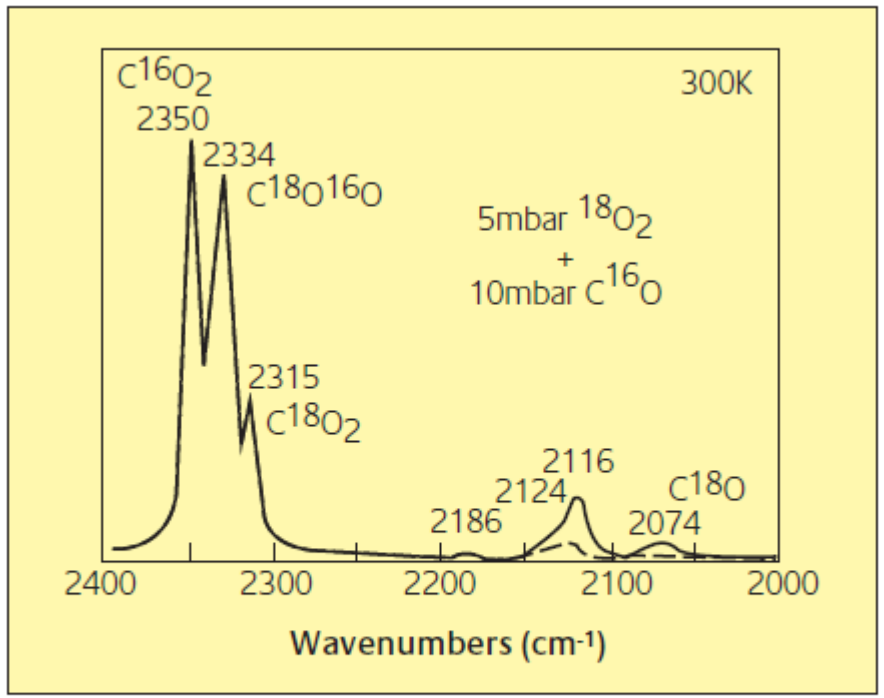

Figure 7
FT-IR spectra for the introduction of $C^{16}O$ at 300 K to Au/TiO_2 after preadsorption of $^{18}O_2$

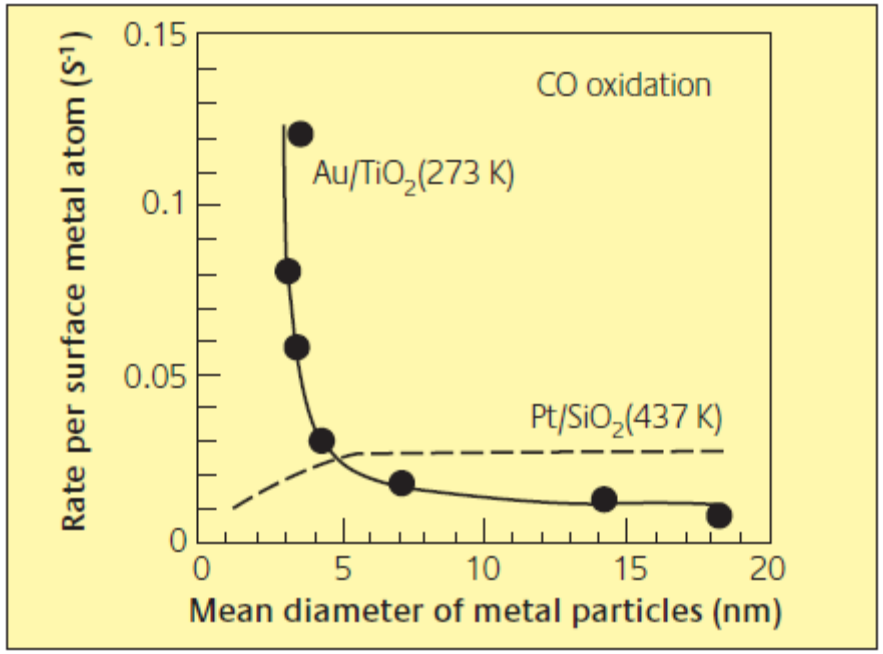

Figure 5
Turnover frequency (TOF) for CO oxidation over Pt/SiO_2 and Au/TiO_2

Gold as a Novel Catalyst in the 21st Century: Preparation, Working Mechanism and Applications

Gold Bulletin 2004 • 37/1–2

Masatake Haruta
Research Institute for Green Technology, AIST
16-1 Onogawa, Tsukuba 305-8569, Japan
E mail:m.haruta@aist.go.jp

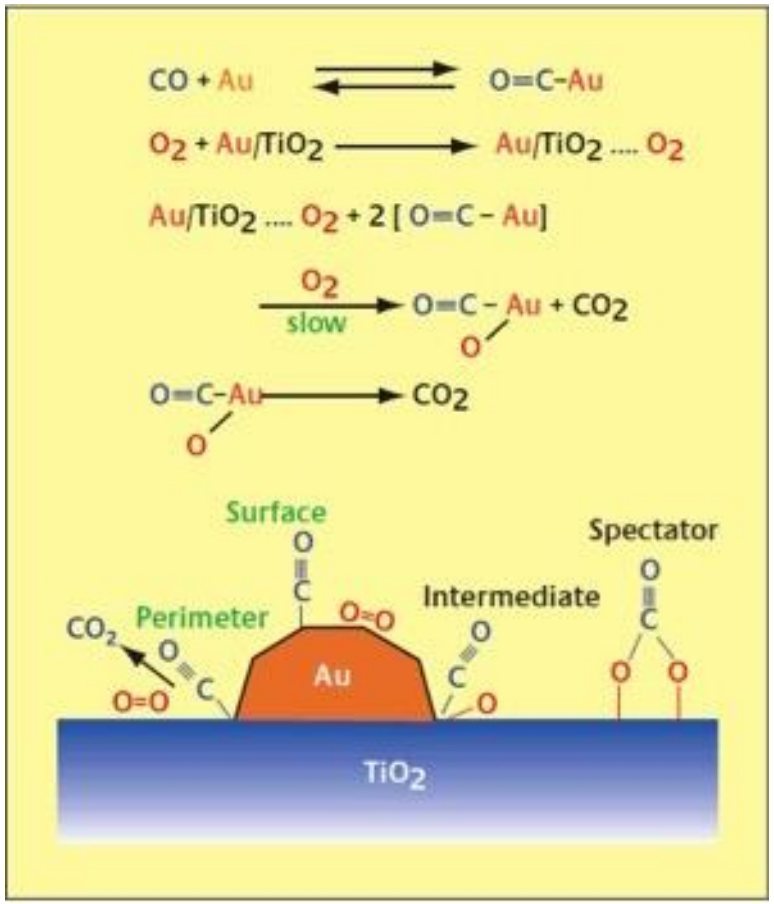

Three pathways to CO oxidation

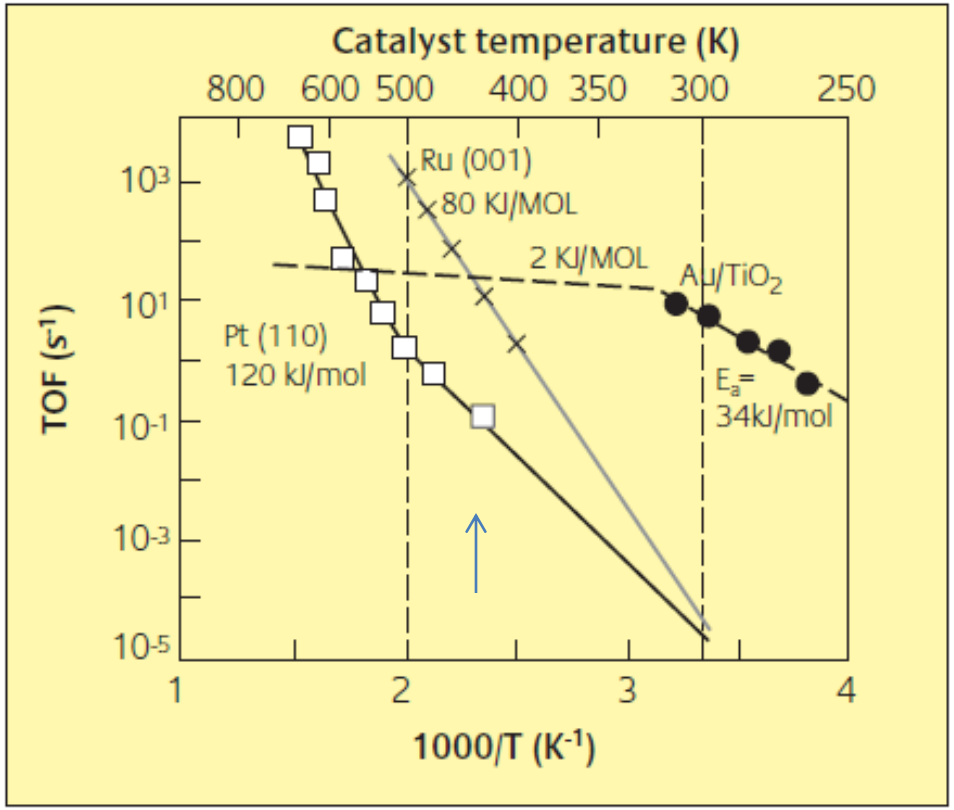

Figure 6

Arrhenius plots of the turn-over frequency (TOF) for CO oxidation over noble metal catalysts. The data for Pt group metals are taken from ref. [41]

- TOF of catalyst drops steeply below 100C on non supported PT and RU, but Au//TiO2 rate decreases much more slowly
- ENABLES THE REACTION AT LOWER TEMPERATURES

Gold Nanoparticles as Ideal Catalyst

- Platelet shape are ideal for maximizing contact with surface.
- Activity of particles increases when particle size shrinks.
- Smaller particles have more corner atoms or “steps” for catalysis.

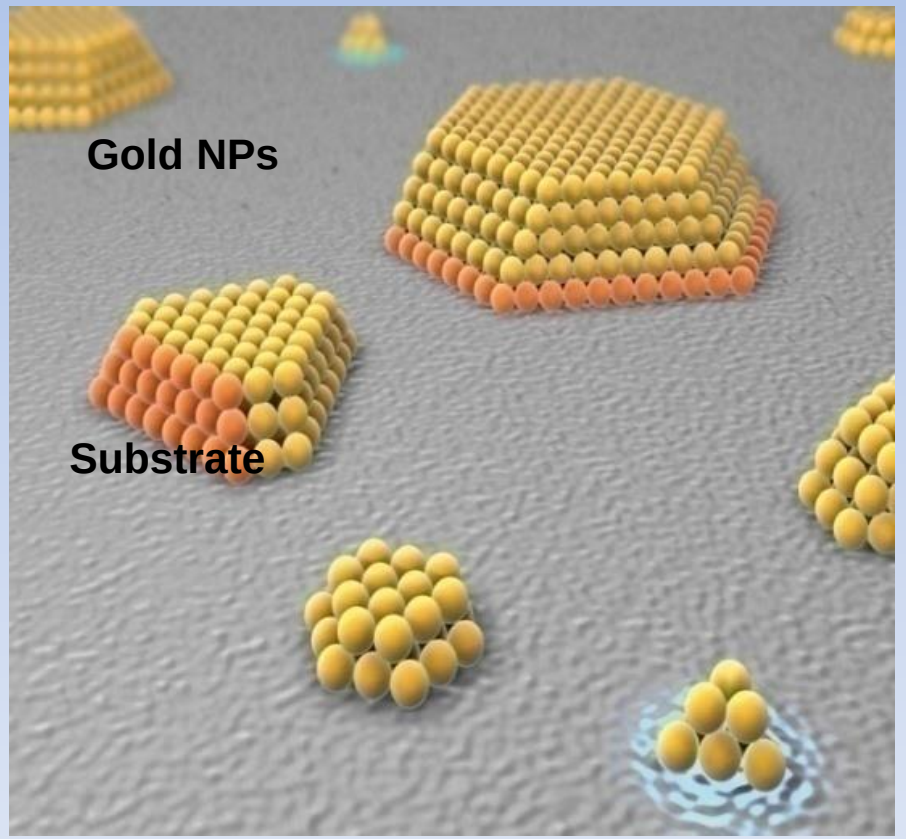

* Adrian Cho, *Science*,Vol.299, pp. 1684-1685

* Jens K. Nørskov, *et al*, *Nanotoday*, Vol.2, Number 4

Colloidal (electrochemical) deposition(Adzic and Bliznakov)

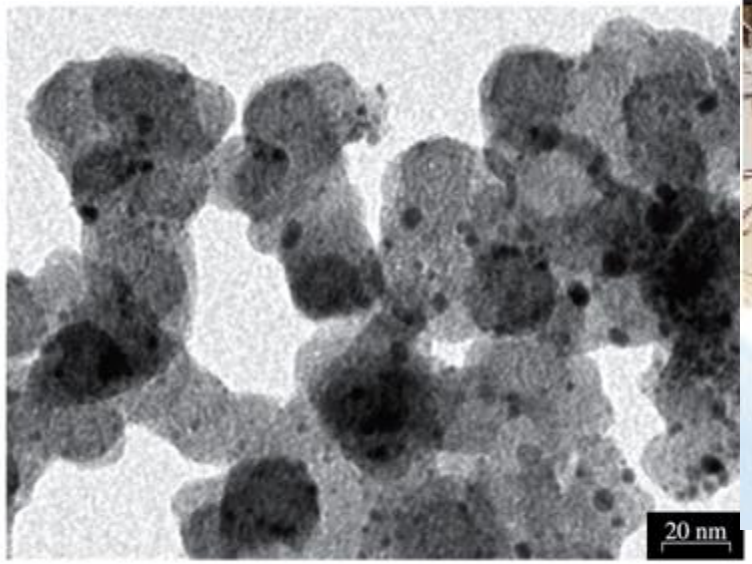

Figure 3. Nanocrystals of PtRu (SD) electrocatalyst dispersed in the carbon matrix. The crystallites have a bimodal distribution with an average size of 2.5 ± 0.4 nm and 5.2 ± 1.2 nm.

Egberto Gomes Franco et al
Mat. Res. vol.8 no.2 São Carlos Apr./June 2005

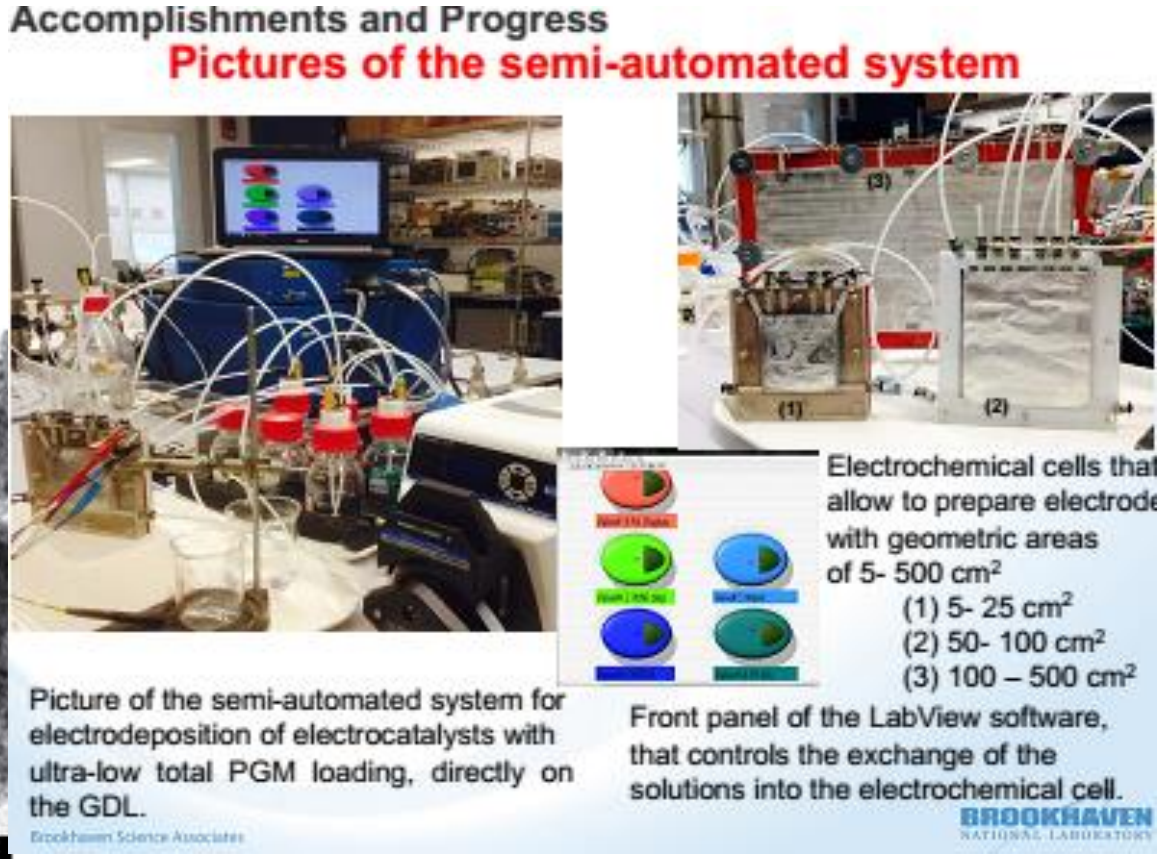

- Requires support
- Chemical solvent deposition (interacts with membrane)

- High temperature deposition> 500C
- Poor control of size
- **Requires support**
- NOT applicable for membranes

Gold as a Novel Catalyst in the 21st Century: Preparation, Working Mechanism and Applications

Gold Bulletin 2004 • 37/1–2

Masatake Haruta
Research Institute for Green Technology, AIST
16-1 Onogawa, Tsukuba 305-8569, Japan
E mail:m.haruta@aist.go.jp

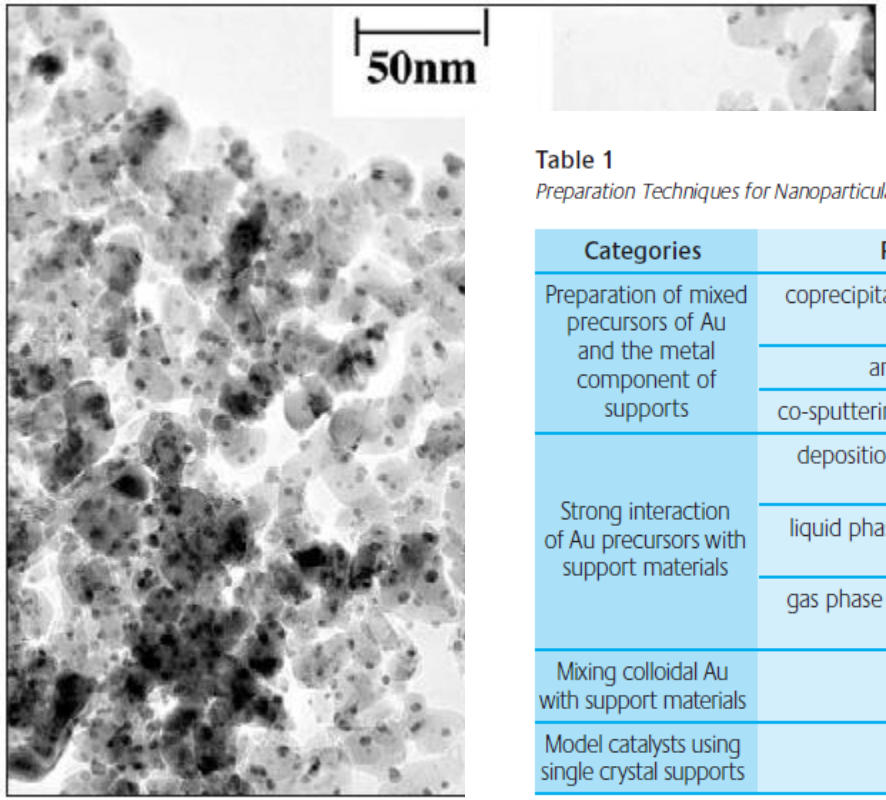

Figure 1
TEM photograph for Au/α-Fe_2O_3 prepared by coprecipitation followed by calcination at 673K

Table 1
Preparation Techniques for Nanoparticulate Gold Catalysts

Categories	Preparation techniques	Support materials	Ref.
Preparation of mixed precursors of Au and the metal component of supports	coprecipitation (hydroxides or carbonates) CP	$Be(OH)_2$, TiO_2*, Mn_2O_3, Fe_2O_3, Co_3O_4, NiO, ZnO, In_2O_3, SnO_2	1, 7, 8, 9, 10
	amorphous alloy (metals) AA	ZrO_2	11
	co-sputtering (oxides) in the presence of O_2 CS	Co_3O_4	12
Strong interaction of Au precursors with support materials	deposition-precipitation ($HAuCl_4$ in aqueous solution) DP	$Mg(OH)_2$*, Al_2O_3, TiO_2, Fe_2O_3, Co_3O_4, NiO, ZnO, ZrO_2, CeO_2, Ti-SiO_2	13, 14
	liquid phase grafting (organogold complex in organic solvents) LG	TiO_2, MnOx, Fe_2O_3	15, 16
	gas phase grafting (organogold complex) GG	all kinds, including SiO_2, Al_2O_3-SiO_2, and activated carbon	17, 18
Mixing colloidal Au with support materials	colloid mixing CM	TiO_2, activated carbon	19, 20
Model catalysts using single crystal supports	vacuum deposition VD (at low temperature)	Defects are the sites for deposition, MgO, SiO_2, TiO_2	21, 22, 23

* The addition of Mg citrate during or after coprecipitation or deposition-precipitation is important for depositing Au as nanoparticles.

Objective: Produce **platelets** of uniform size that can be applied as a film directly on the membrane, and will not block gas diffusion.

- Small (<5nm) gold nanoparticles
- No support
- Low temperature deposition

Ideal model:

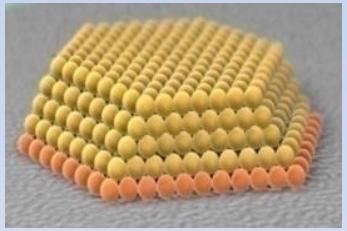

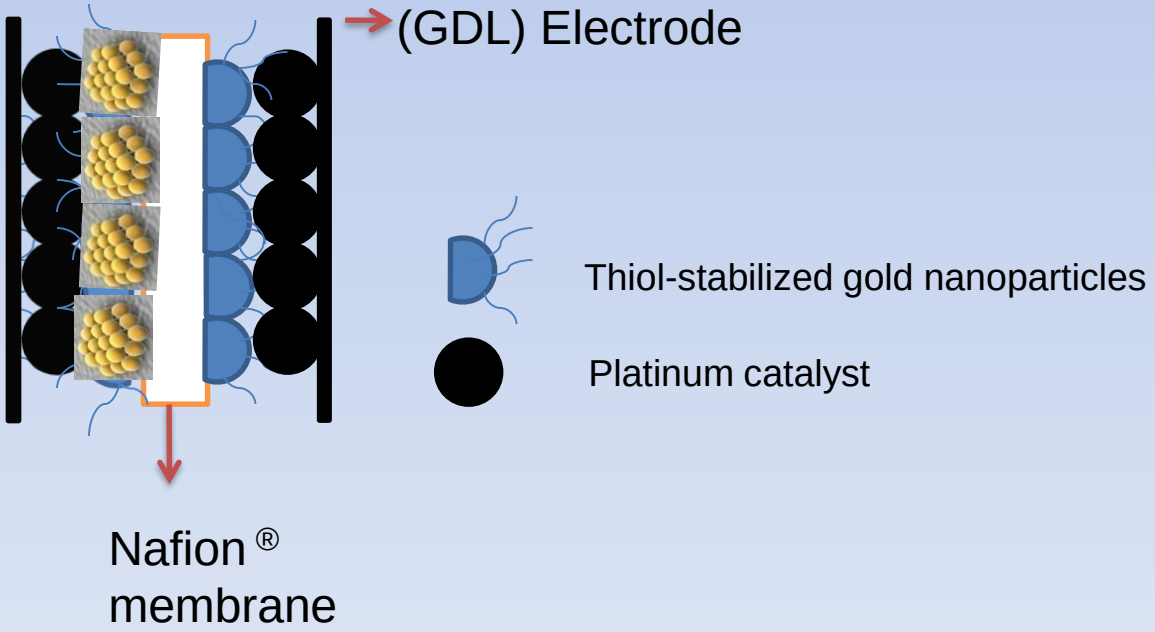

Two-phase Method

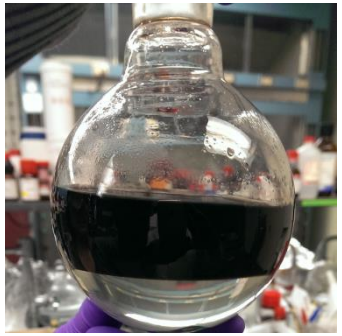

Produces particles that have a weakly bound Au core and tightly bound Au/S shell

Dodecanethiolate palladium nanoparticles: Pd-C12, 2-phase
Dodecanethiolate Pd/Au nanoparticle: Pd-Au , 2- phase

Dodecanethiolate gold nanoparticles: Au-C10, 2-phase

$(Au_m)(C_{12}H_{25}SH)_n(C_6H_5Me)$

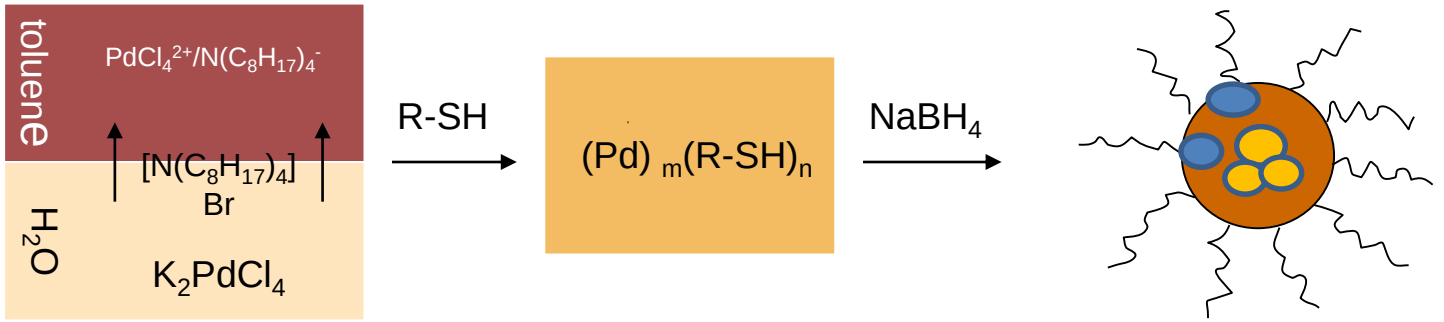

- 0.5 mmol of K_2PdC_{14} dissolved in 20mL H_2O
- 1312 mg of $(C_8H_{17})_4NBr$ dissolved in 20mL of toluene is added, and stirred to extract Pd salt out of H_2O phase
- 0.5 mmol of $C_{12}SH$ is added and mixture is reduced with 227 mg of $NaBH_4$

[2] Brust, M.; Walker, M.; Bethell, D.; Schiffrin, D. J.; Whyman, R. *J. Chem. Soc., Chem. Commun.* 1994, 801.

TEM Determination of Size for Au thiol nanoparticles

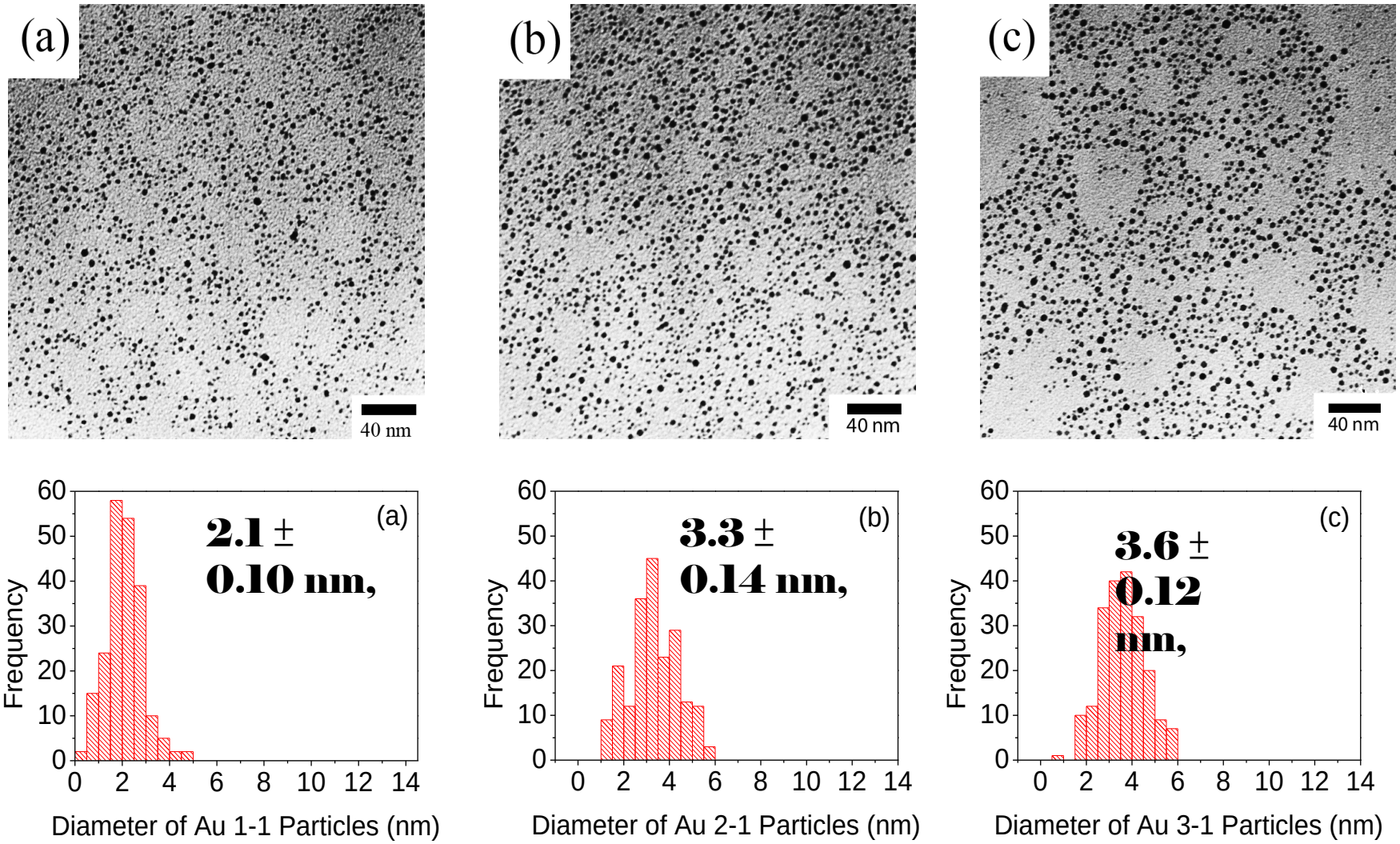

Unit Cell Lattice Parameter: Electron Diffraction

Pd-C12, 1-phase

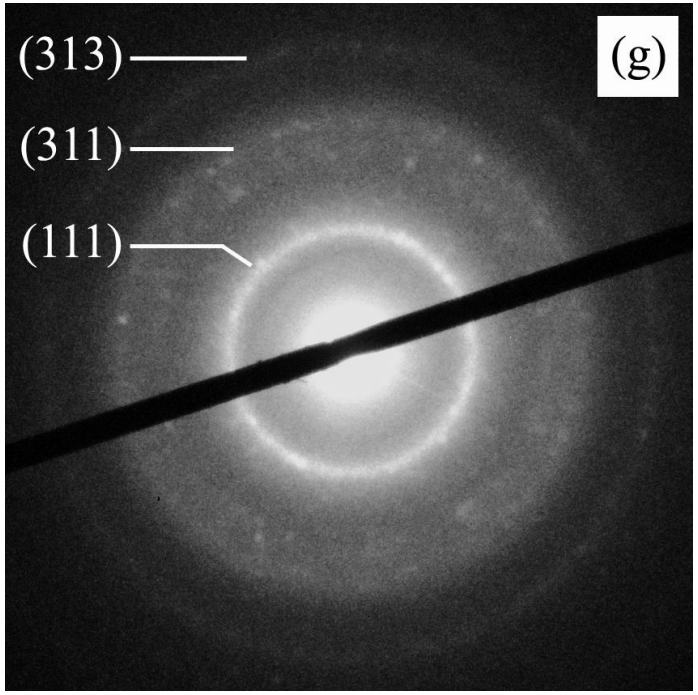

Pd-C12, 2-phase

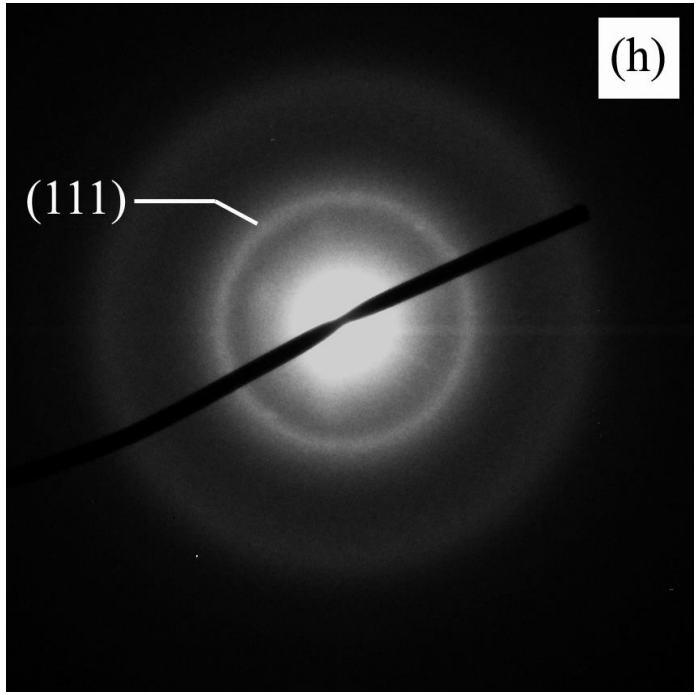

FCC

	Pd-C12, 1-phase	Pd-C12, 2-phase	Bulk Pd
Cell Parameter a_0 (Å)	3.98 ± 0.01	3.90 ± 0.01	3.8907 [3]

[3] JCPDS-International Centre for Diffraction Data.

Preparation of Monolayer of Platelet Gold Nanoparticles

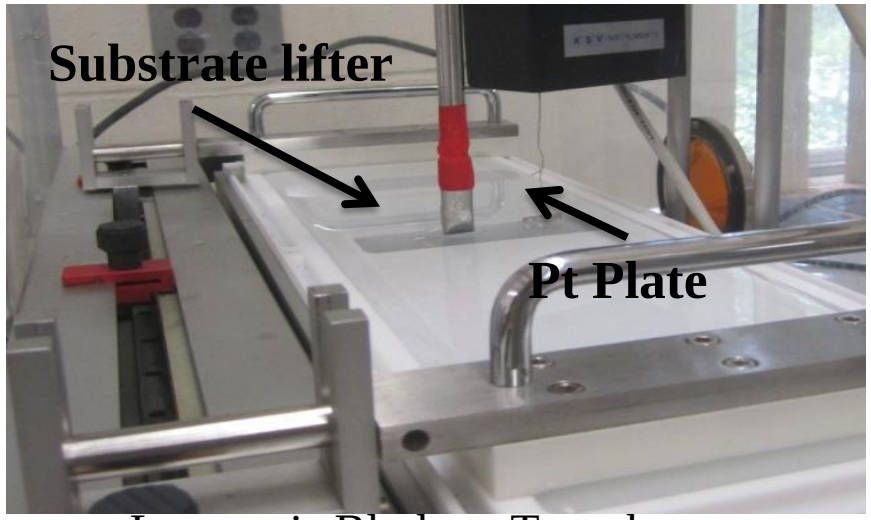

Langmuir-Blodgett Trough

Components:

- Trough with subphase;
- Teflon Barrier;
- Pt plate detector;

Function:

- Create platelet gold nanoparticles by spreading as prepared gold nanoparticles at the interface of water and air.*
- Directly deposit platelet gold nanoparticles onto membrane

* Sun Y, et al., *Langmuir, Vol. 22, No. 2, 2006*

Deposition of Monolayer of Gold Nanoparticles

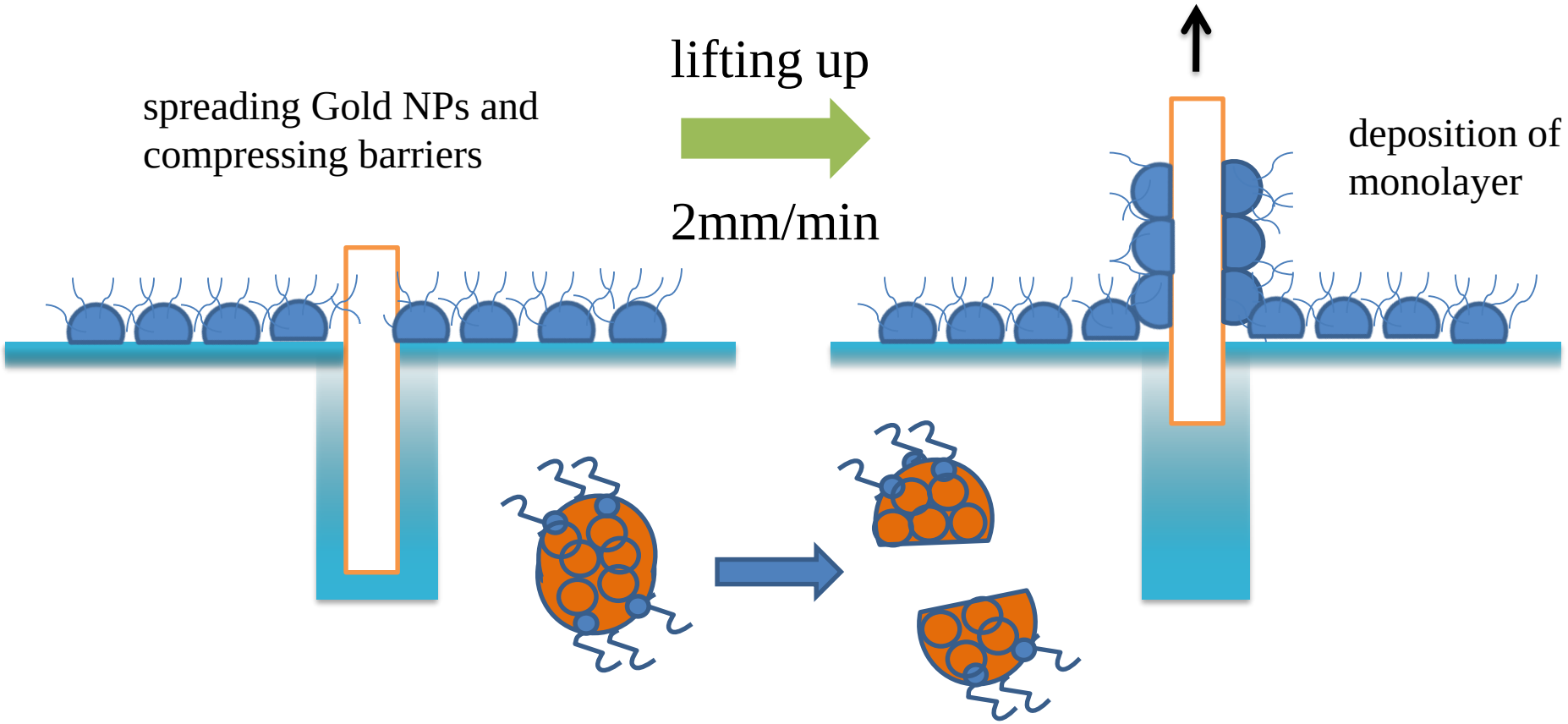

Au clusters are weakly bound, while Au/S bond is strong.
Water displaces the Au/Sulfur hydrophobic complexes, forming platelets.

LB Isotherm Curve for Gold Nanoparticles

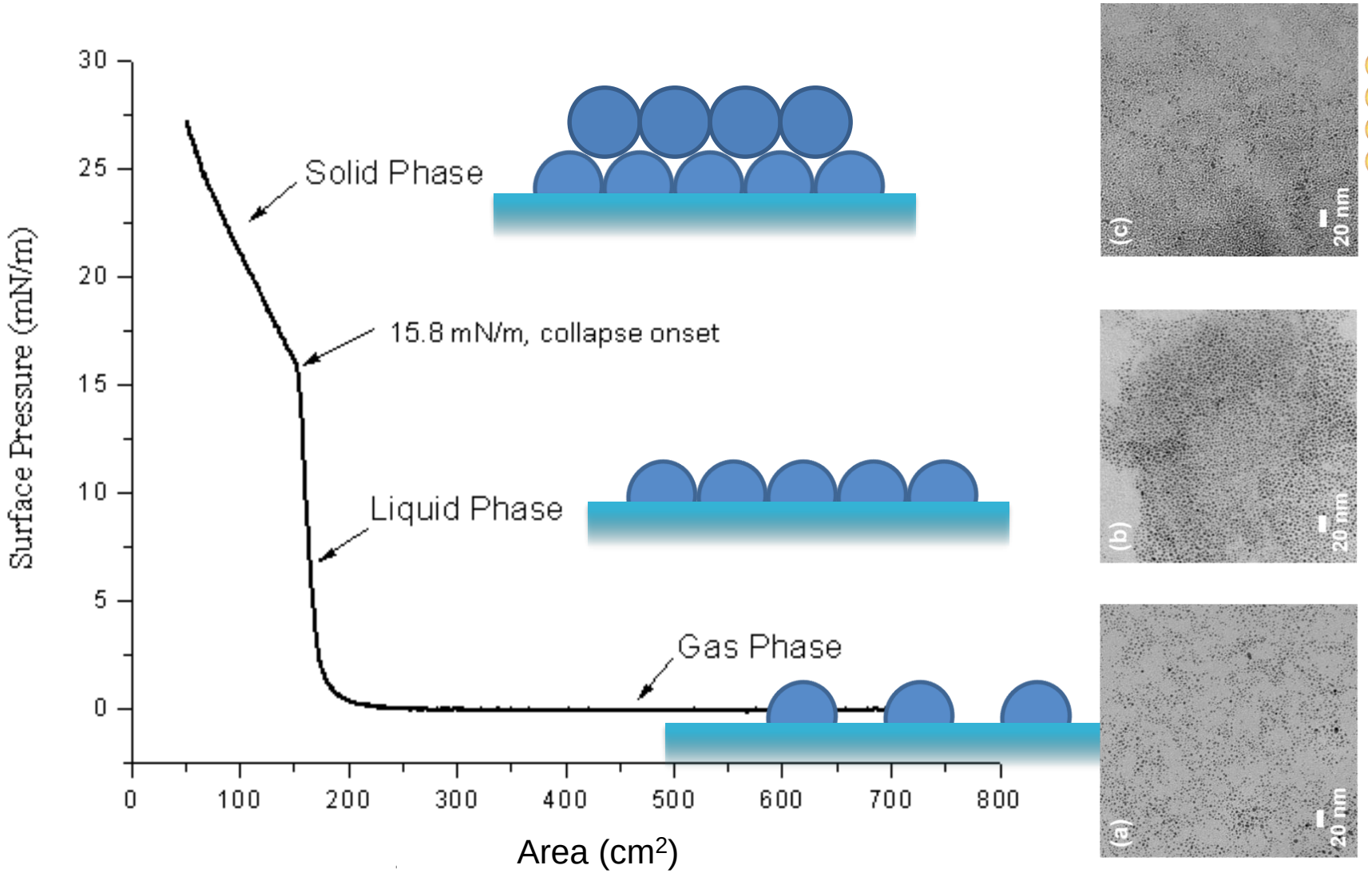

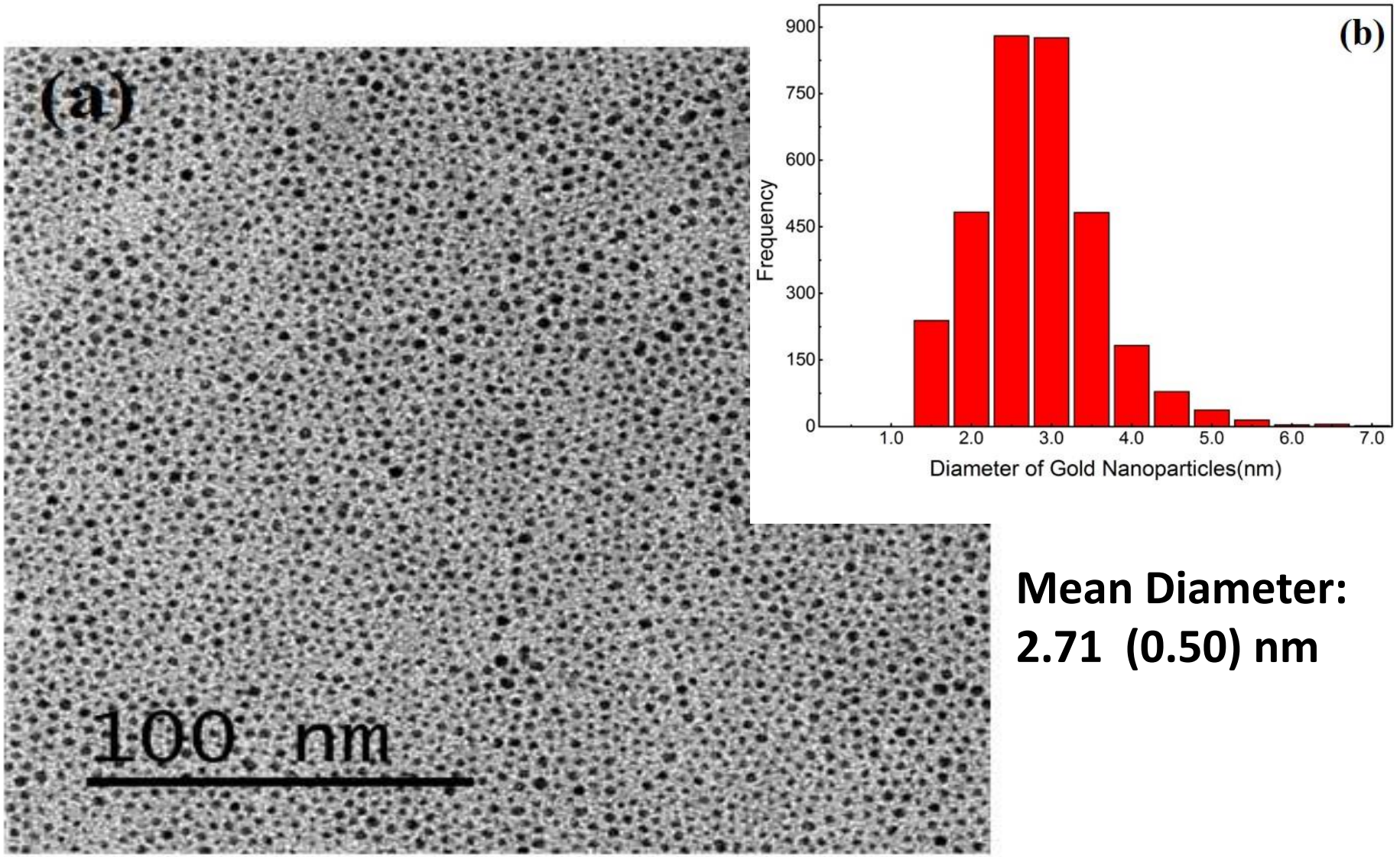

Mean Diameter:
2.71 (0.50) nm

Highly ordered nanoplatelet film at the correct pressure

Characterization of prepared AuPd NPs

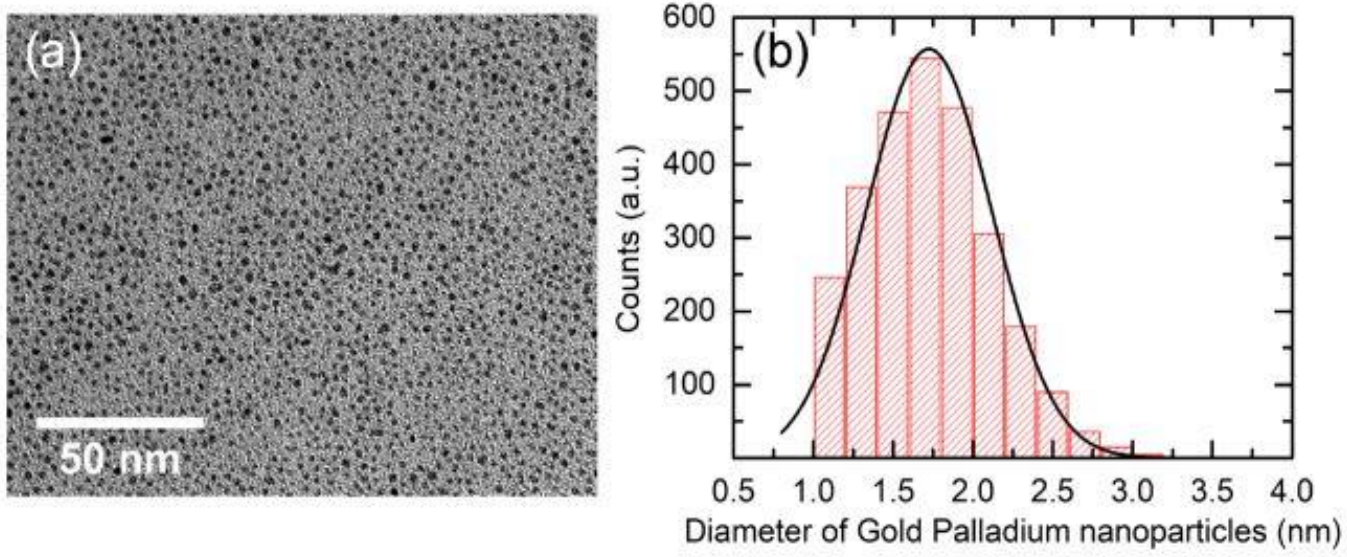

Uniform distribution with
Average size = 1.86 nm

Lattice constant of a = 0.400 nm, which is intermediate between lattice constants for Au, 0.408 nm, and Pd, 0.389 nm

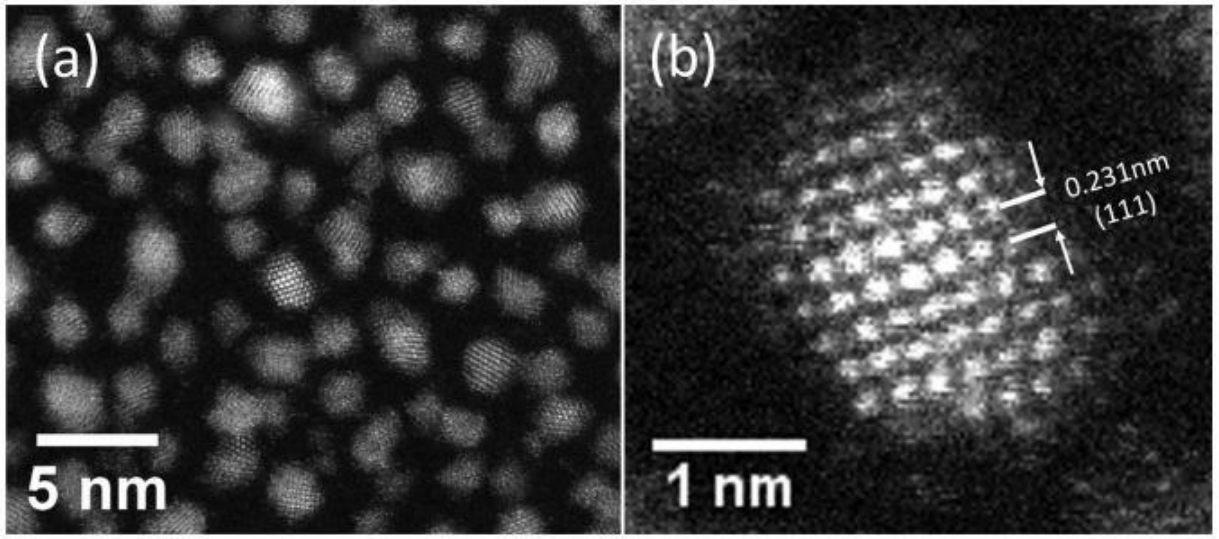

- X-ray Reflectivity -

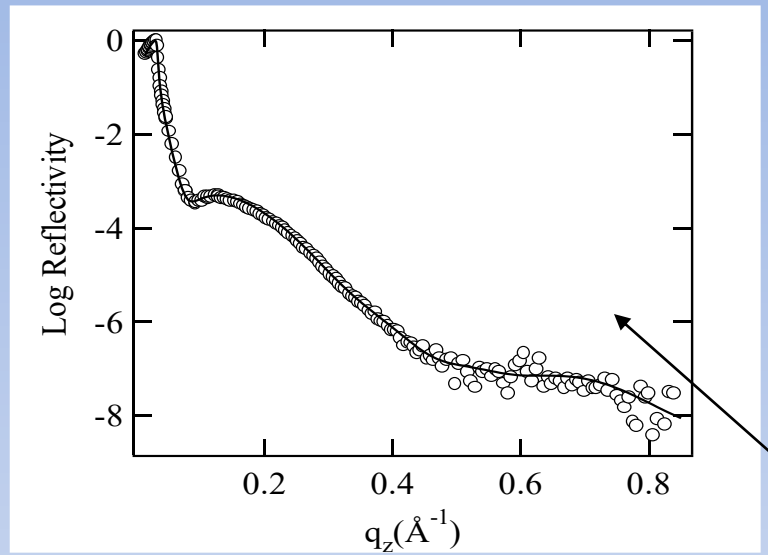

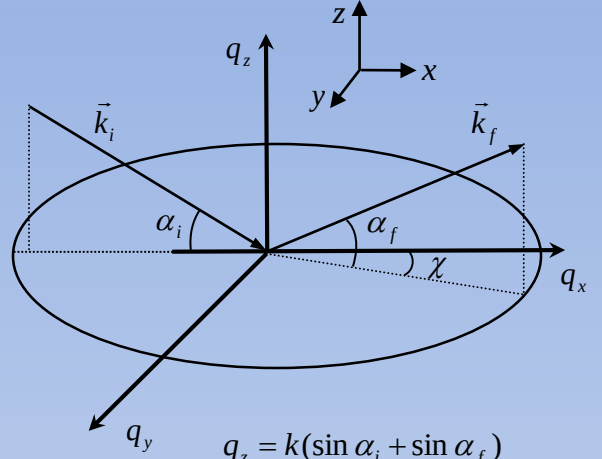

$$q_z = k(\sin\alpha_i + \sin\alpha_f)$$
$$q_x = k(\cos\alpha_f \cos\chi - \cos\alpha_i)$$
$$q_y = k\cos\alpha_f \sin\chi$$
$$q_{xy} = (q_x^2 + q_y^2)^{1/2}$$

Fitting Parameters

	s	t	δ×10⁶
air	5.5	--	--
thiol	4.5	7.2	1.0
Pd/thiol	**5.0**	**13.3**	**3.1**
thiol	3.0	12.5	0.53
SiO_2	--	13.0	2.54

s – roughness (Å),

t – thickness (Å),

δ– dispersive component of the refractive index.

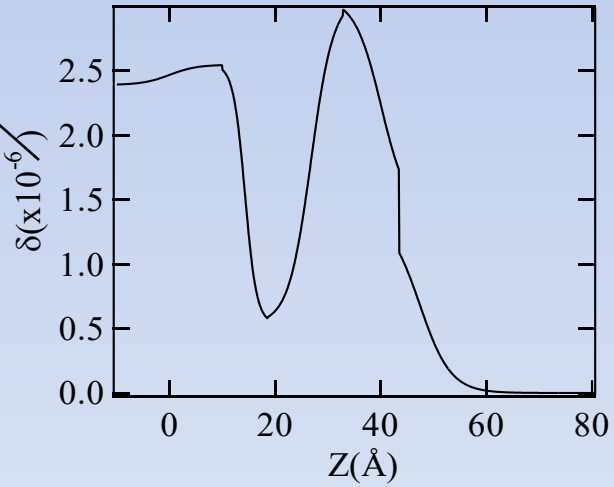

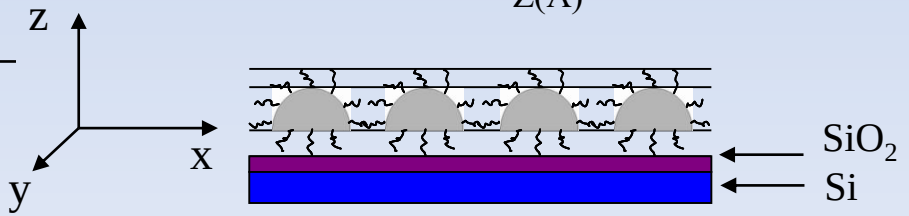

Lifted AuNP monolayer directly on Nafion membrane

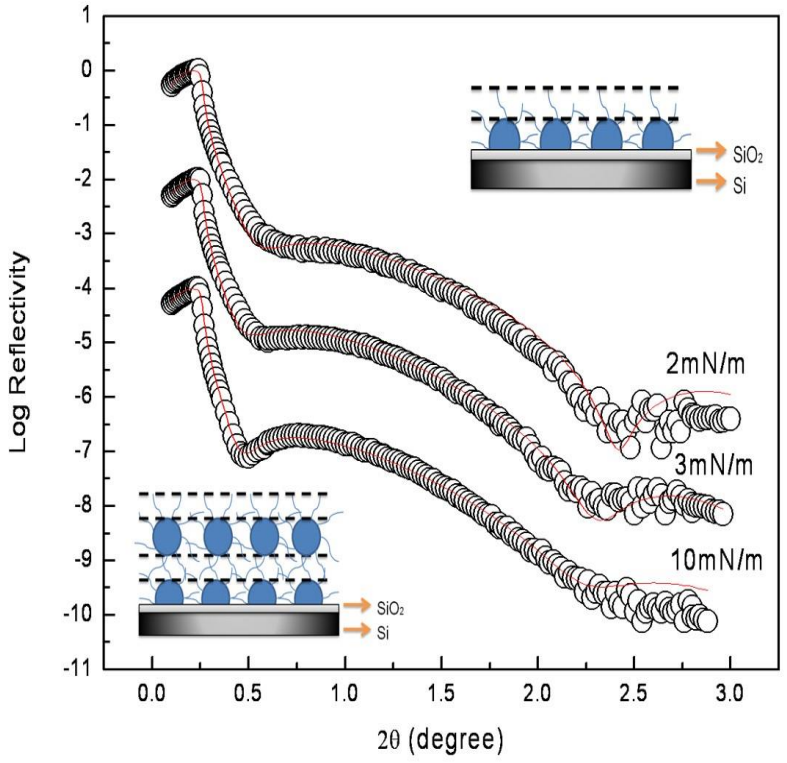

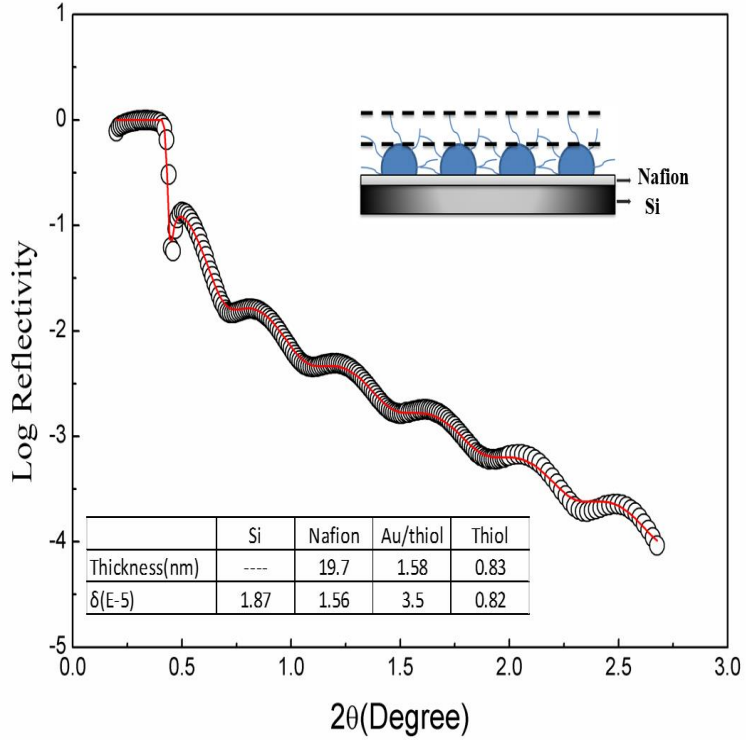

	Si	Nafion	Au/thiol	Thiol
Thickness(nm)	----	19.7	1.58	0.83
δ(E-5)	1.87	1.56	3.5	0.82

Reflectivity of films lifted at different pressures on SiOx. Bare Au surface is unstable and recombination occurs.

Optimal surface pressure

XRR indicate the platelet shape of the AuPd NPs in the water air interface

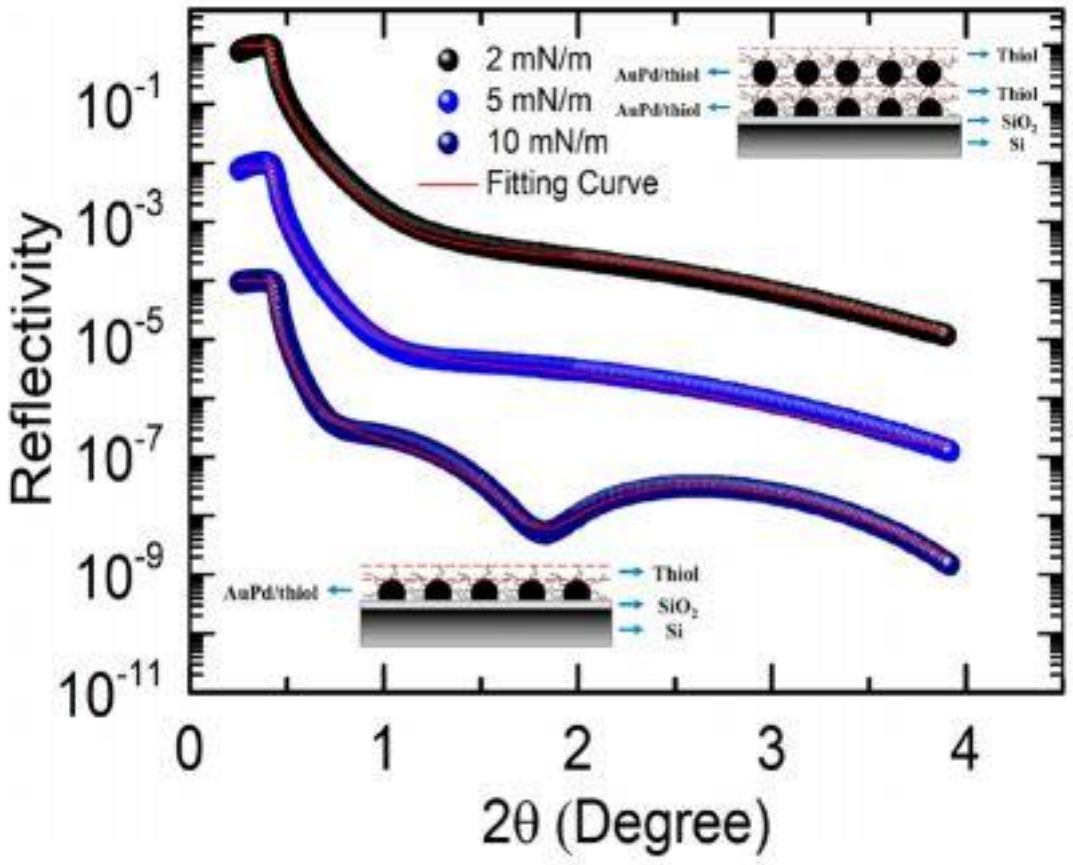

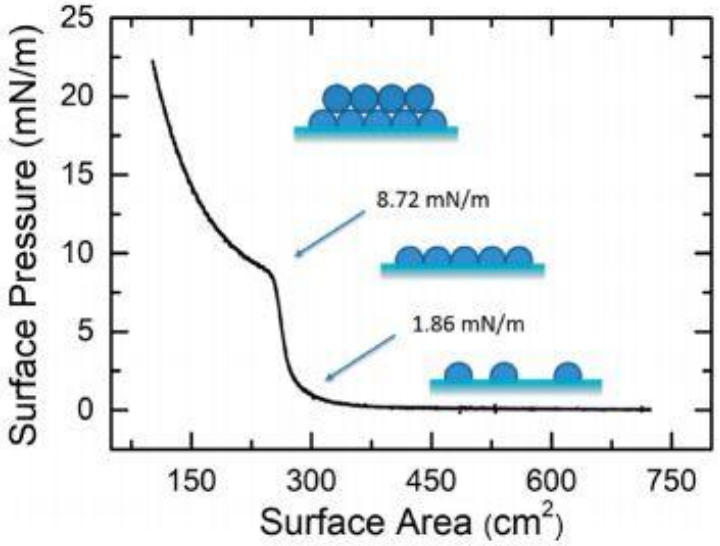

	2 mN/m		5 mN/m		10 mN/m	
	t (Å)	δ (×10^{-5})	t (Å)	δ (×10^{-5})	t (Å)	δ (×10^{-5})
Si	N/A	1.85	N/A	1.85	N/A	1.85
SiO_2	15	1.9	15	1.9	15	1.9
AuPd/thiol	11.5	2.09	11.6	2.27	11.8	2.85
Thiol	4.5	0.41	4.6	0.45	4.86	0.42
AuPd/thiol	N/A	N/A	N/A	N/A	21.3	1.41
Thiol	N/A	N/A	N/A	N/A	4.38	0.31

Confirmation of platelet structure: X-ray Reflectivity Results (Angstroms)

	2 mN/m		3 mN/m		10 mN/m	
	t (Å)	δ (×10^6)	t (Å)	δ (×10^6)	t (Å)	δ (×10^6)
Si		2.239		2.239		2.239
SiO_2	17.1	2.31	17.1	2.31	17.1	2.31
Au/thiol	15.8	4.33	17.4	4.33	18.5	4.33
thiol	5.0	0.95	6.1	0.95	9.6	0.95
Au/thiol					34.5	3.03
thiol					7.0	0.85

Thickness at Z direction < 28.5 Å (average diameter of particles under TEM)
Shape changes from spherical to oblate*

t: thickness
δ: scattering length density

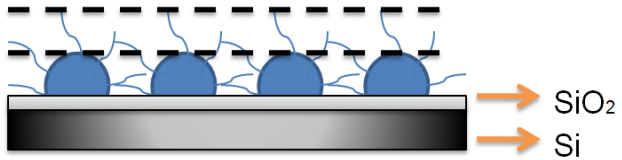

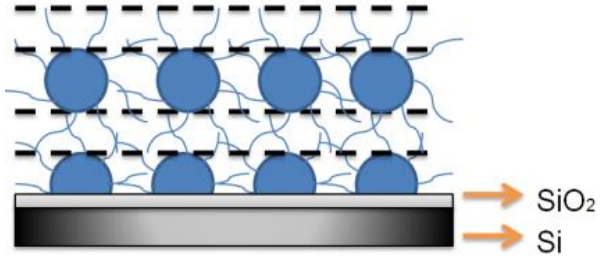

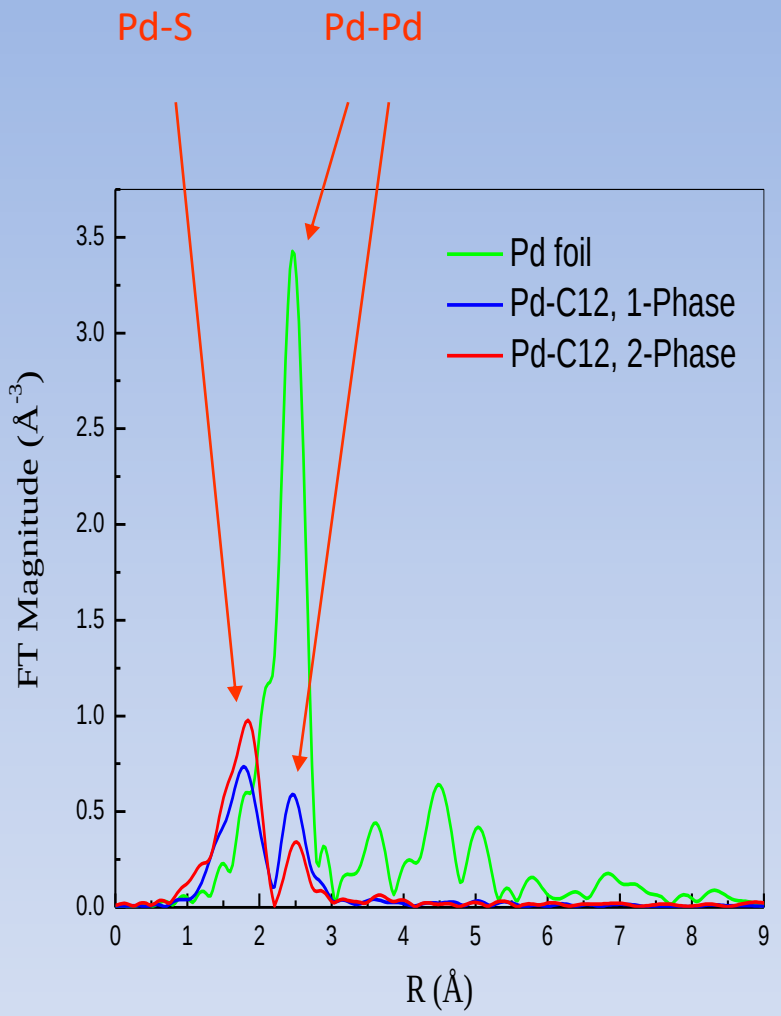

The Fourier-transformed EXAFS data

- CN= 2.9(5)

	EXAFS	TEM
Pd-C12, 1-phase	<10 Å	46 Å
Pd-C12, 2-phase	<10 Å	25 Å

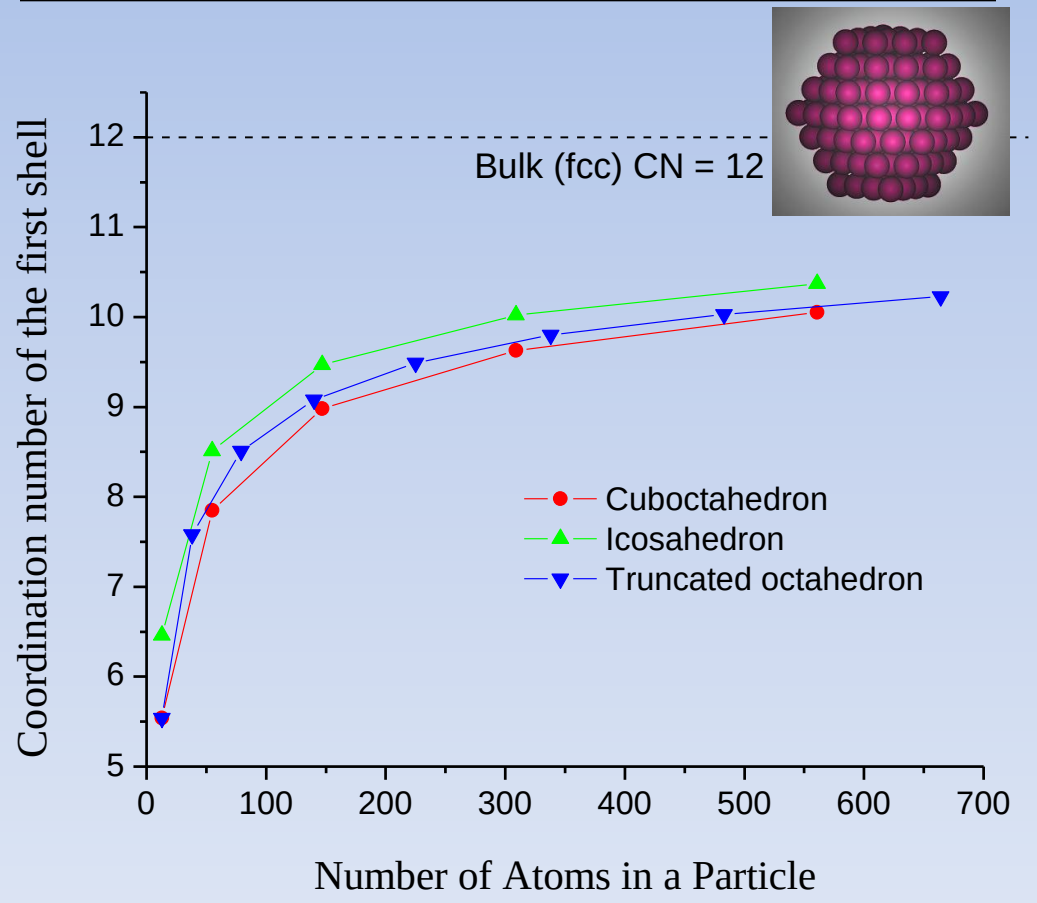

- EXAFS Fitting and Modeling (Anatoly Frenkel-)

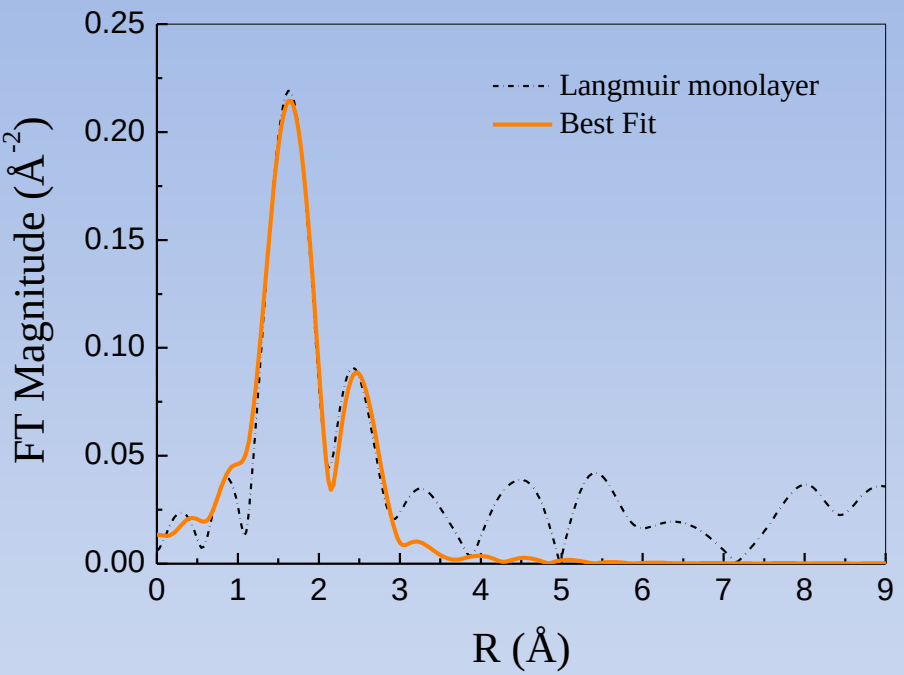

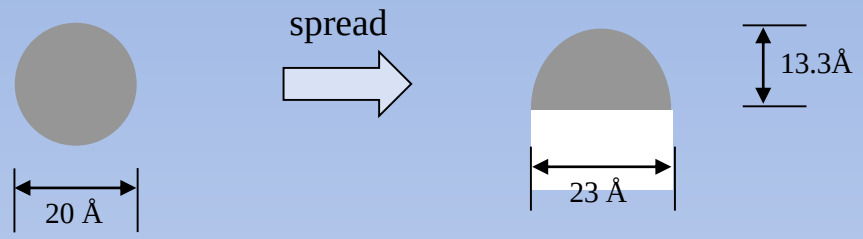

sample	CN	R
LB	6.0(2)	2.76(2)
2 phase	2.3(1)	2.77(2)

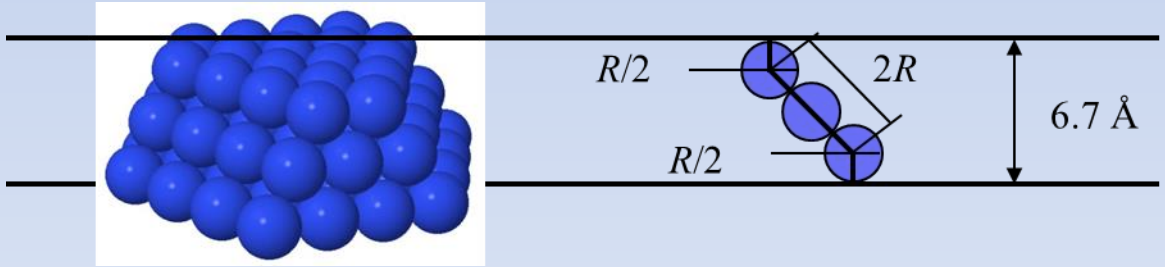

Isothermal curve

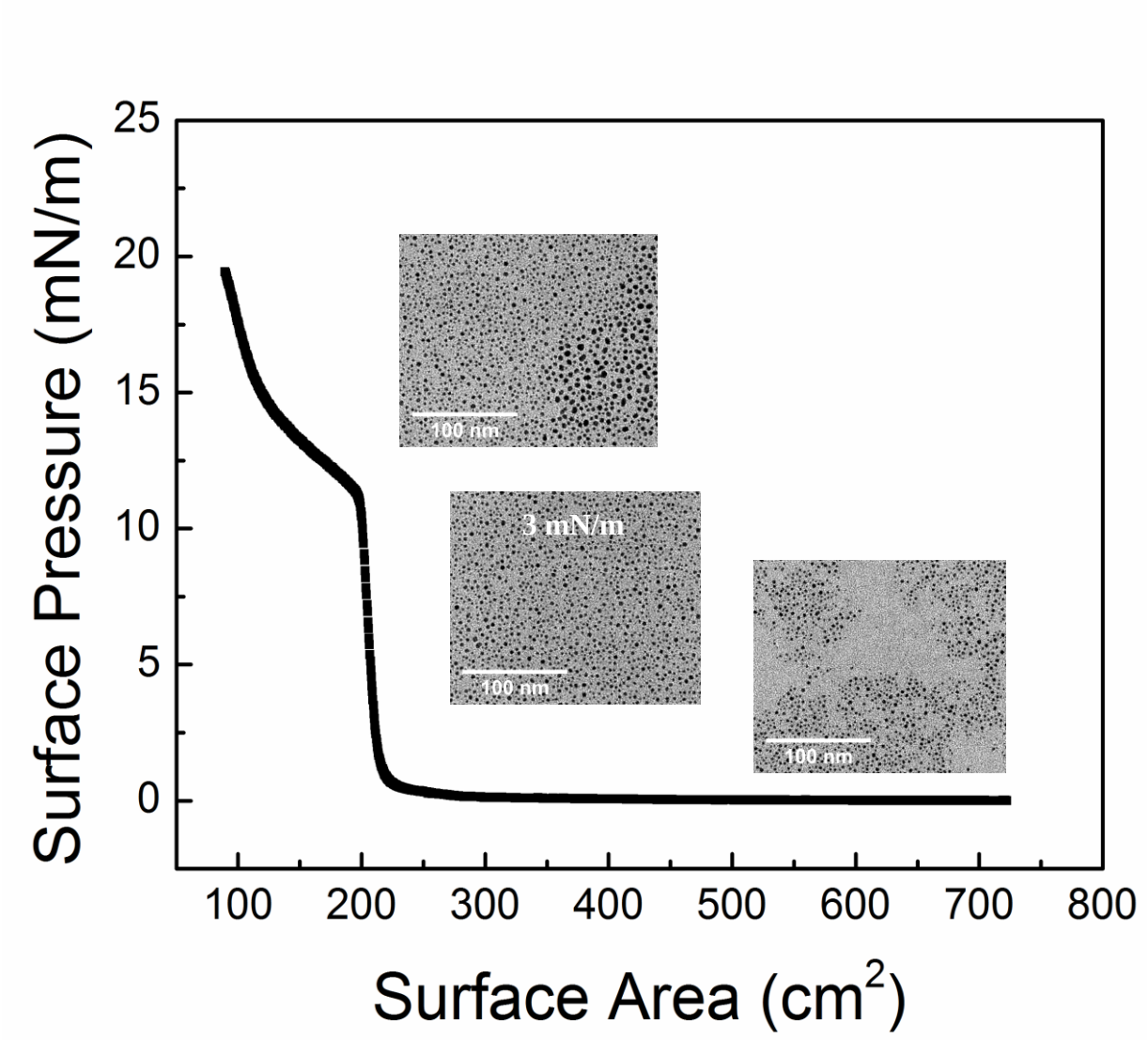

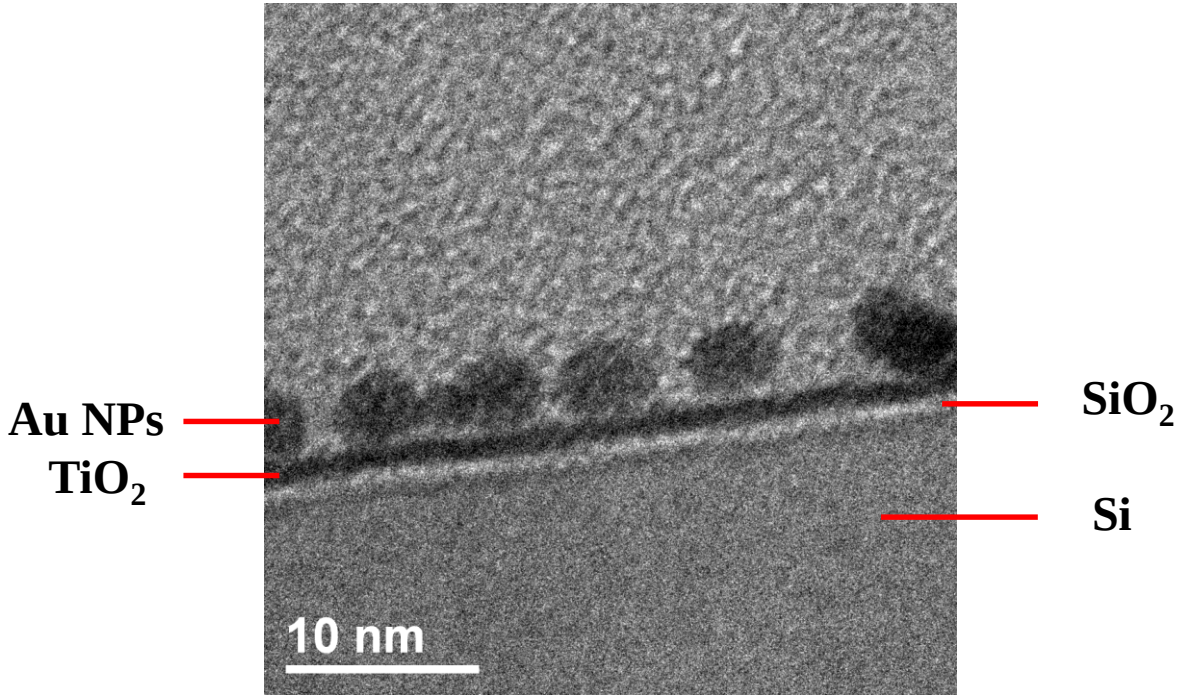

Cross-section TEM image of Au NPs assembled at 3 mN m^{-1} on a TiO_2-coated (20 ALD cycles) Si substrate.

FIB TEM and elemental mapping

AuPd NPs lifted on a silicon wafer at surface pressure of 5 mN/m

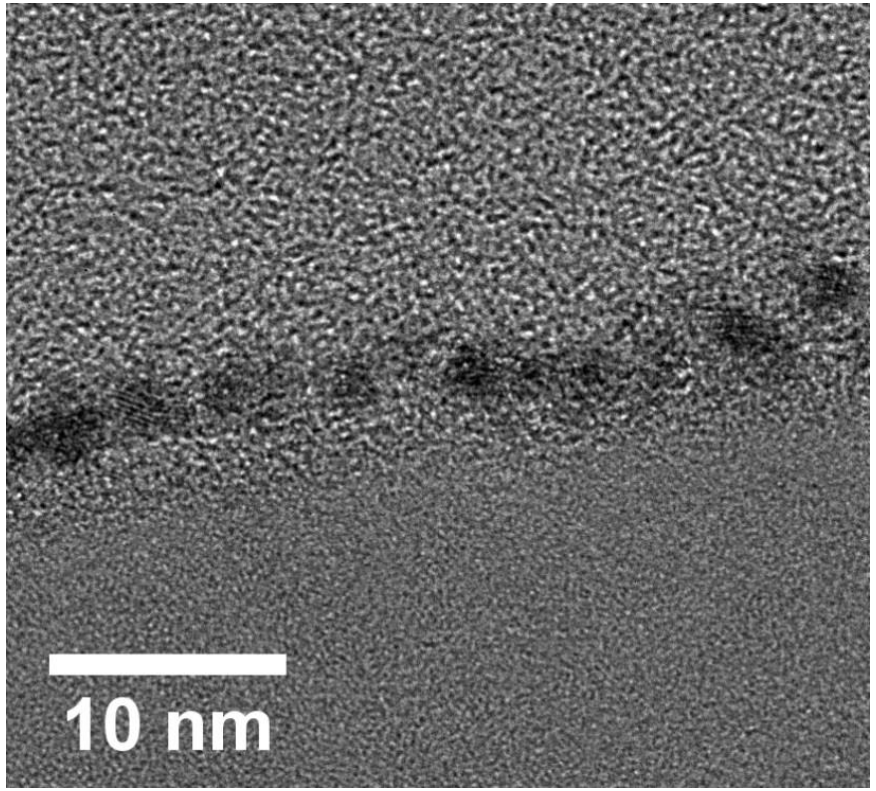

Cross-sectional TEM

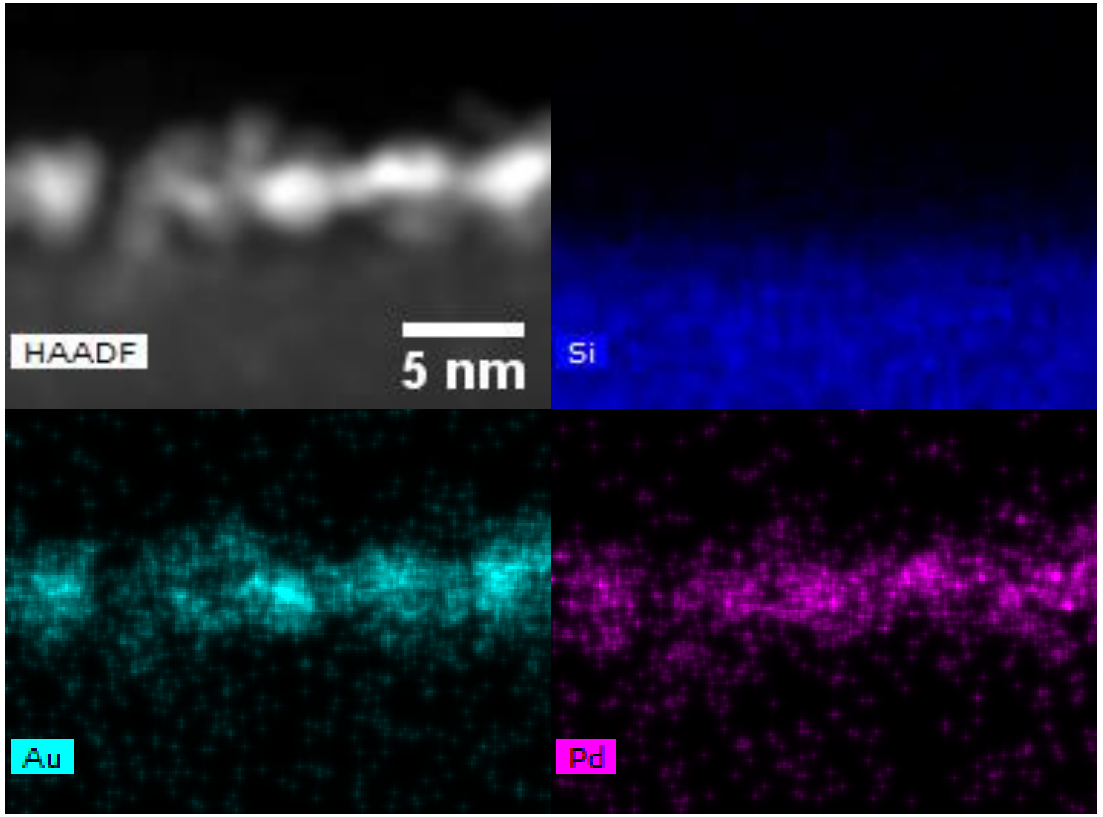

STEM elemental mapping

Power further increased by optimizing particle diameter.

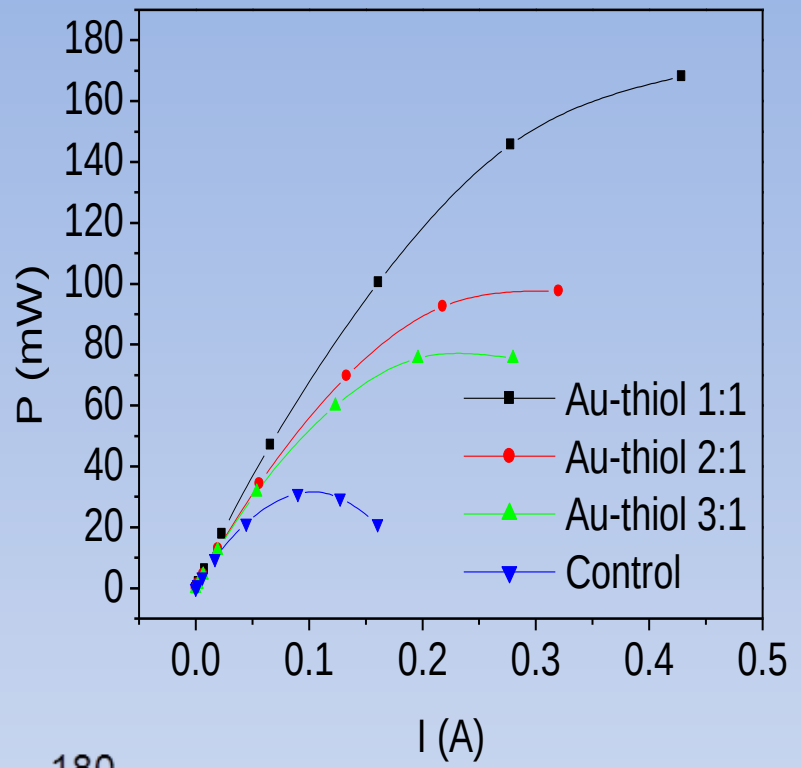

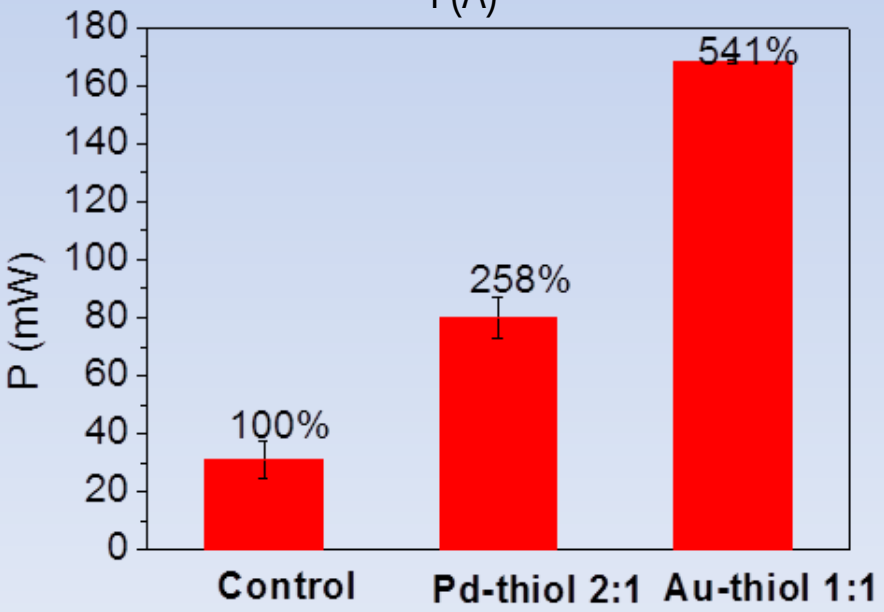

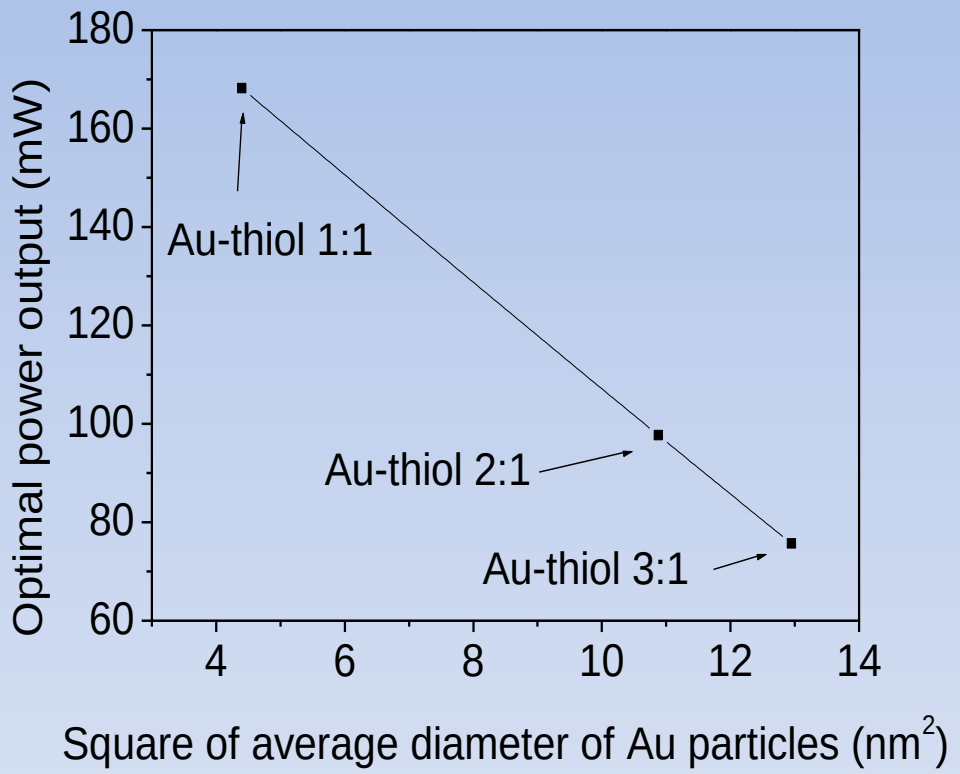

3 stack MEA: Improvement is additive

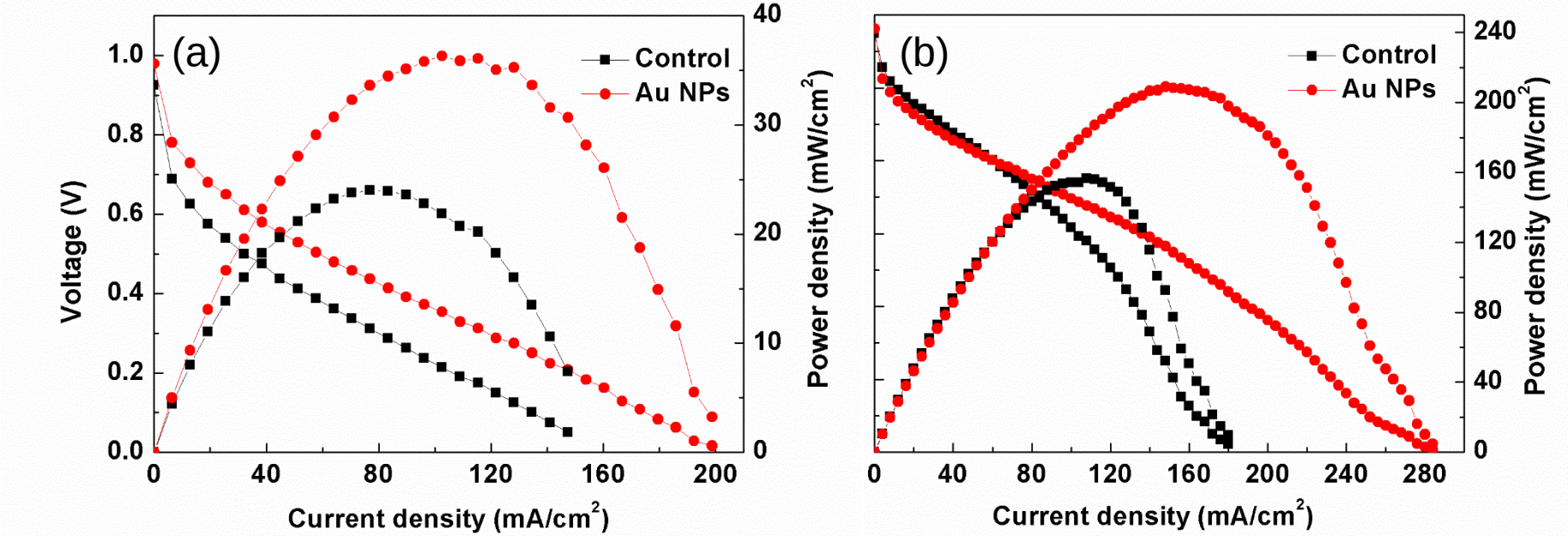

Single MEA

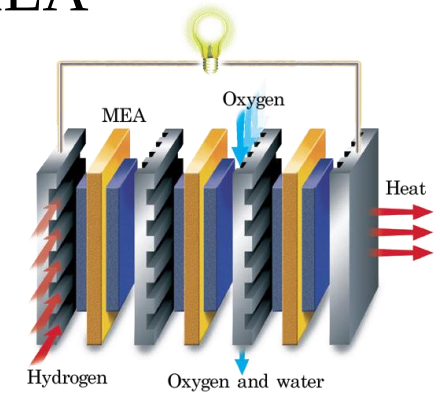

Three stack MEA

PEMFC performance and durability

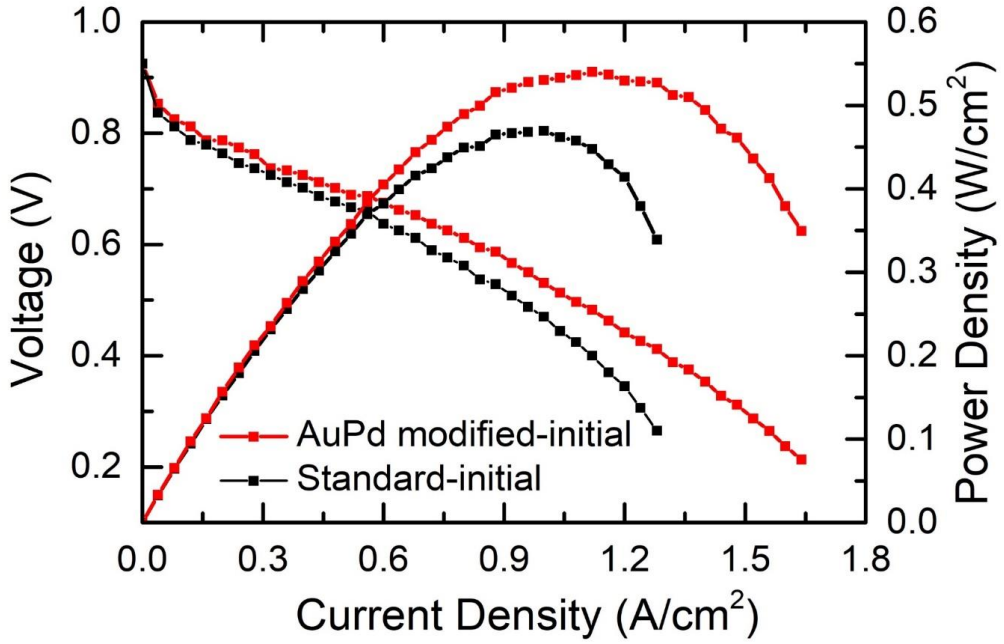

A 15% enhancement of the maximum power density 0.540 W/cm^2 to 0.469 W/cm^2

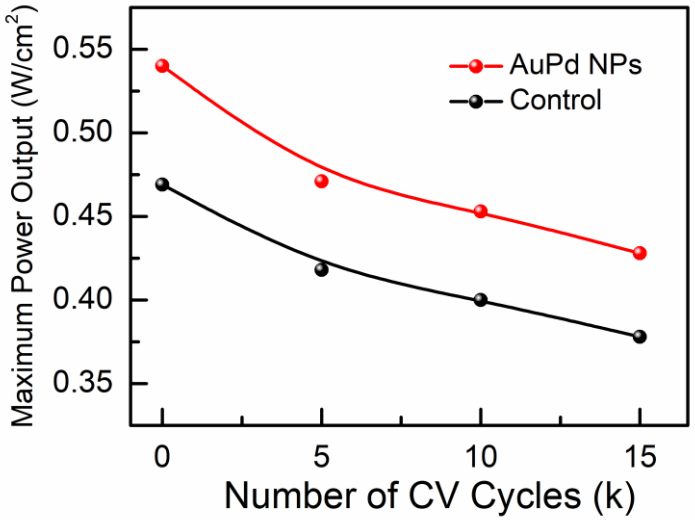

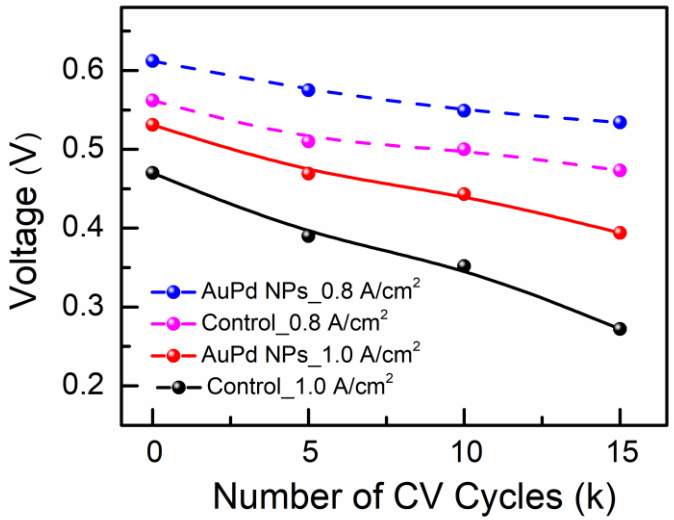

At 1.0 A/cm^2, the voltage of the coated cell was 13% higher initially and reached 45% after 15k cycles.

GO Characterization

Graphene oxide (GO) is an oxidized form of graphene, functionated with oxygen-containing groups, such as epoxide, carbonyl, carboxyl, and hydroxyl groups

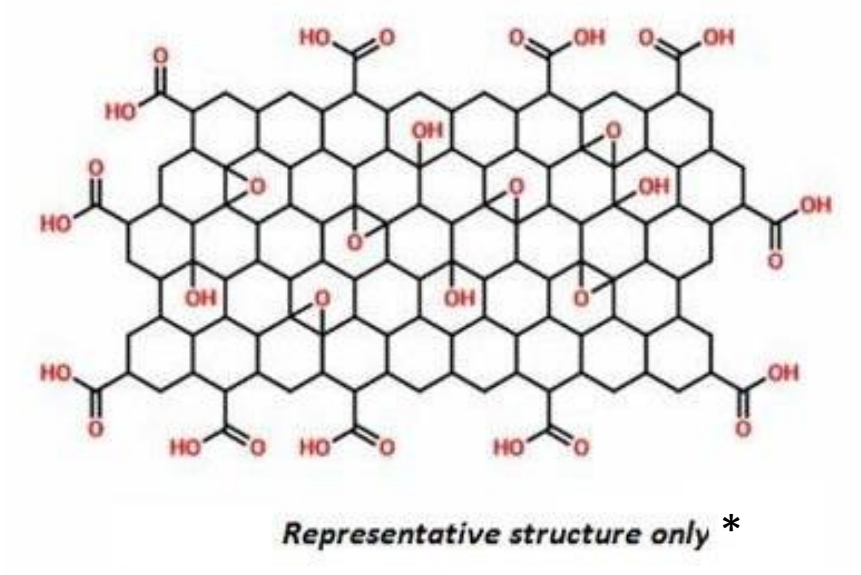

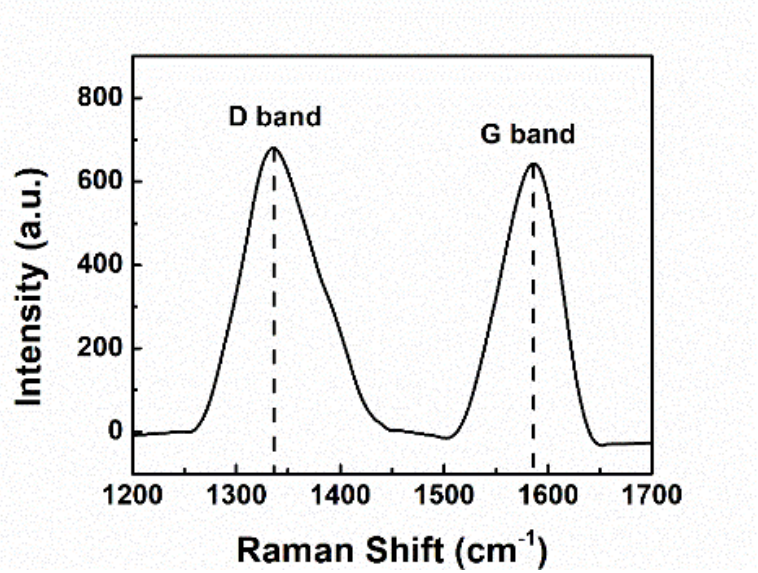

Raman, XPS was conducted to investigate the nature and components of the synthesized GO**

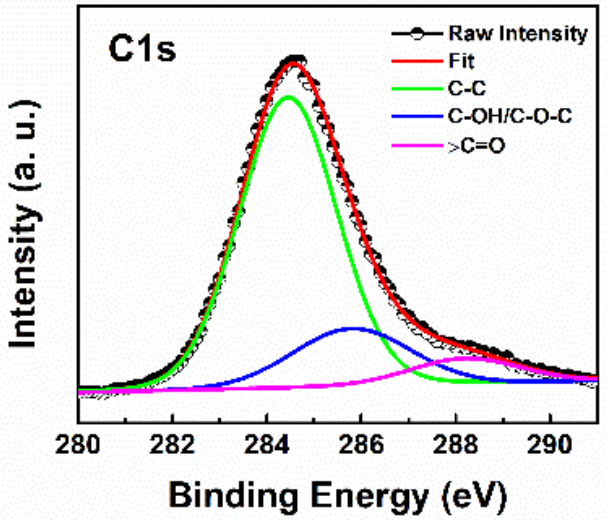

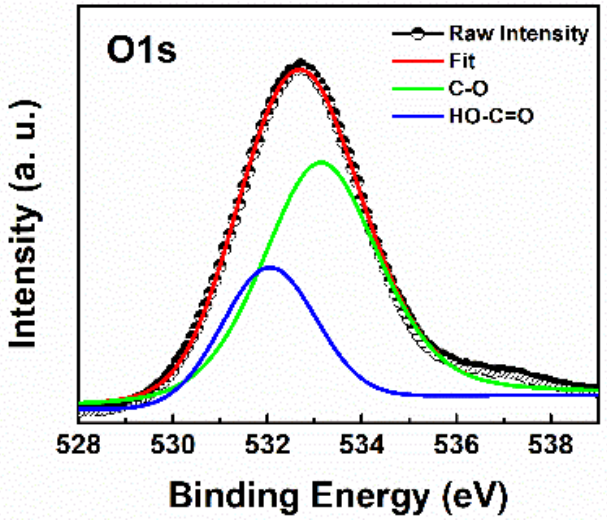

* *https://www.ossila.com/products/graphene-oxide-powders?variant=52280147640 61*

** L. Wang, et al., 2020. *Appl. Energy*, **261**, 114277.

PEMFC performance

60% maximum power enhancement by 1 μg/cm^2 graphene oxide (GO) on the surface of membrane or electrode, which decreases at higher GO loading.

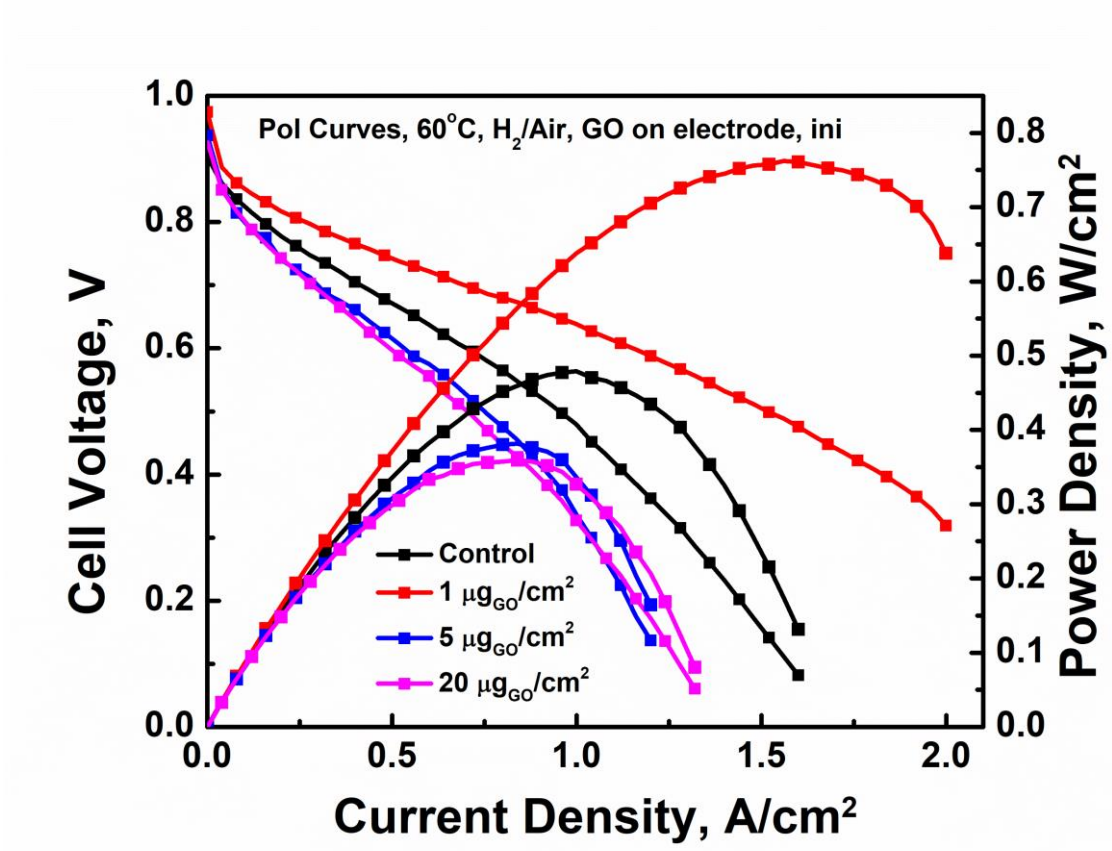

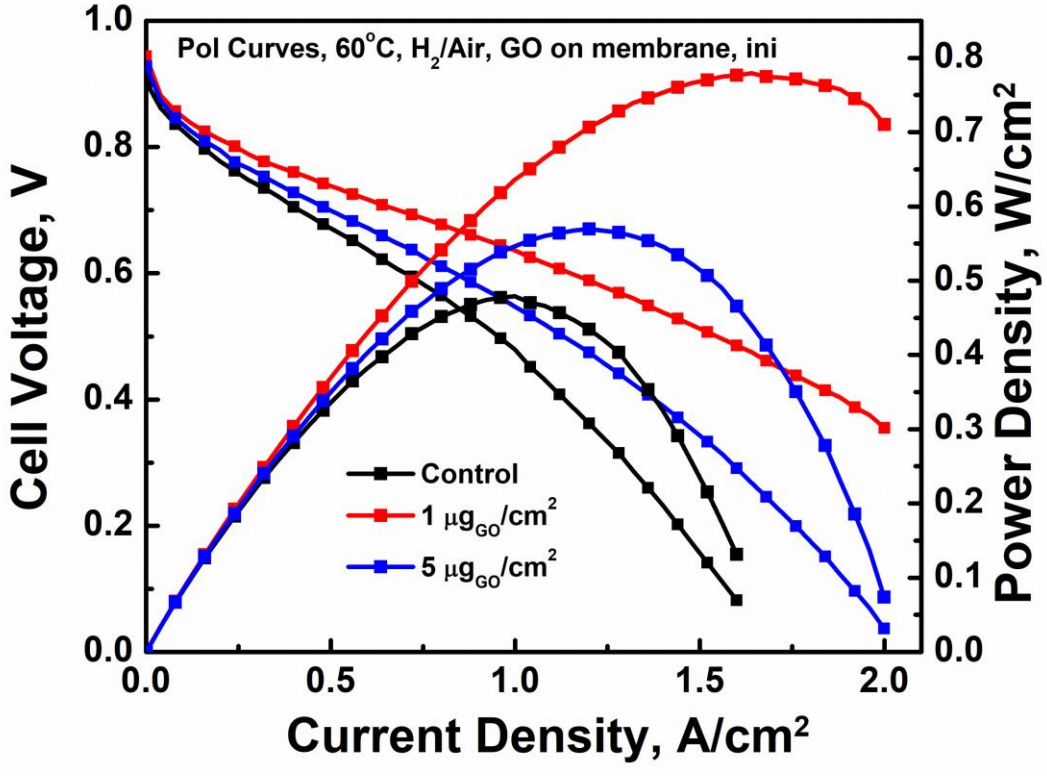

Electrochemical Impedance Spectroscopy (EIS) study

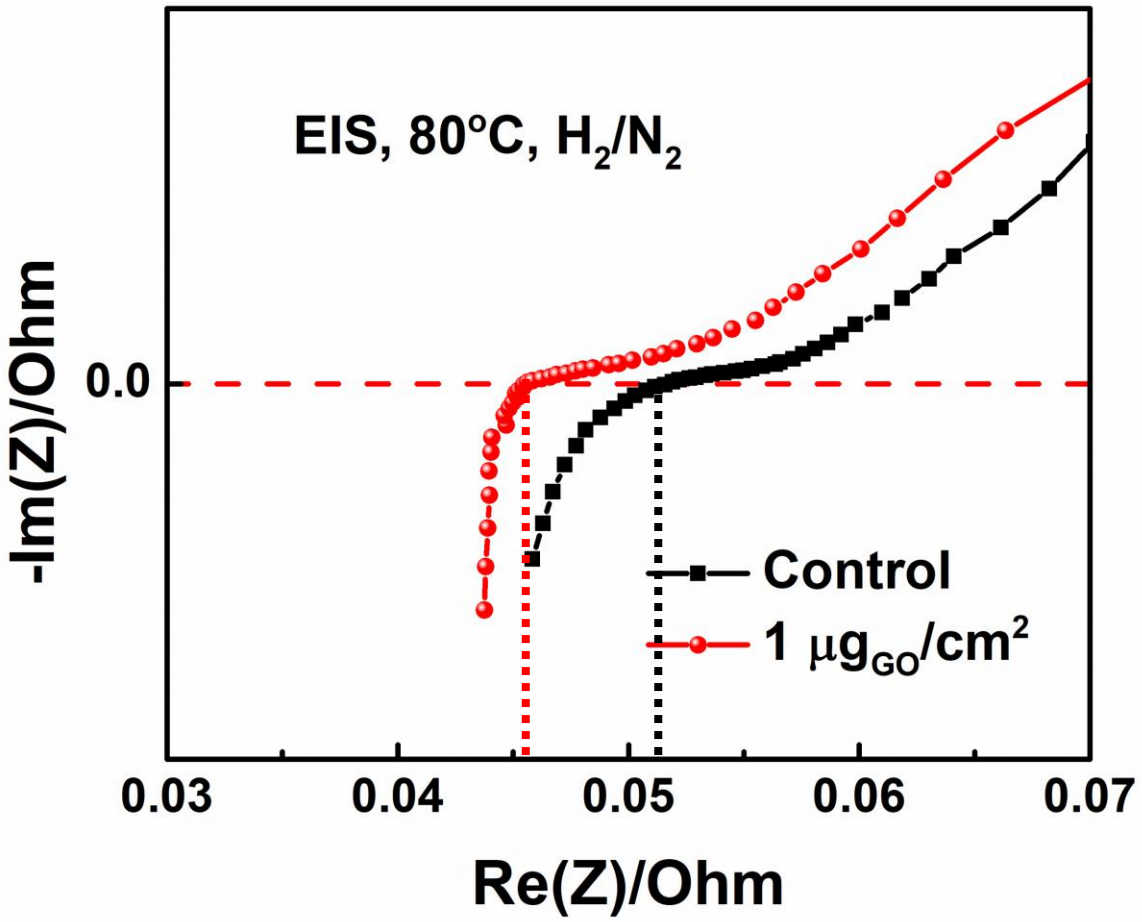

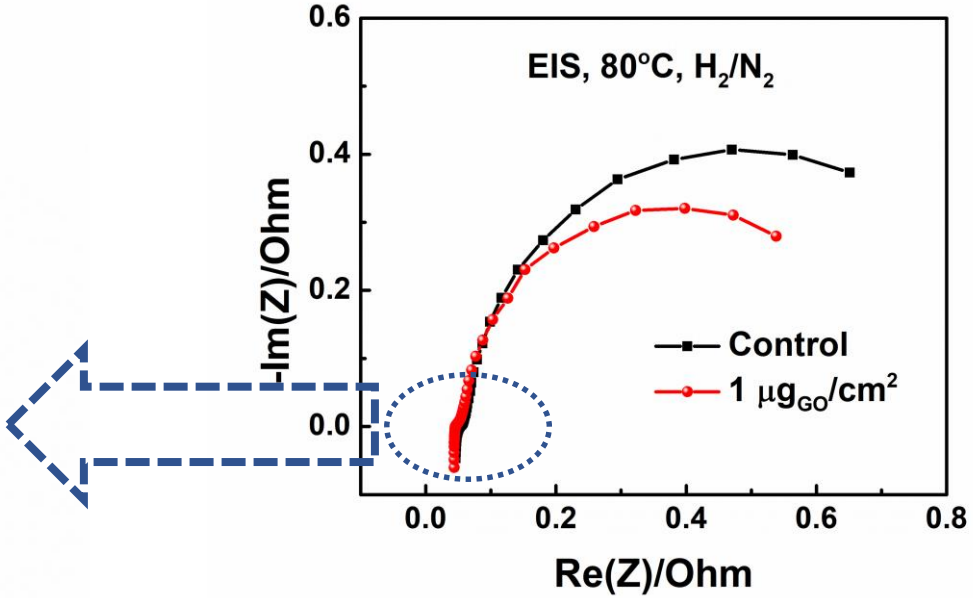

The ohmic resistance of the cell with GO coated electrodes is 0.045 Ω, 13% lower than the control of 0.051 Ω

Mechanism study

As a **surface effect** on both anode and cathode

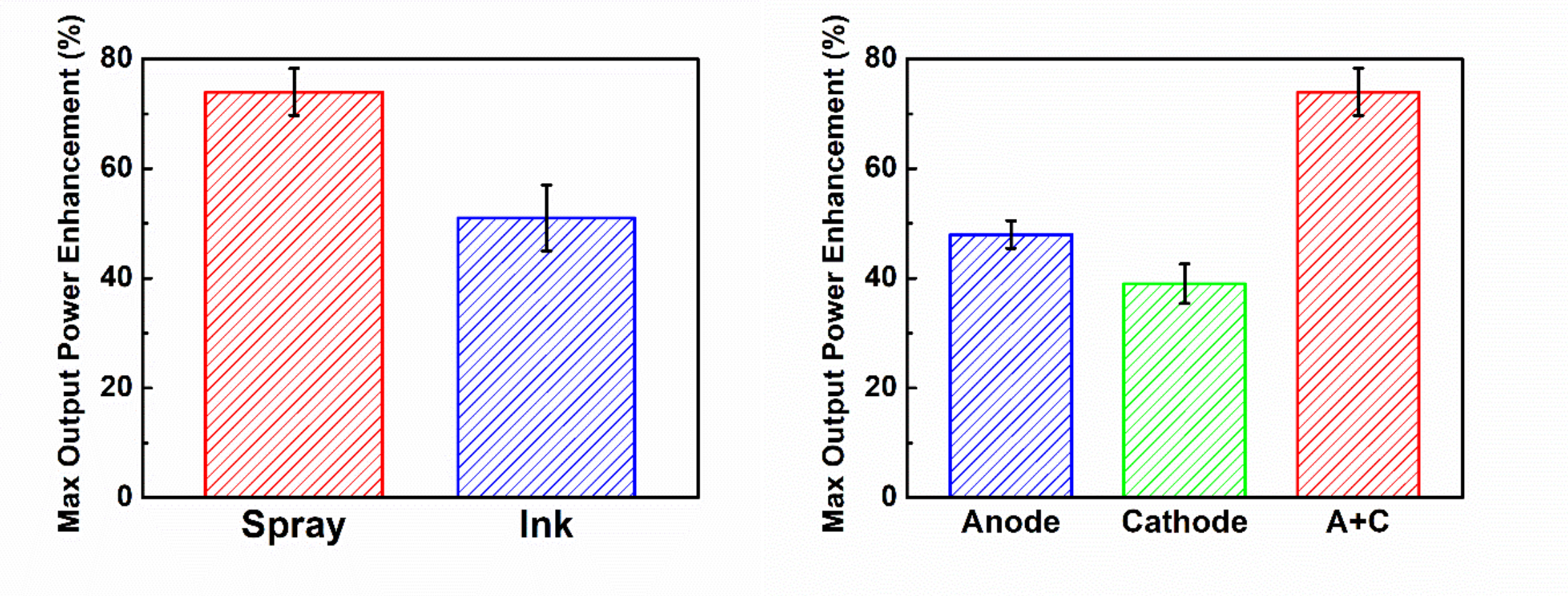

Summary of maximum power enhancement percentage of PEMFC with GO spray-coated on electrode or added into the catalyst ink; GO coated electrode at only anode, cathode or both.

CO poisoning and pure oxygen testing

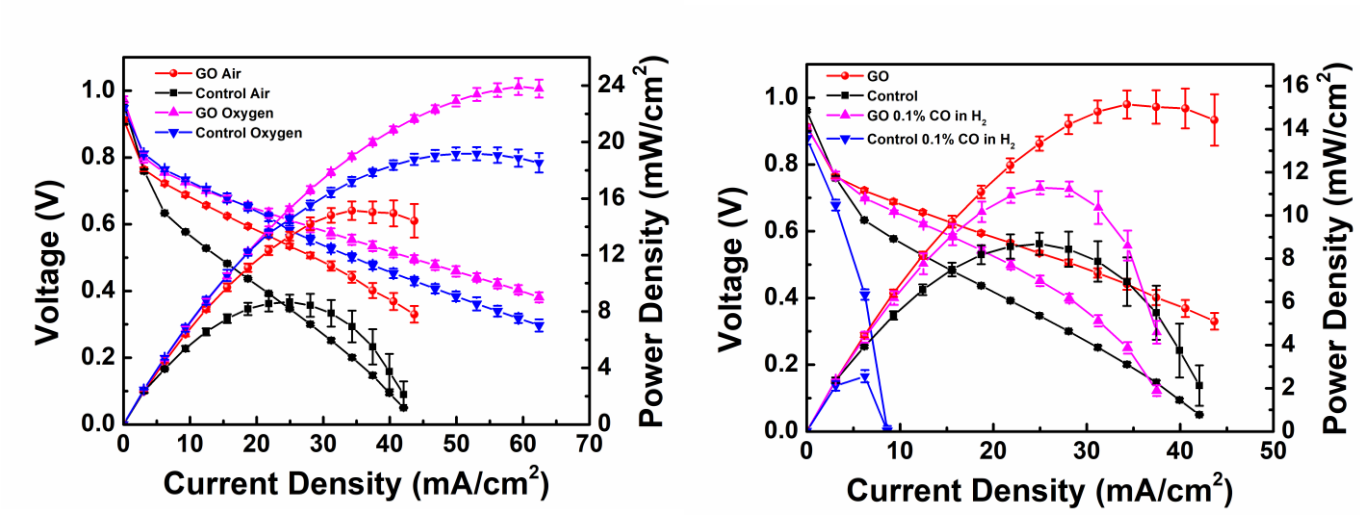

The power enhancement is only 25% in pure O_2 while it is 60% in air for the coated MEA

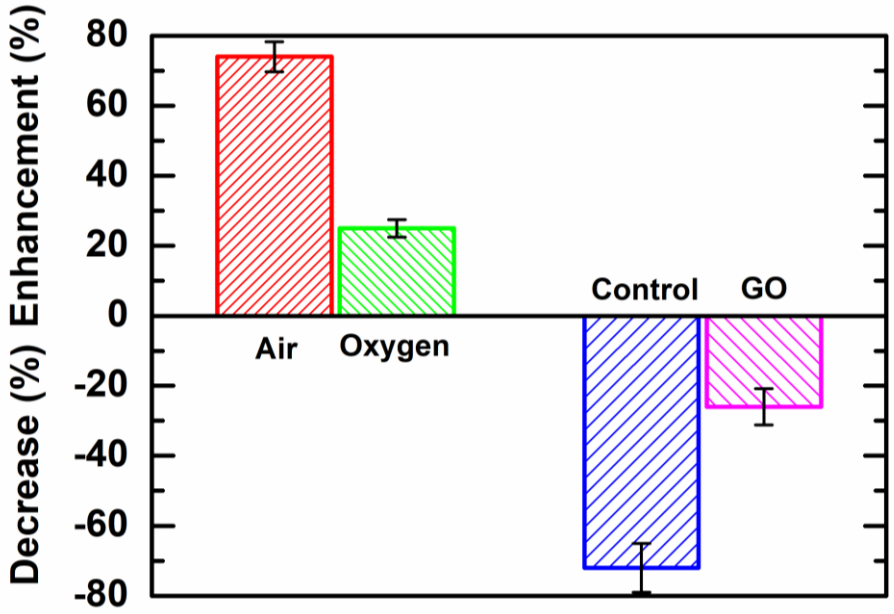

Under 0.1% CO in H_2 (O_2), the maximum power decreases only 26% for the MEA with GO coating while over 70% for the MEA without.

PEMFC Durability

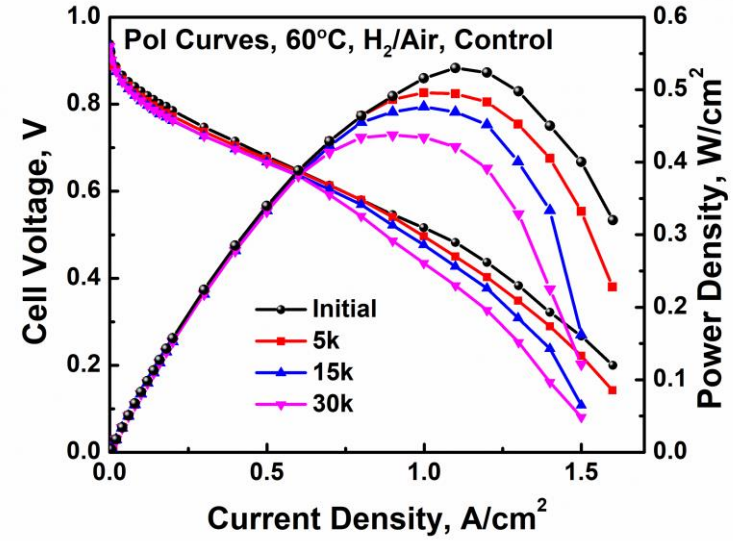

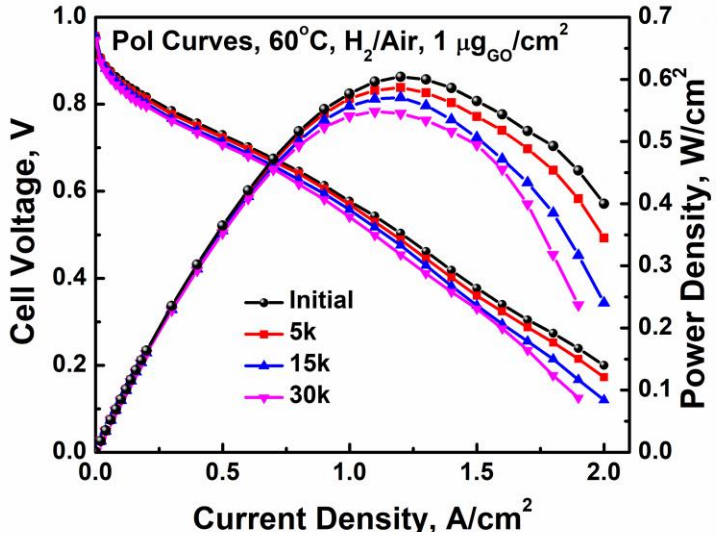

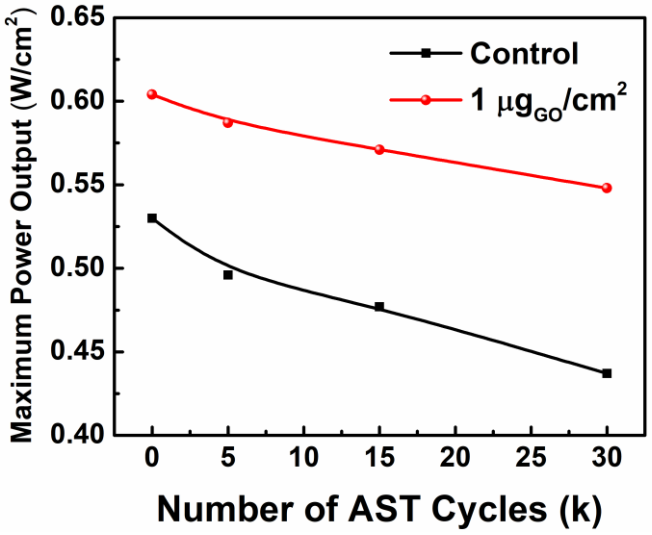

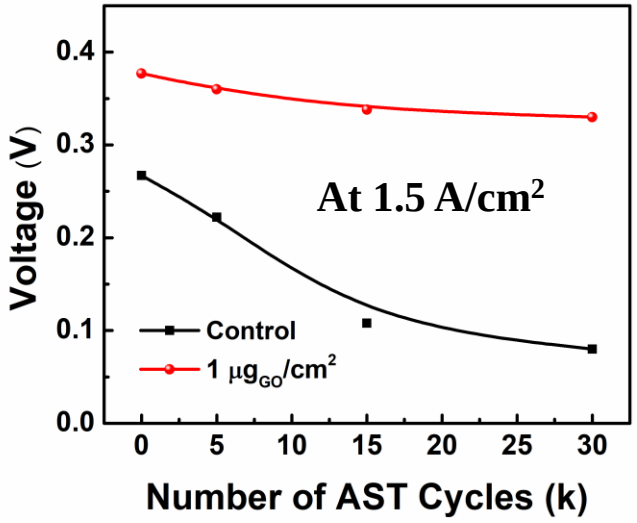

Maximum power density decrease (W/cm2)

	Control	1μg$_{GO}$/cm^2
Initial	0.530	0.604
5k	0.496	0.587
15k	0.477	0.571
30k	0.437	0.548
Decrease (%)	**18**	**9**

The voltage at 1.5 A/cm^2 decreased 13% for the coated MEA while 70% for MEA without after 30k cycles.

Challenges in AEMFCs

- Most significant challenge of AEMFC technology is durability.
- Reported lifetime of AEMFCs significantly inferior to that of PEMFCs.
- For PEMFCs, perfluorosulfonic acids (PFSAs) are known to be chemically, and electrochemically stable.
- For AEMFCs, no such materials available for now.
- Although recent improvement in performance and durability of AEMFCs is impressive even with hydrocarbon-based materials, the current durability of AEMFCs needs to be significantly further improved to achieve commercially viable systems.

Fuel cell performance

	AEM	Anode catalyst	Anode loading (mg/cm^2)	Cathode catalyst	Cathode loading (mg/cm^2)
1	Sustainion	Pt/C	0.76	Pt/C	0.76
2	Sustainion	Pt/C	0.76	FeCo-N-C	0.7
3	mTPN1-TMA	Pt/C	0.76	Pt/C	0.76

Table 3: AEMs with different catalyst and loadings on anode and cathode

- Power Output of Sustainion AEM

a) Pt/C cathode electrode – 0.42 W/cm^2

b) FeCo-N-C cathode electrode – 0.39 W/cm^2

- Power Output of mTPN1-TMA AEM

a) Pt/C cathode electrode – 0.35 W/cm^2

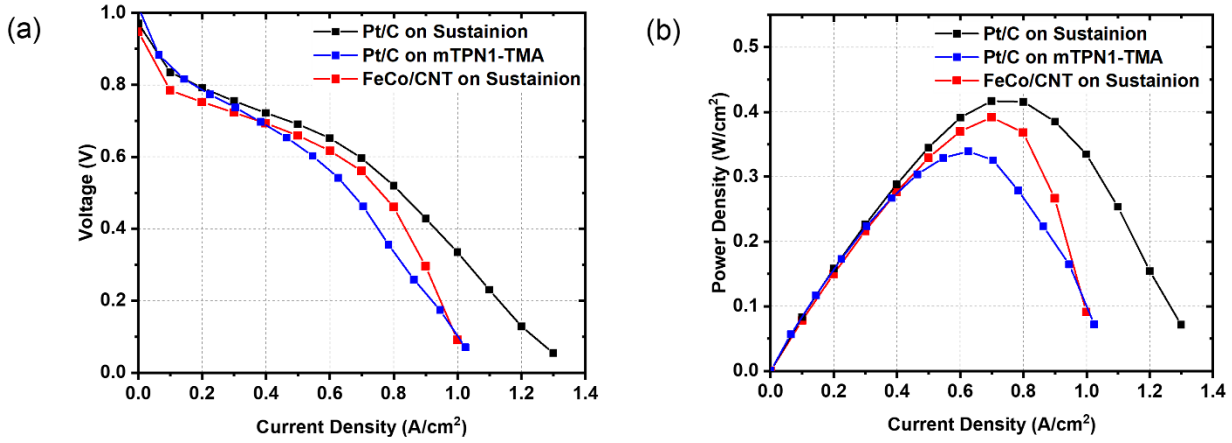

Fig. 9: (a) Polarization, and (b) power density versus current density curves of AEMFCs with Pt/C and FeCo/CNT on the cathode

Durability

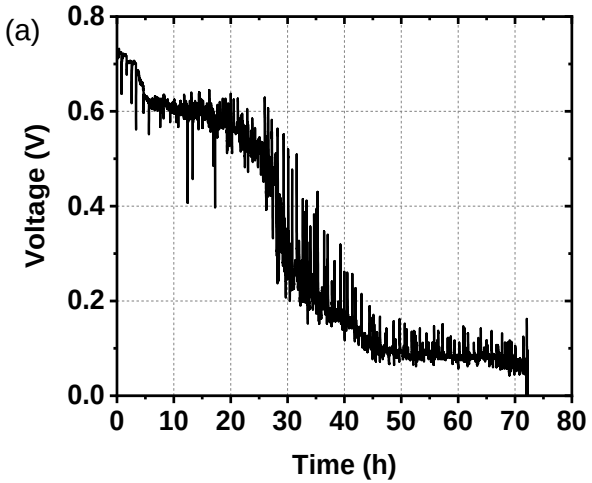

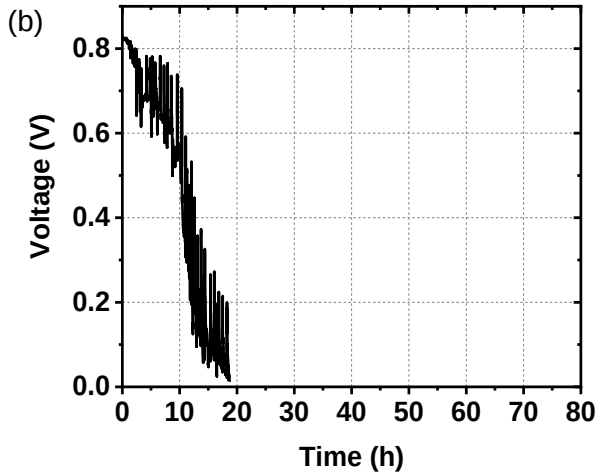

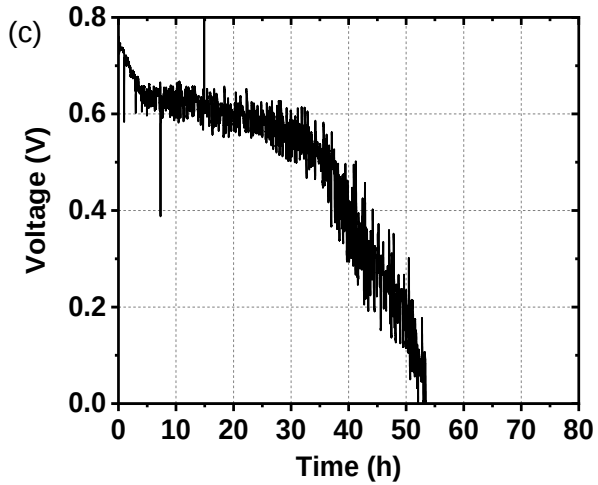

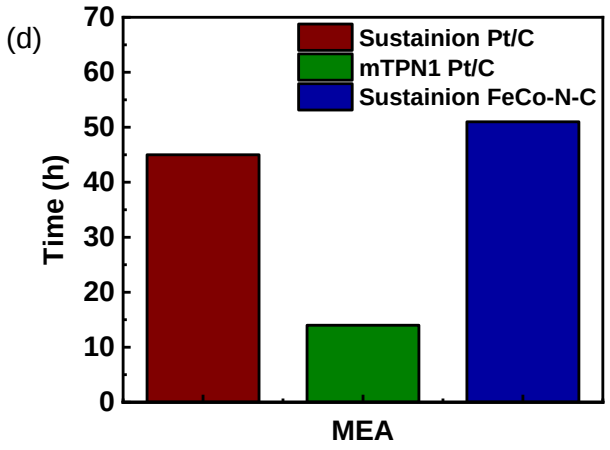

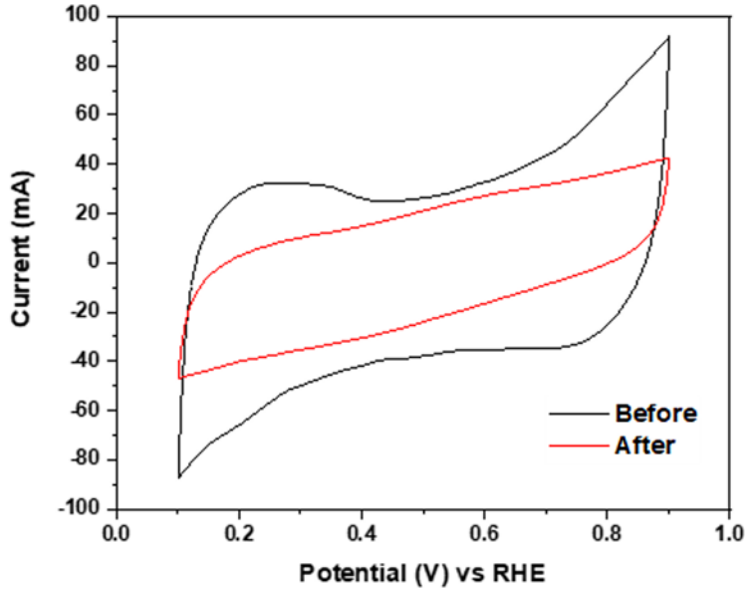

Time (h)	Initial ECSA of Pt (m^2/g)	Final ECSA of Pt (m^2/g)	Change (%)
70	63.78	28.95	54.60

Durability tests of the AEMFC with (a) Sustainion AEM and Pt/C cathode electrode (b) mTPN1-TMA AEM and Pt/C cathode electrode (c) Sustainion AEM and FeCo-CNT cathode electrode where the voltage is plotted as a function of time at a constant current of 0.15A/cm^2 (d) Time needed for MEAs to reach 0.1 V

X-ray Computed Tomography

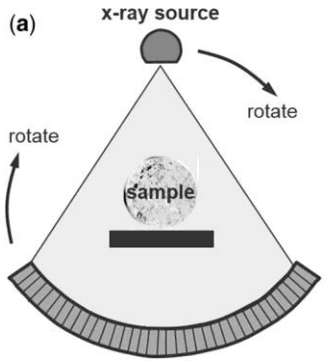

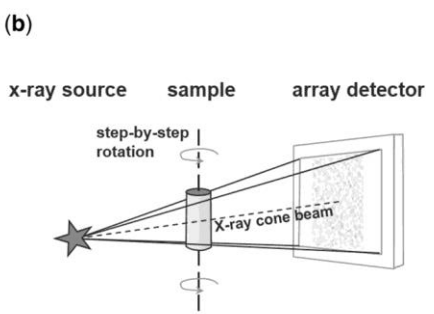

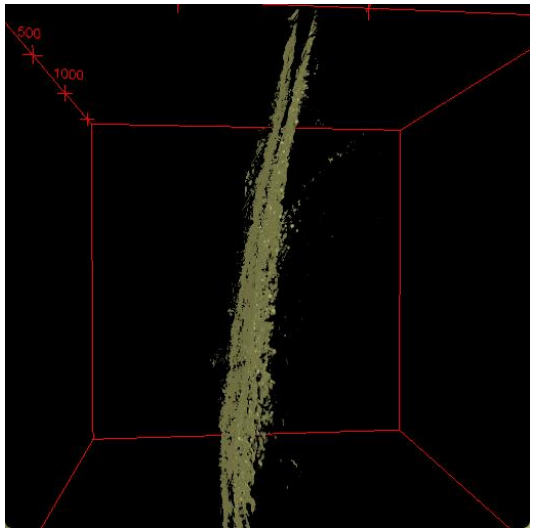

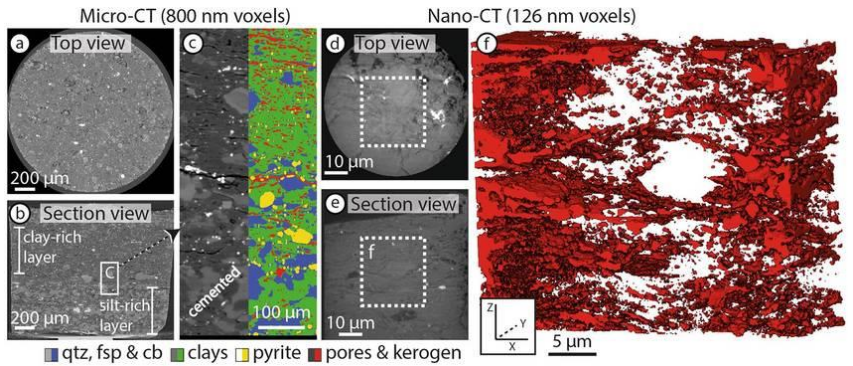

Experiment setting: Full-field X-ray computed tomography data sets were collected for a series of specimens, employing a Zeiss Xradia 520 Versa X-ray microscope. The X-ray source was operated at 40.20 kV and 74.7 µA (3W). The isotropic voxel size was set to 2.1 µm and a series of 1601 projections were collected over 360° with a 2.5 s image collection time per step. Data reconstruction was performed using a filtered-back projection algorithm. Data was visualized in ImageJ software.

* Wennberg, Ole Petter, and Lars Rennan. "A brief introduction to the use of X-ray computed tomography (CT) for analysis of natural deformation structures in reservoir rocks." *Geological Society, London, Special Publications* 459.1 (2018): 101-120.

* Backeberg, Nils R., et al. "Quantifying the anisotropy and tortuosity of permeable pathways in clay-rich mudstones using models based on X-ray tomography." *Scientific reports 7.1 (2017): 1-12.*

SEM-EDX

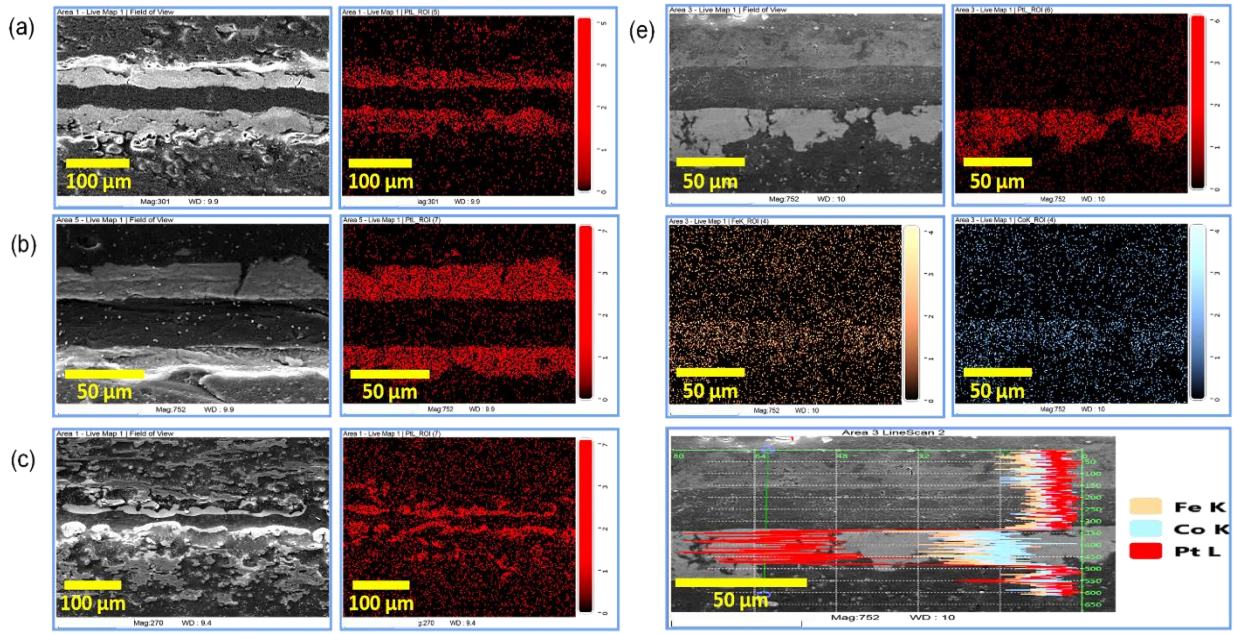

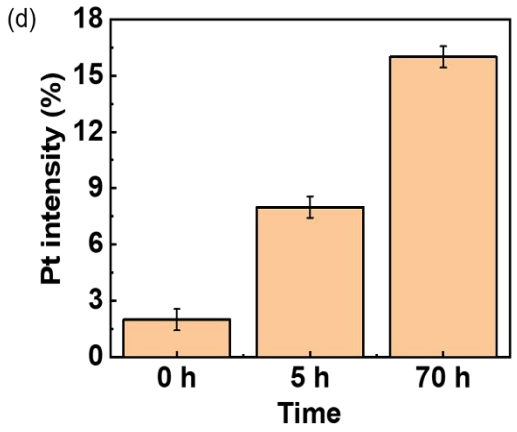

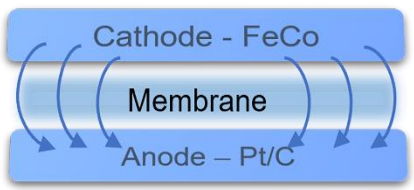

- Pt is seen inside the membrane at 0 h, 5 h and 70 h but the intensity is different
- Membrane is completely degraded after 70 h of durability testing
- Metal migration is confirmed from the MEA with FeCo-N-C catalyst at the cathode.
- Fe and Co migrates from cathode to anode without degrading the membrane and co-localized within the Pt layer at the anode.

Fig. 14: SEM-EDX of sample MEAs with (a) Sustainion AEM and Pt/C cathode electrode after 0 h (b) 5 h and (c) 70 h. (d) Comparison of Pt intensity in the membrane after 0 h, 5 h and 70 h. (e) Sustainion AEM and FeCo-N-C cathode electrode after 52 h. (f) Image representation of MEA with FeCo-N-C catalyst

micro-CT

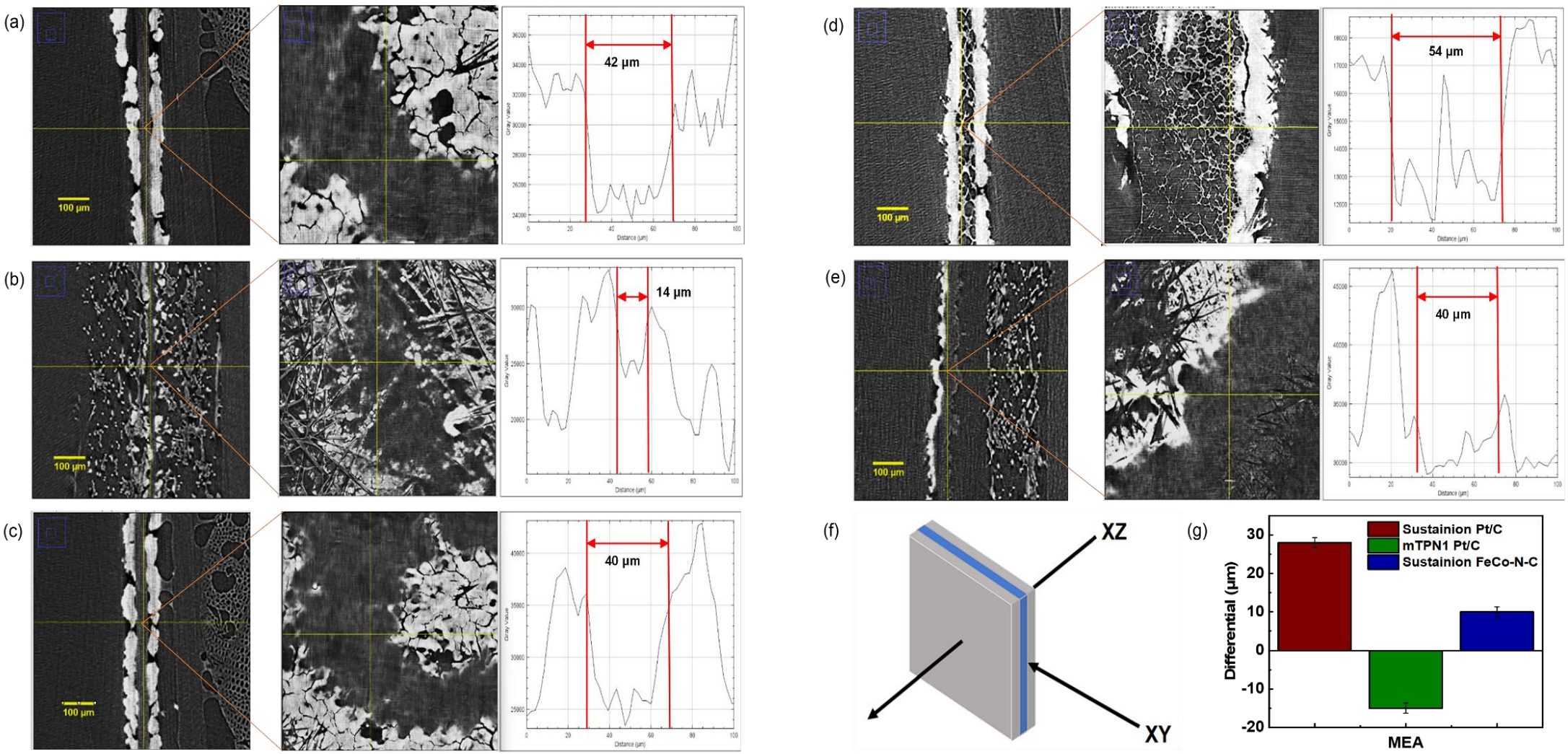

Micro-CT images obtained in the XY and XZ planes and thickness of MEAs assembled with (a) Sustainion AEM and Pt/C cathode electrode after 5 h (b) and after 70 h; (c) mTPN1-TMA AEM and Pt/C cathode electrode after 5 h (d) after 19 h; (e) Sustainion AEM with FeCo-N-C cathode electrode after 52 h; (f) Image representation of MEA with XY and XZ plane; (g) The thickness differential in the membranes of MEAs operated for 5 h and after failure at times above.

micro-CT

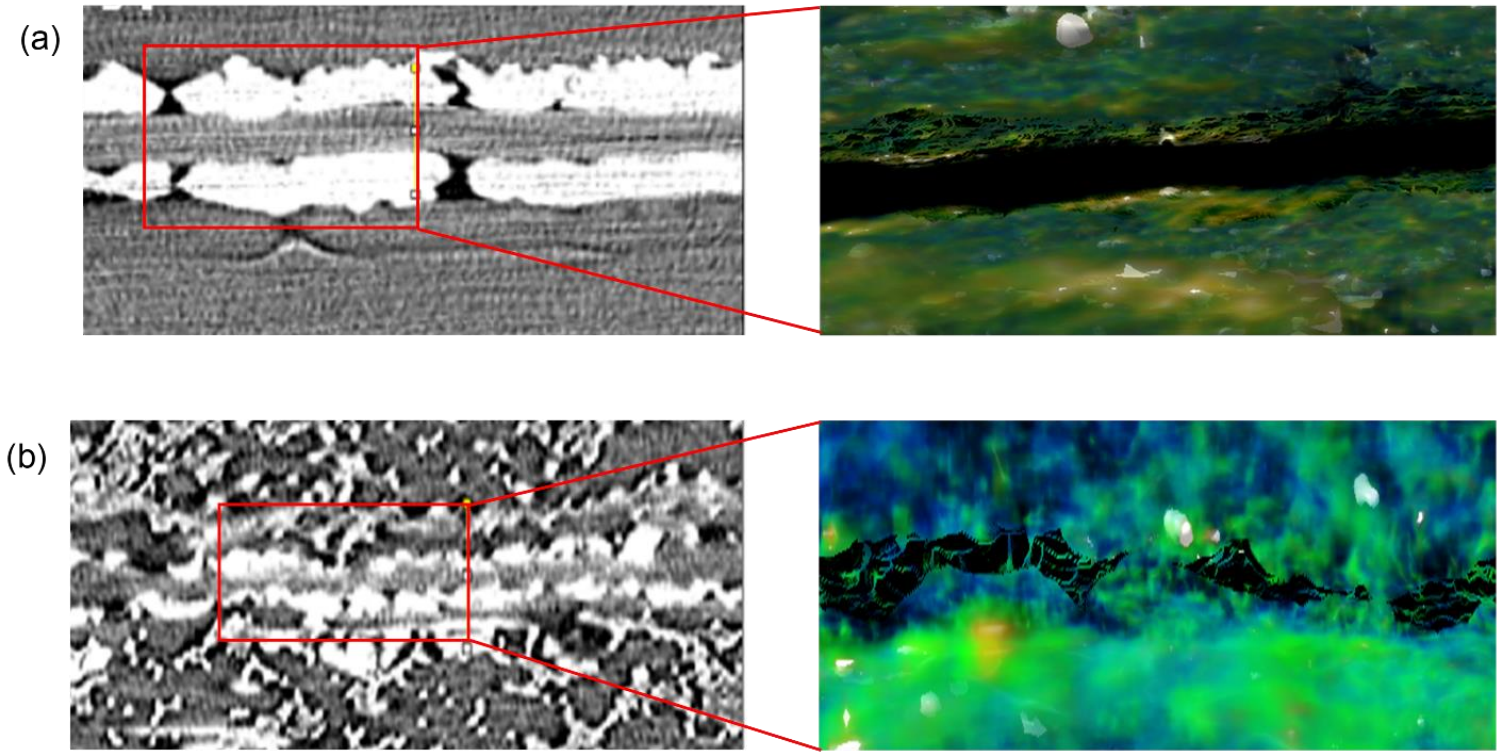

3D reconstruction micro-CT images of the cross-section MEAs with Sustainion AEM and Pt/C cathode electrode after (a) 5 h and (b) 70 h of operation at 0.15 A/cm^2.

Pt ion migration from cathode to anode is the main cause of degradation—Pt ions penetrate the membrane and attack the carbon support. The decreased potential makes ionization 4X easier in alkaline medium.

Conclusion

- The primary cause of decreasing durability and performance in AEMFCs was identified as the dissolution of the Pt catalyst combined with reduction of Pt ions in the membrane.
- MEAs assembled with Sustainion and mTPN1-TMA membranes, which have different chemical compositions, were tested at 0.15 A/cm^2 for 5 hours and until failure.
- The mTPN1-TMA membrane failed after 19 hours, exhibiting the presence of a Pt lattice between the electrodes, causing electrical shorts and MEA failure.
- The Sustainion membrane lasted longer (70 hours), but showed significant shrinking and the presence of Pt domains within the membrane, leading to failure.
- Substituting Pt/C with FeCo-N-C catalyst at the cathode resulted in more stable operation, but a performance decrease was observed after 30 hours, with migration of Fe and Co ions to the anode.
- SEM analysis suggested that the Fe and Co ions possibly alloyed with Pt, increasing its stability against dissolution and enhancing overall MEA stability.

Graphene-based Materials

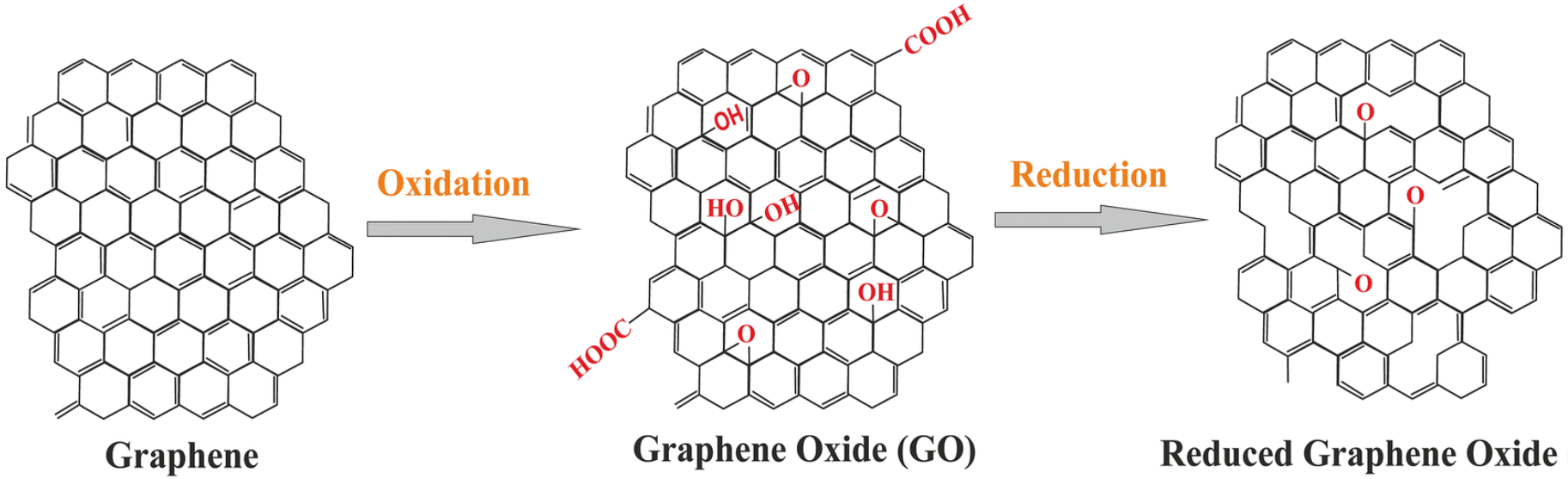

- GO is an oxidized form of graphene, functionated with oxygen-containing groups, such as epoxide, carbonyl, carboxyl, and hydroxyl groups.
- Reduced graphene oxide (r-GO) removes the oxygen groups and repairs the defects in GO to restore the long-range conjugated network of Graphene and thus restores conductivity.

Characterization of Graphene, GO and r-GO

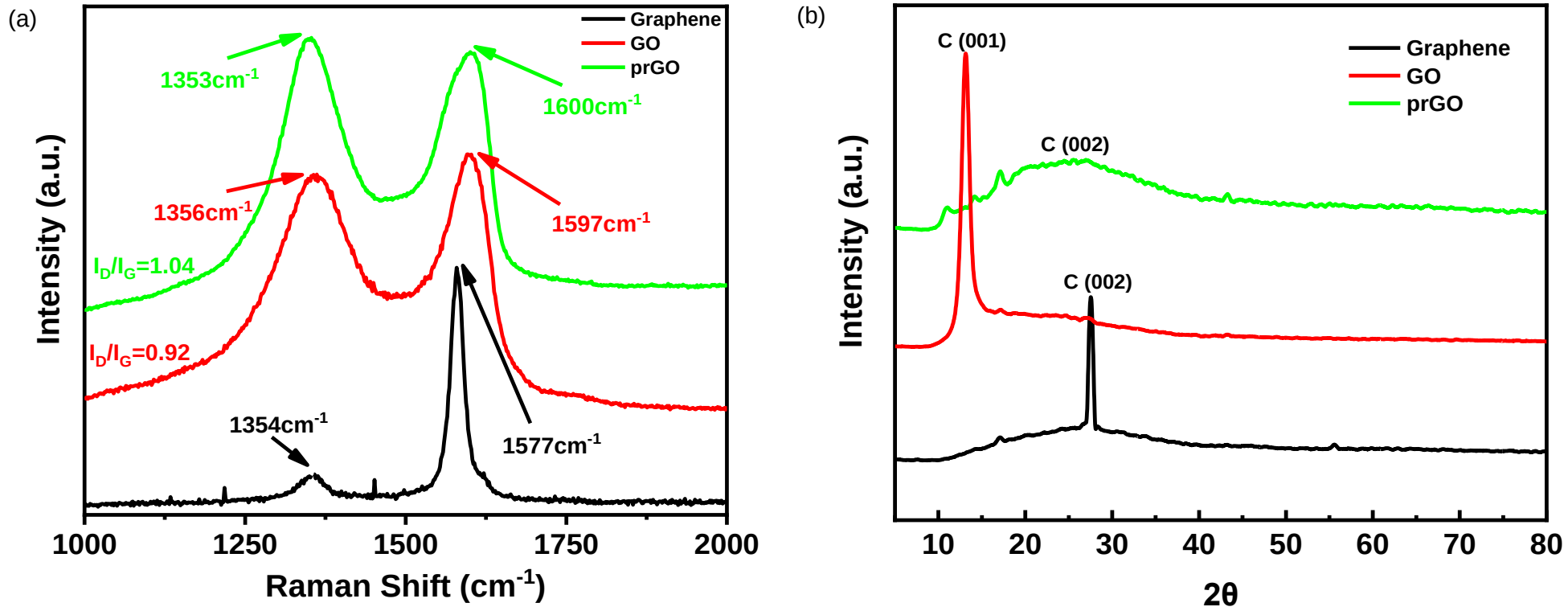

Fig. 17: (a) Raman spectroscopy results of Graphene NPs, freshly prepared GO and prGO (b) XRD results of Graphene NPs, freshly prepared GO and prGO

- GO was synthesized using modified Hummer's method, and then reduced using $NaBH_4$.
- XRD and Raman confirms the formation of GO and prGO.

Characterization of Graphene, GO and r-GO

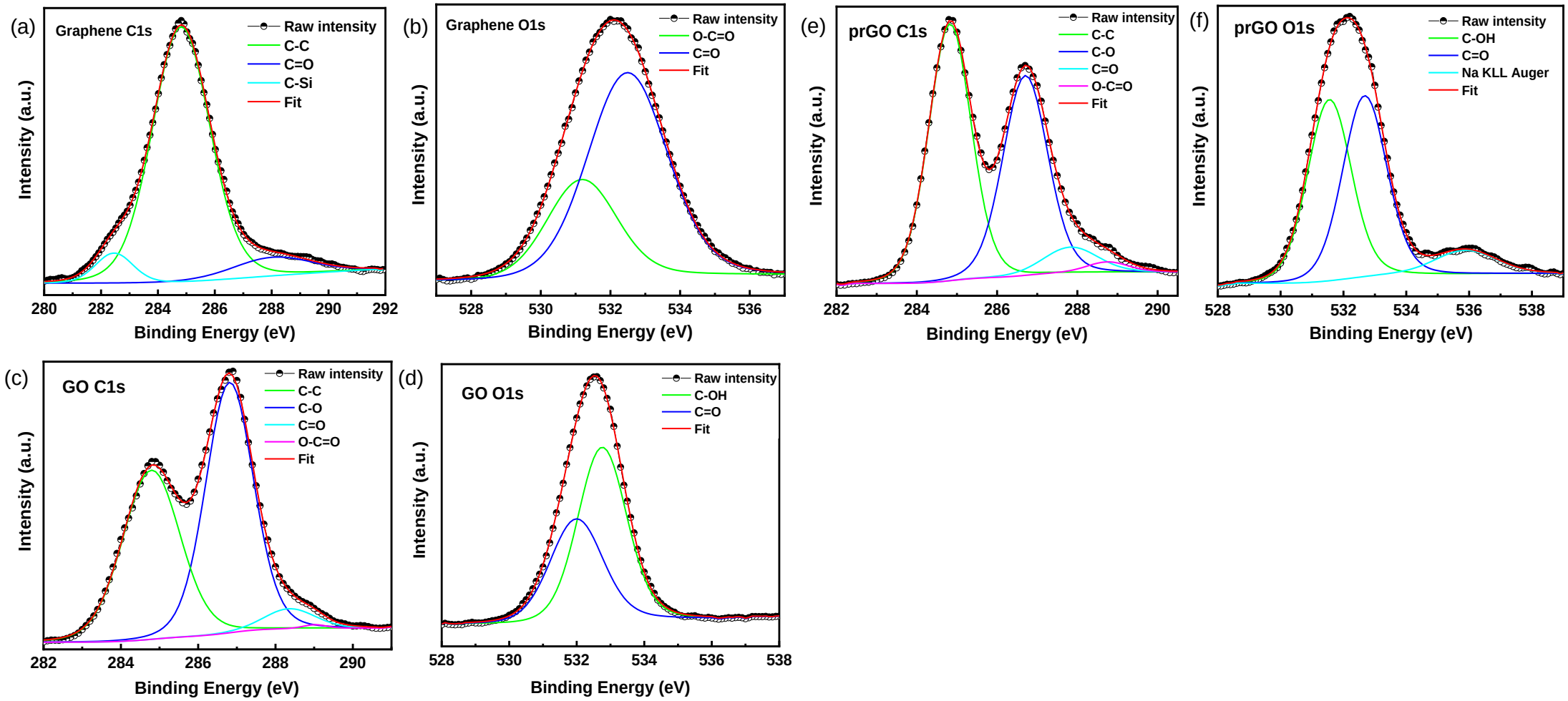

Fig. 18: (a,b) high-resolution XPS spectrum of Graphene (c,d) high-resolution XPS spectrum of freshly prepared GO (e,f) high-resolution XPS spectrum of freshly prepared prGO

Fuel cell performance

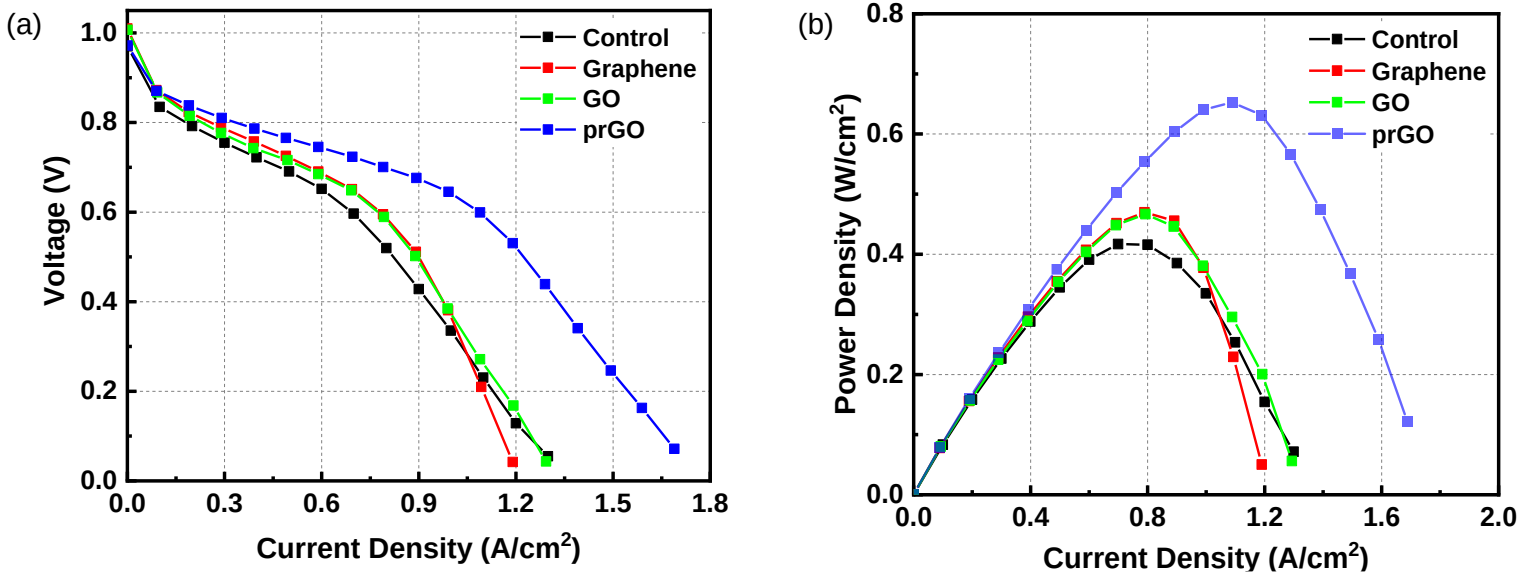

Fig. 19: (a) Polarization, and (b) power density versus current density curves of AEMFCs with different graphene materials sprayed on the membrane

- Unmodified membrane, P_{max}= 0.417 W/cm^2
- Graphene and GO-coated membranes enhanced the performance by almost 12.5% with P_{max}= 0.469 W/cm^2 and P_{max}= 0.466 W/cm^2 respectively.
- The prGO in contrast increased the maximum power density by almost 56% with P_{max}= 0.652 W/cm^2.

Characterization of different reductions of prGO

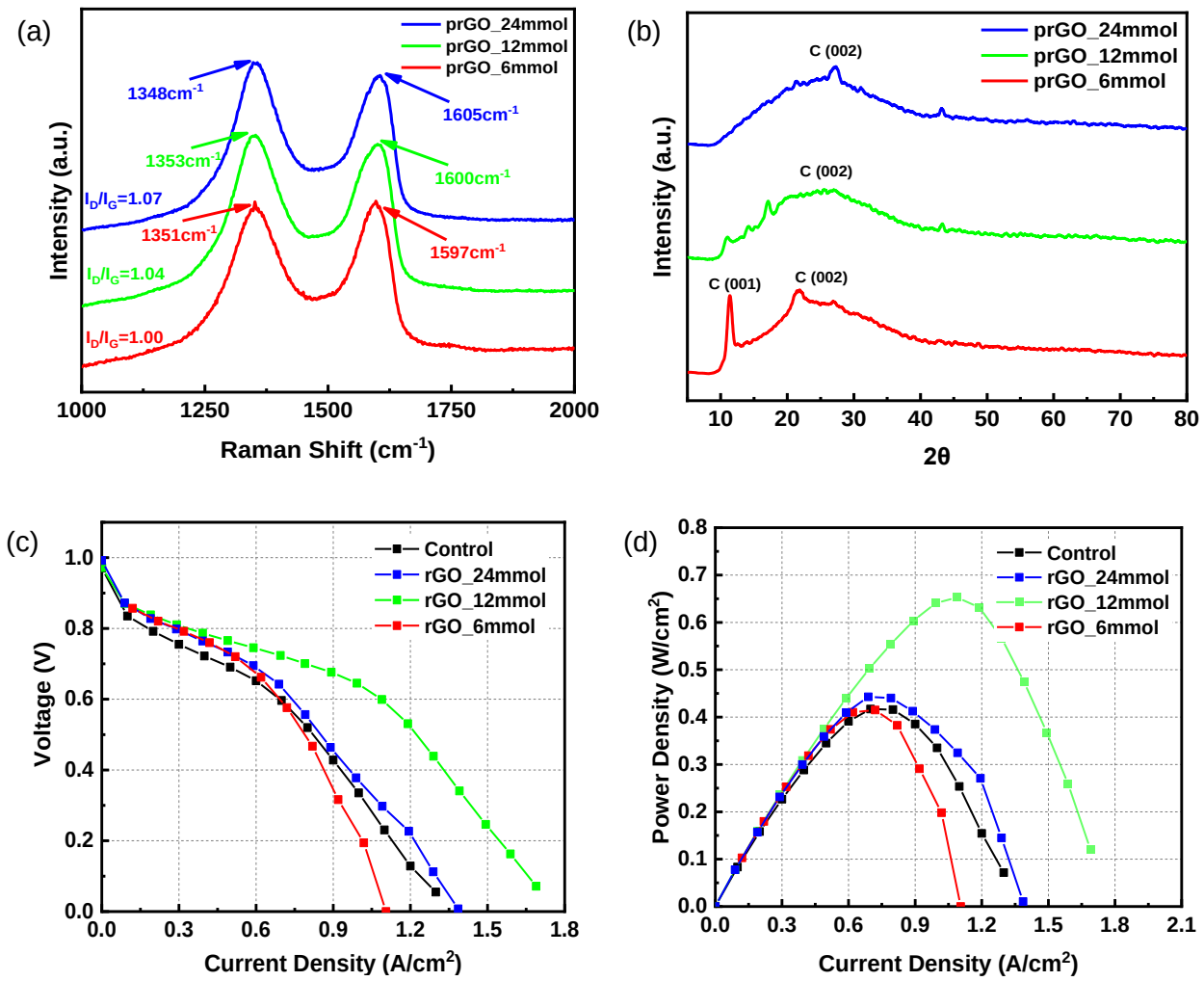

- To investigate the dependence of the enhancement on the degree to which the GO was reduced, we also sprayed prGO that had been reduced with higher and lower molarities of $NaBH_4$, 6, and 24 mmol.
- For prGO 6mmol, P_{max} = 0.45 W/cm^2
- For prGO 24mmol, P_{max} = 0.415 W/cm^2

Fig. 20: Raman spectra (a) and XRD pattern (b) of GO reduced with 6, 12, and 24 mmol of $NaBH_4$ (c) Polarization and (d) power curves of AEMFC with GO reduced with different degrees sprayed on the membrane and the electrode

Performance Comparison

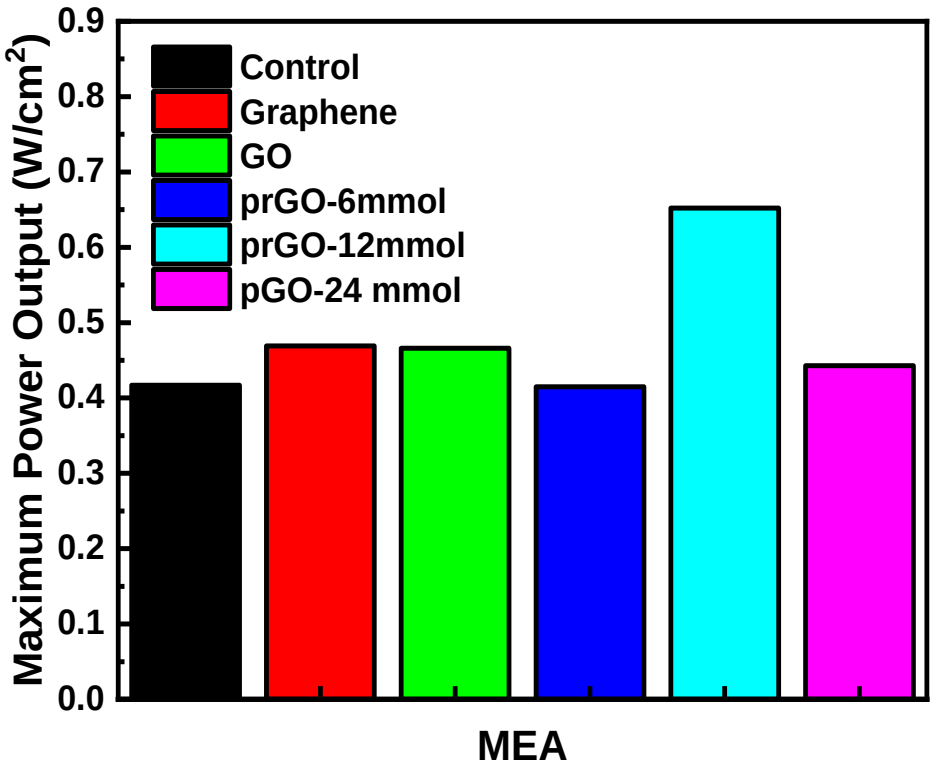

- Power output displayed by Graphene and GO coated AEMs was somewhat similar to the ones demonstrated by 6mmol and 24mmol prGO coated AEMs
- Sustainion membrane coated with Graphene oxide partially reduced with 12 mmol $NaBH_4$ showed maximum power enhancement ~56%

Fig. 21: Power density versus current density data of AEMFCs with different graphene materials sprayed on the membrane

FeCo-N-C catalyst fuel cell performance

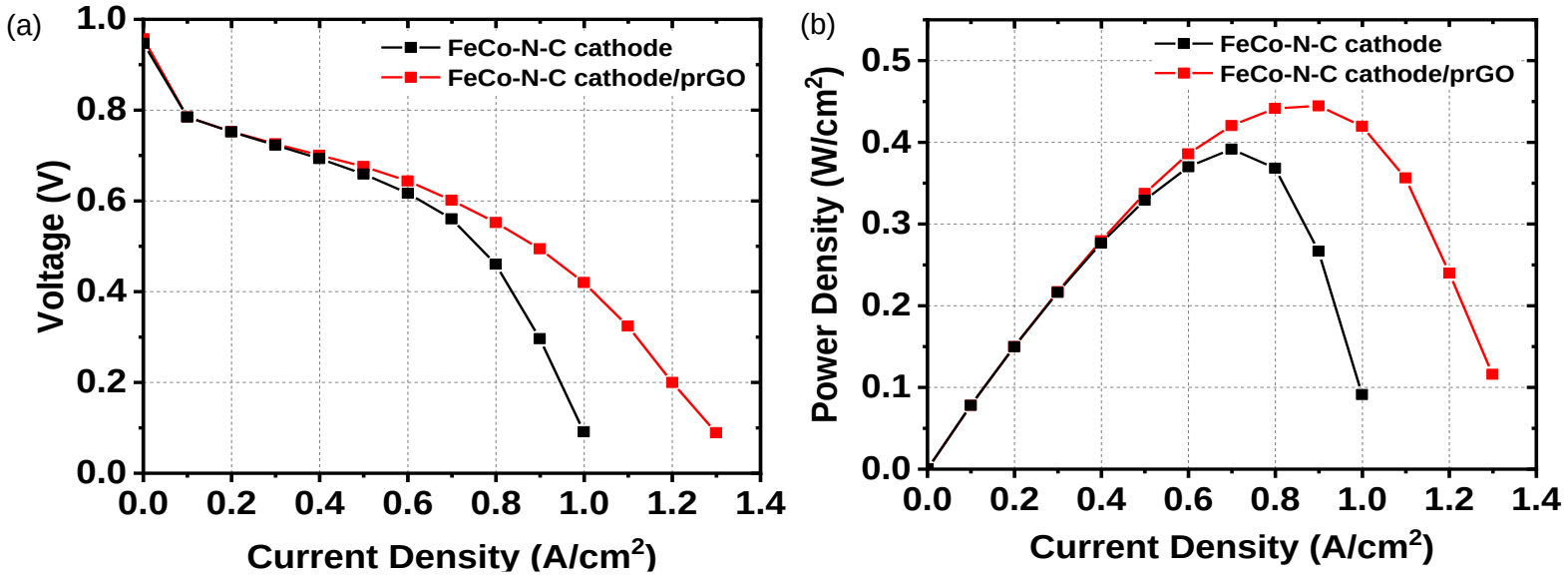

Fig. 22: (a) Polarization and (b) power curves of AEMFC with FeCo-N-C cathode catalyst with and without prGO sprayed on the membrane

- P_{max} of the MEA with FeCo-N-C catalyst = 0.392 W/cm^2 as compared to P_{max} with Pt/C catalyst = 0.417 W/cm^2
- The maximum power enhancement or 0.441 W/cm^2 is only 16% as opposed to 56% with Pt/C, which suggests that the effect is specific to the supported Pt/C metal catalyst.

Durability

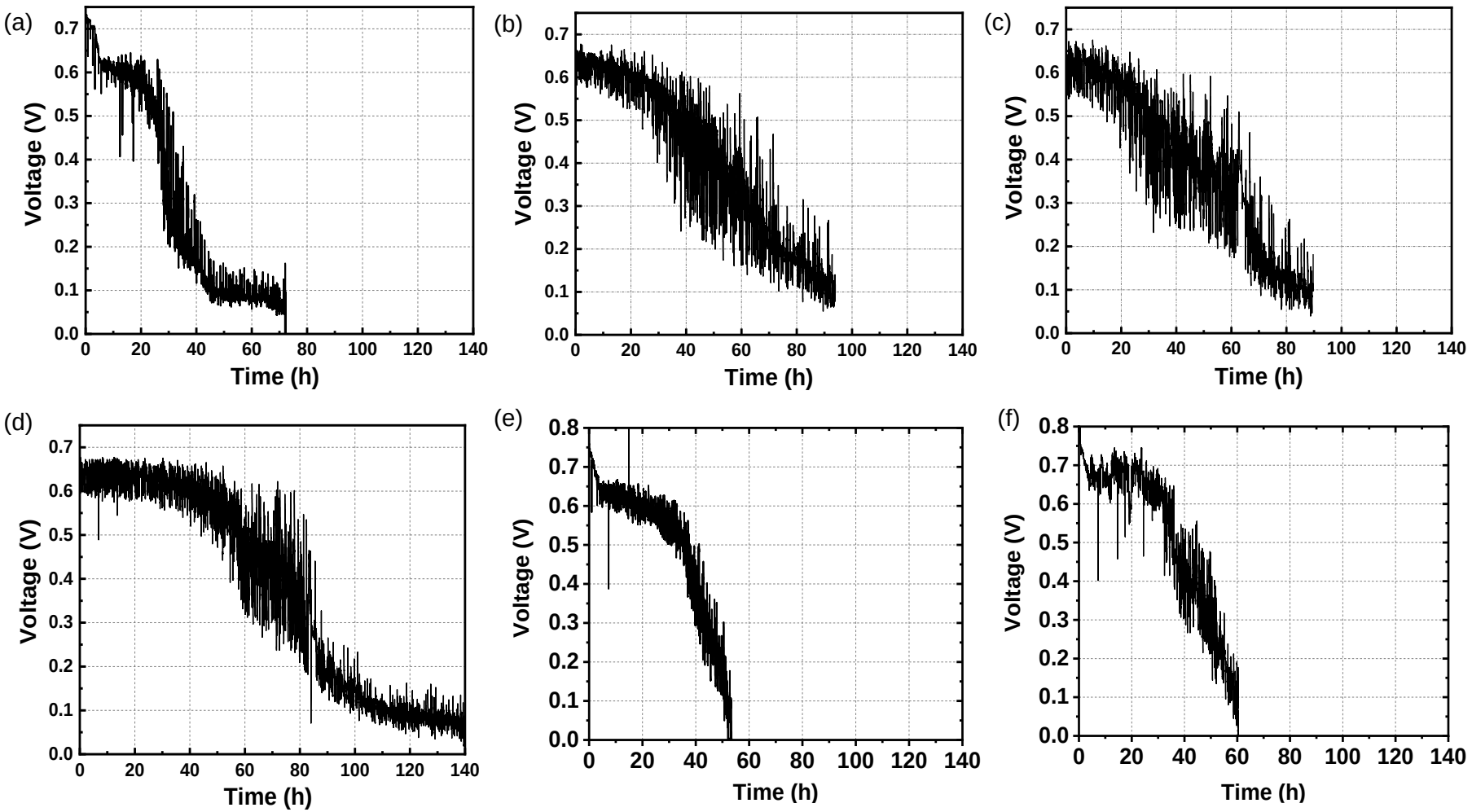

Fig. 23: Durability tests of the AEMFC with (a) plainSustainion AEM, (b) 1 μg/cm² Graphene, (c) 1 μg/cm² GO, and (d) 1 μg/cm² prGO coated (e) FeCo-N-C cathode catalyst (f) FeCo-N-C cathode and 1 μg/cm² prGO coated onto the membrane where the voltage is plotted as a function of time at a constant current density of 0.15 A/cm².

Cyclic Voltammetry/ Electrochemical Active Surface Area (ECSA)

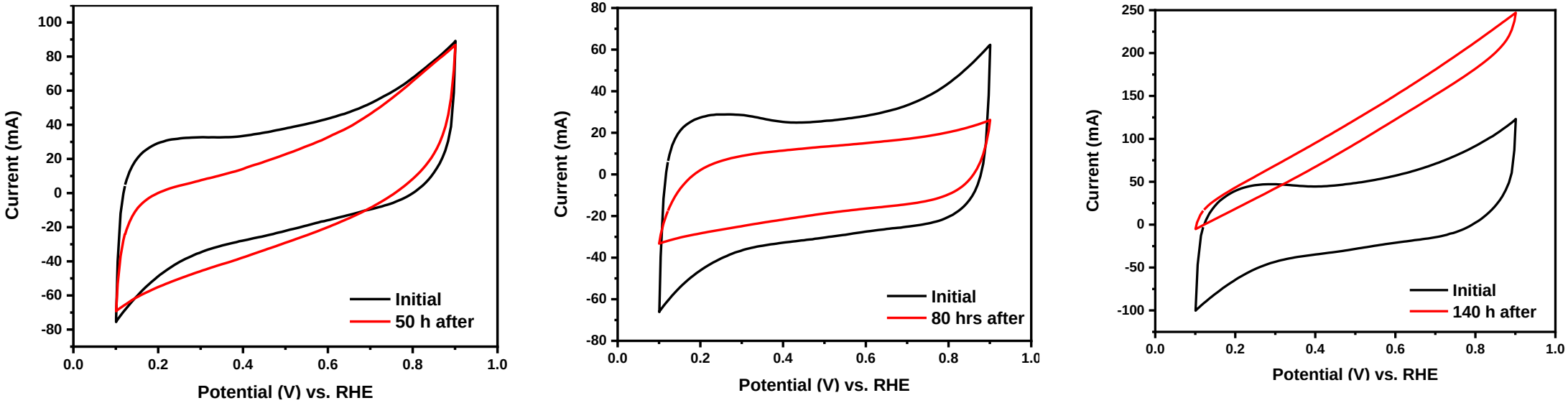

Fig. 24: Cyclic voltammograms of the cathode electrode in the inert gas atmosphere for the membrane sprayed with prGO after (a) 50 h (b) 80 h (c) 140 h

Time (h)	Initial ECSA of Pt (mg/cm^2)	Final ECSA of Pt (mg/cm^2)	Change (%)
50	60.70	50.03	17.57
80	56.12	36.94	34.17
140	72.05	??	??

Table 5: The active Pt surface area change

micro-CT

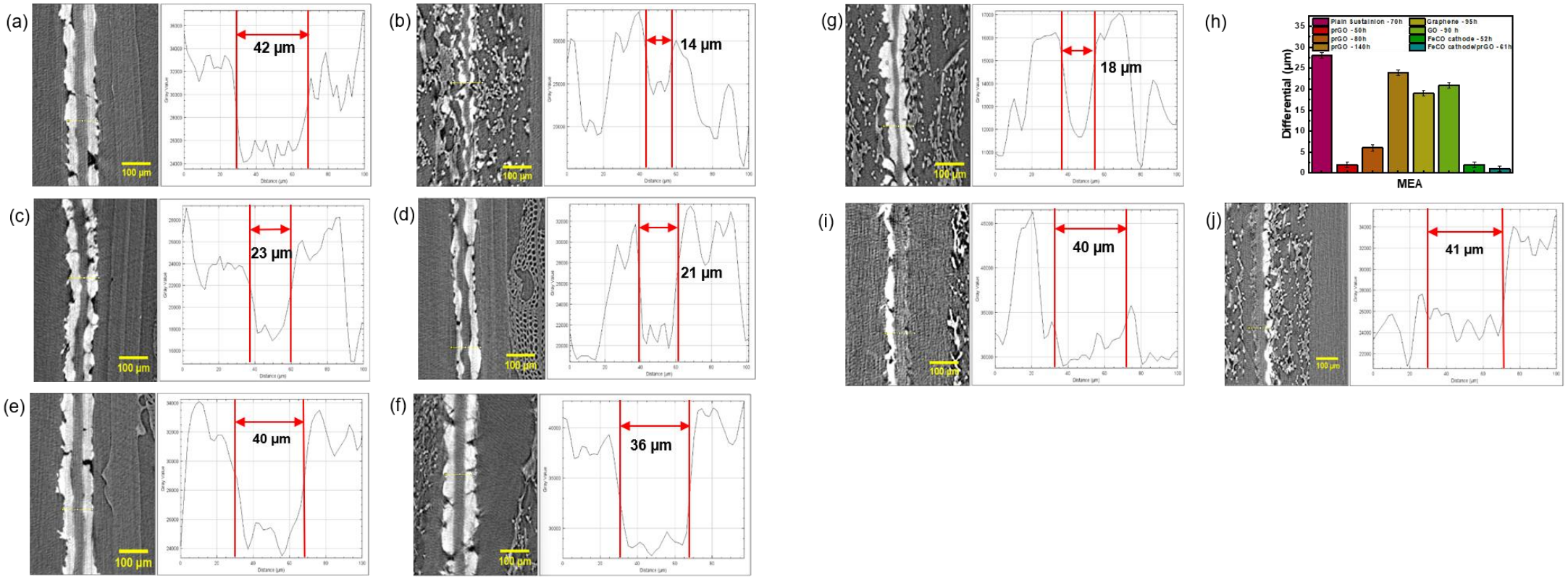

Fig. 25: XCT cross-sectional images of Sustainion AEM with Pt/C cathode electodes, maintained at 0.15 A/cm^2 (a) Without graphene materials after 5 h (b) after 70 h; (c) With Graphene after 95 h; (d) With GO after 90 h (e) With prGO after 50 h (f) after 80 h (g) after 140 h; (h) The thickness differential in the membranes of MEAs operated for 5 h and after failure at times above; (i) FeCo-N-C cathode electrode after 52 h (j) FeCo-N-C cathode electrode with prGO after 61 h.

micro-CT: Graphene strikes again!

Graphene and GO block Pt ion penetration.

The OH groups on prGO Reduce Pt effectively and possibly also carbon products from CO, preventing their penetration into the membrane—Hence increase both power and durability.

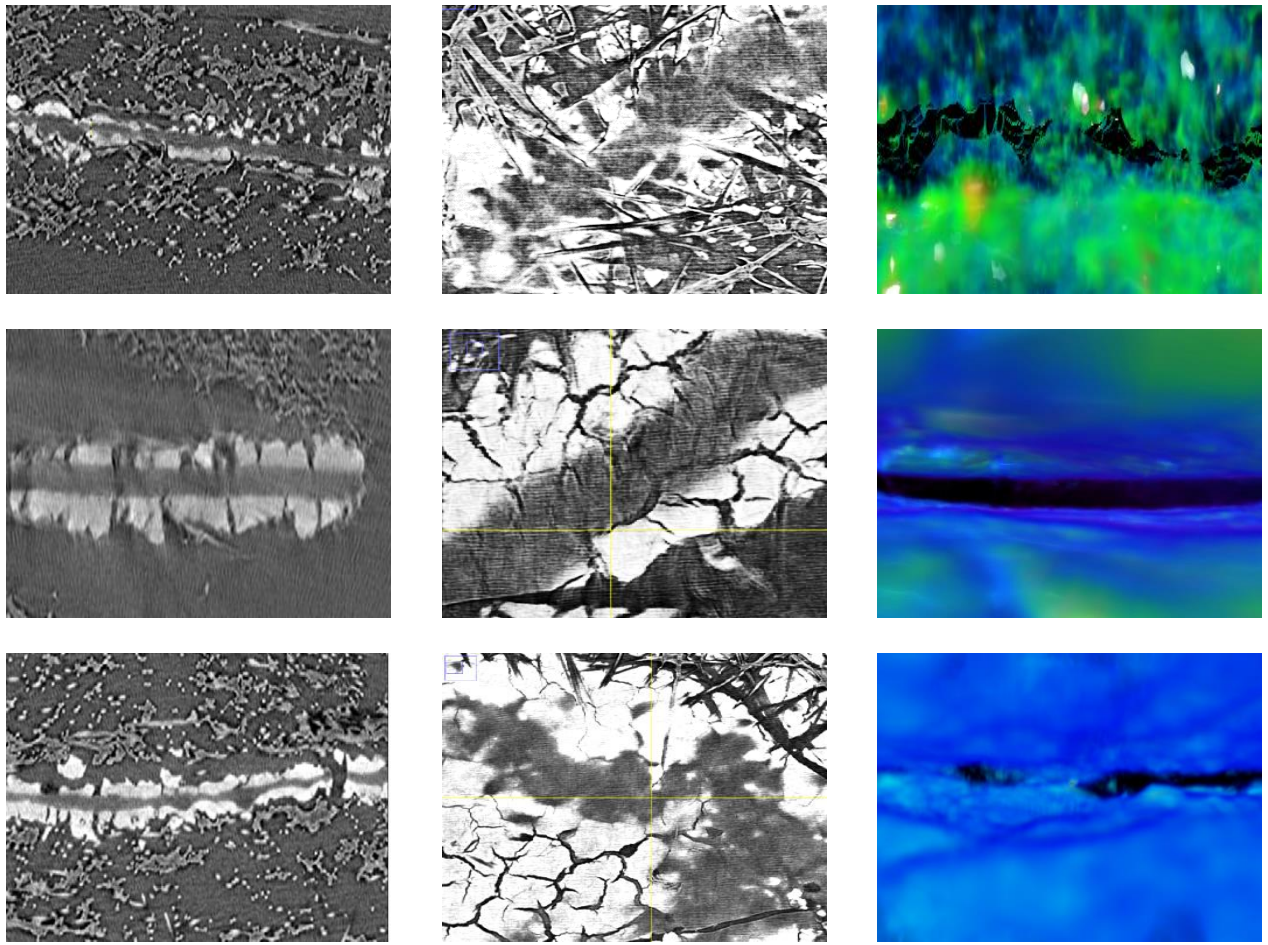

Fig. 26: XY plane, XZ plane micro-CT images and their 3D reconstruction of the MEAs with Sustainion membrane (a) without prGO after 70 h (b) with prGO after 80 h (c) with prGO after 140 h (d) Image representation of MEA with XY and XZ plane

Conclusions

- Power output and durability are major challenges in anion exchange fuel cells.
- This study investigates the impact of applying graphene materials to anion exchange membrane fuel cells.
- Graphene oxide and partially reduced graphene oxide (prGO) with different degrees of reduction were synthesized and characterized.
- AEMs with graphene materials demonstrated increased power output and improved durability compared to unmodified membranes.
- The addition of prGO with intermediate reduction showed the most significant enhancement in power output and durability, suggesting its potential as a catalyst for anion exchange fuel cells.
- The synergy with prGO was specific to Pt/C catalyst.
- Graphene materials, oxide, and partially reduced oxides are known to reduce the ions, nucleating particle formation, which we postulate traps the ions from further migration into the membrane, increasing the durability by preserving the catalyst and reducing degradation.

Can we make a PEMFC using recyclable and “green” materials?

Cellulose Nanofiber (CNF)

a. Most abundant biopolymer
b. Environmentally friendly
c. Tunable surface functionalizations
d. Inexpensive

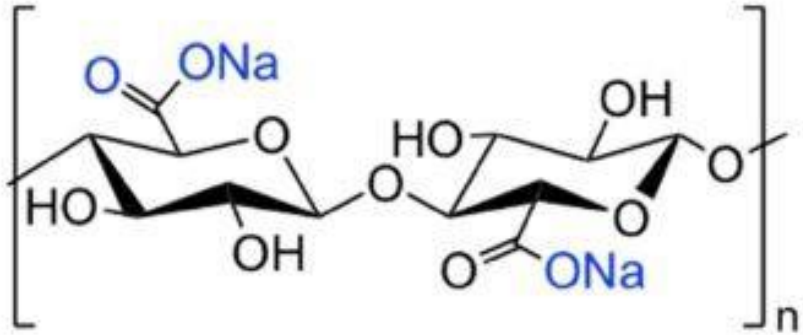

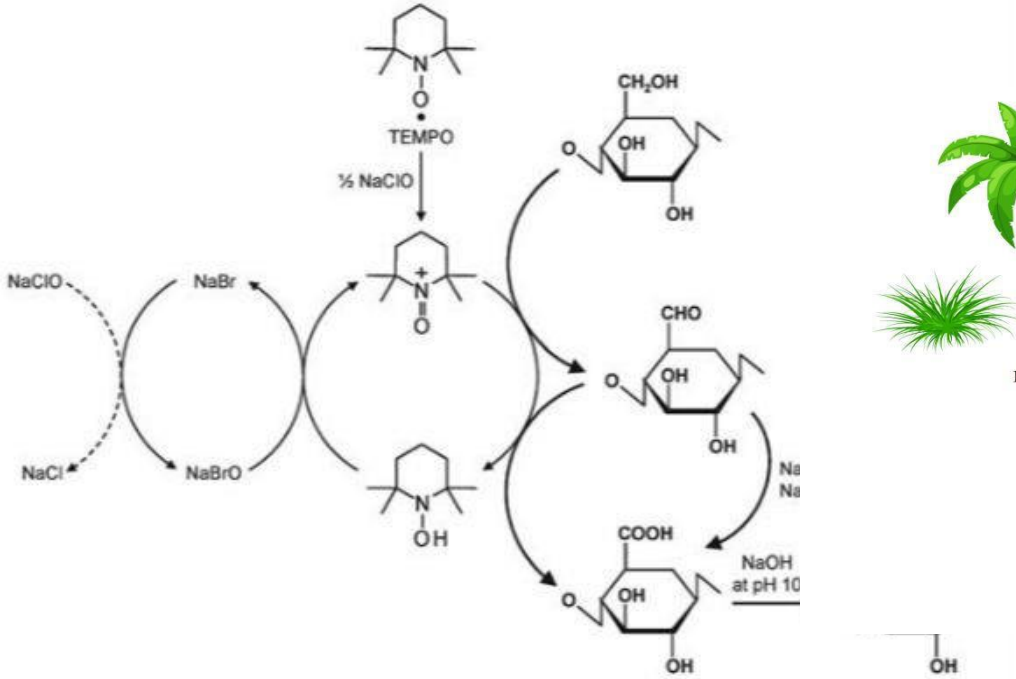

Nanoscale, 2017, 9, 14758-14781, *Nanoscale* 2011, 3 (1), 71–85

Reducing cost and recycle: cellulose scaffold

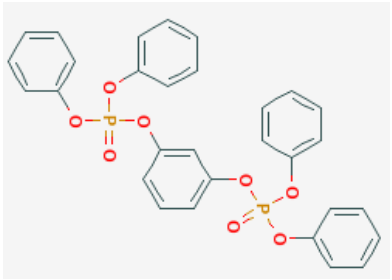

Chemical Formula of RDP

- Commercial filter paper: Ahlstrom cellulose filter papers--$20.00/200 sheets, 195um
- The cellulose fibers construct a perfect **scaffold** for the membrane.
- Resorcinol bis(diphenyl phosphate) (RDP) - inexpensive liquid form
  - Easily incorporated into the cellulose membrane simply by immersion.
- **Hydrogen bonds to cellulose** enriching the fibers in PO_4-H functionalities

Compare nanocellulose to filter paper-macro

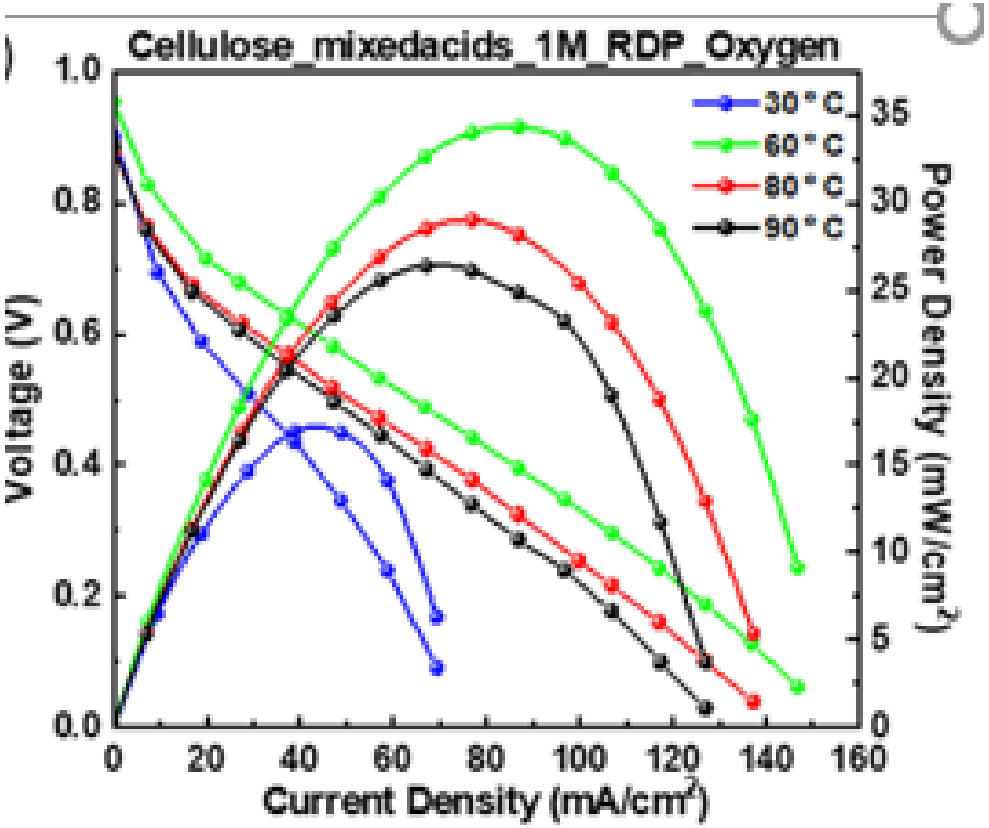

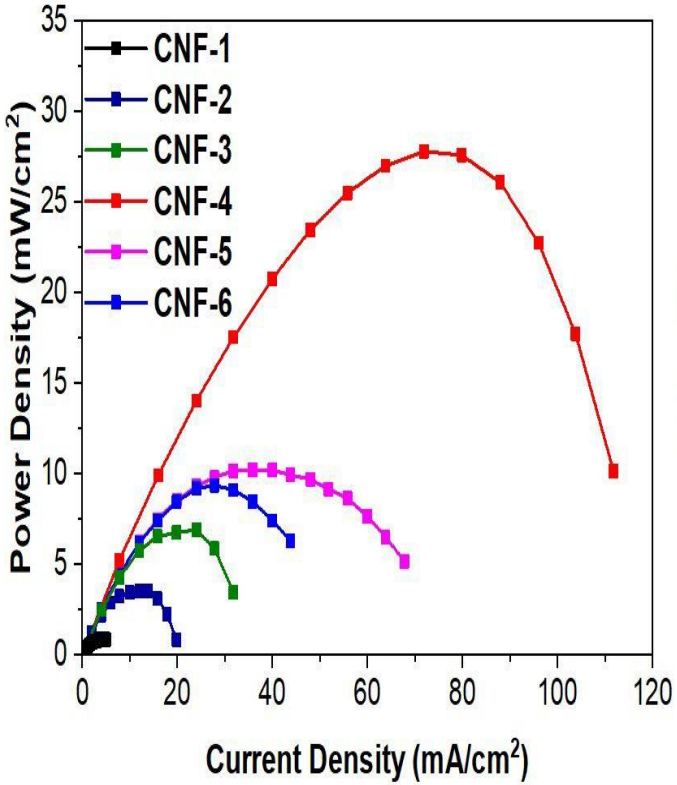

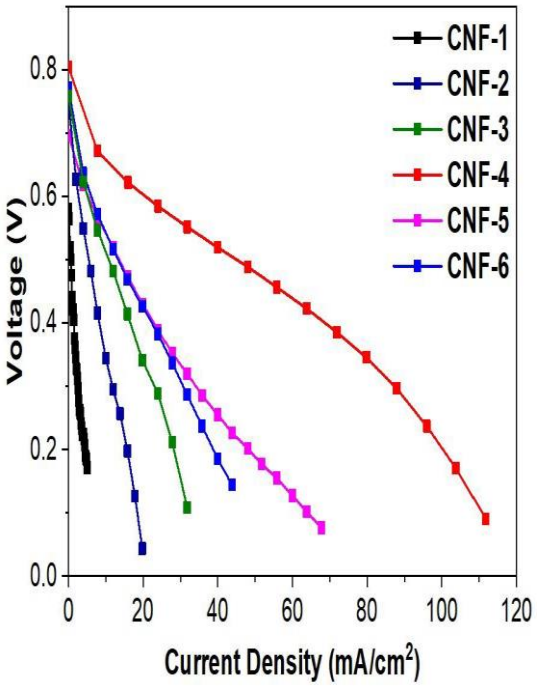

28%

Filter paper-mixed acids RDP -micro cellulose fibers in O2

35.2 mW/cm²

Density: 150.0 mA/cm²

Nanocellulose in O2

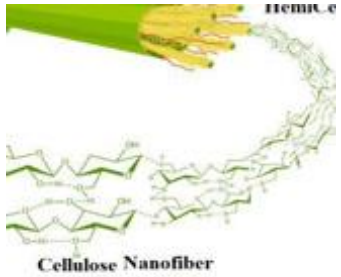

27.7 mW/cm²

Density: 111.8 mA/cm²

Sustainable Energy Fuels, 2022,**6**, 3669-3680

Assembling the nanocellulose MEA and testing the power output

1. **Low Pt group metal loading**

   0.1 mg/cm^2 Pt/C

2. **Polarization**

   5 cm^2, 100 sccm H_2 & O_2, 80 °C, 100 % RH

3. **40 h Durability:**

   11 mA/cm^2 constant current density load

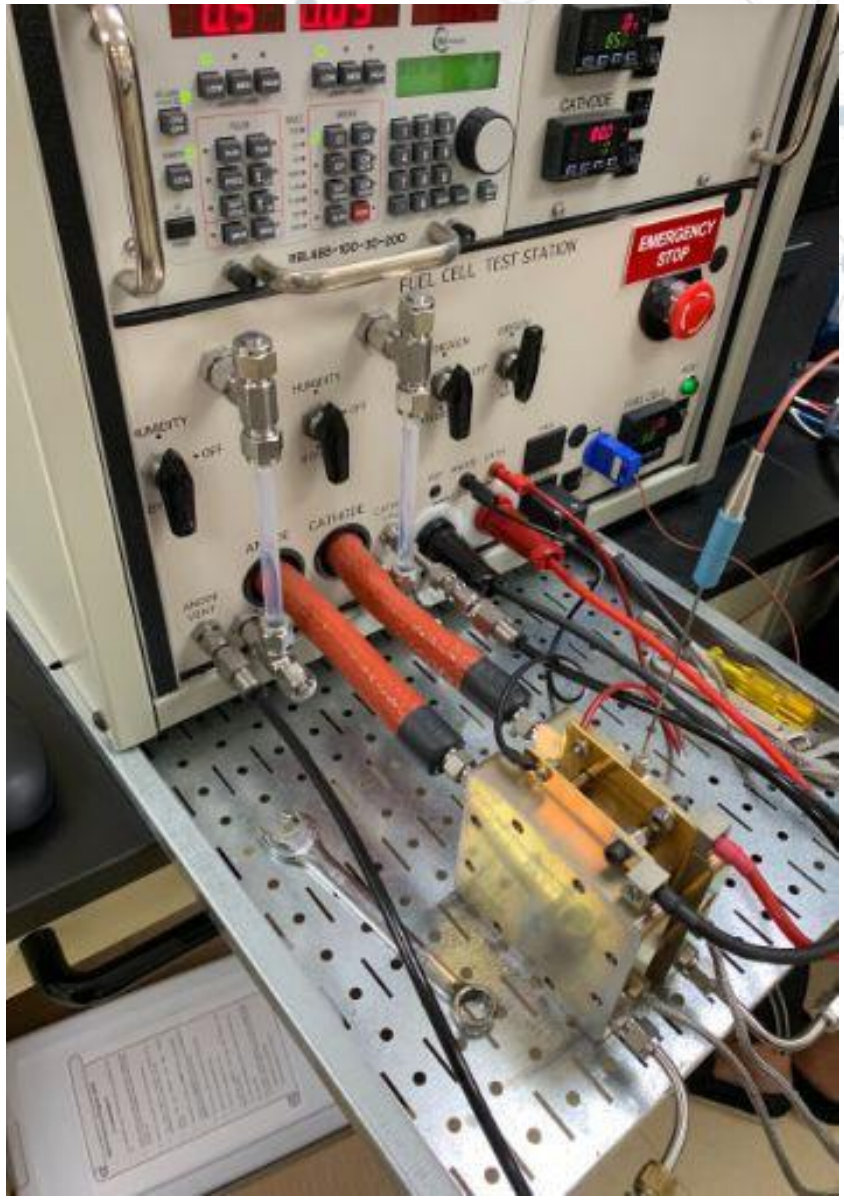

Fuel cell performance

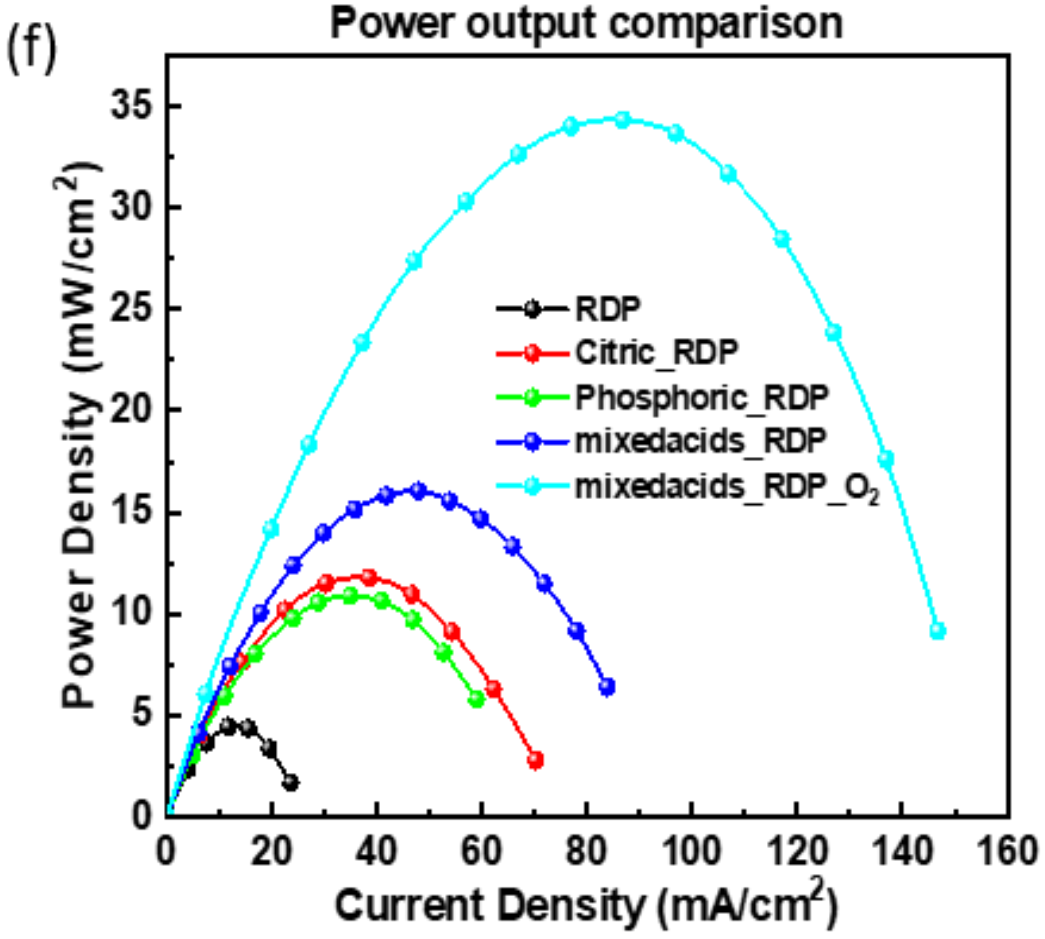

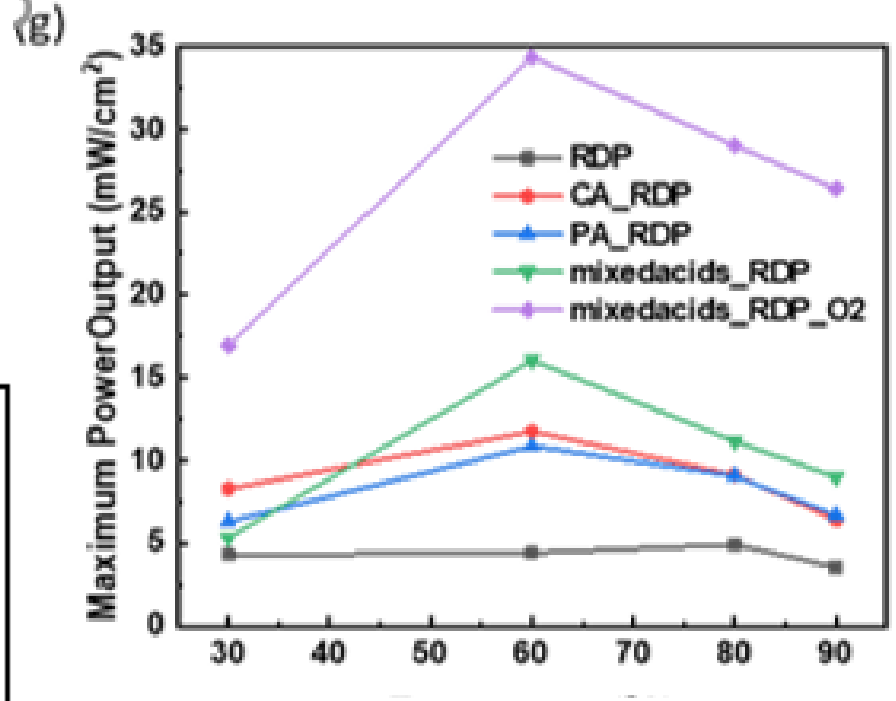

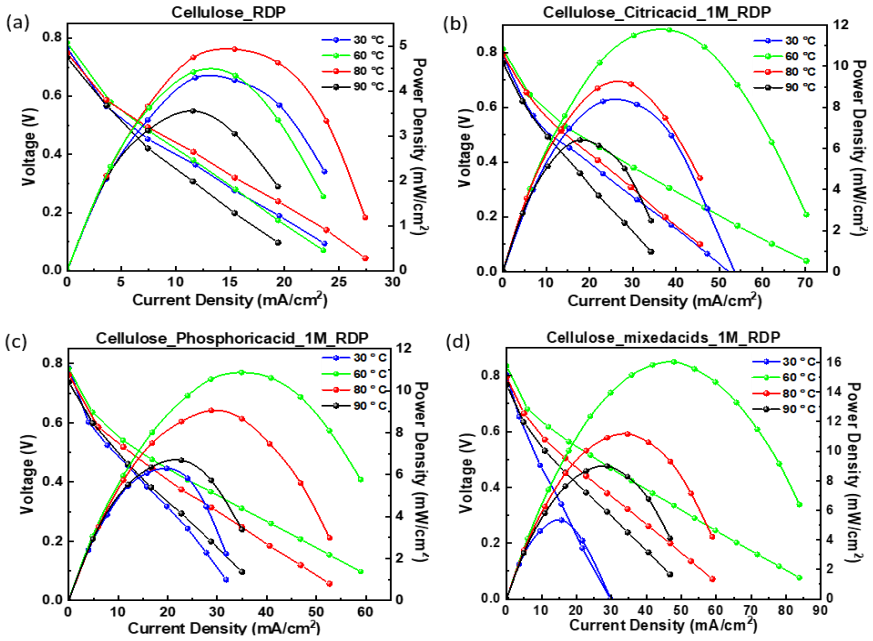

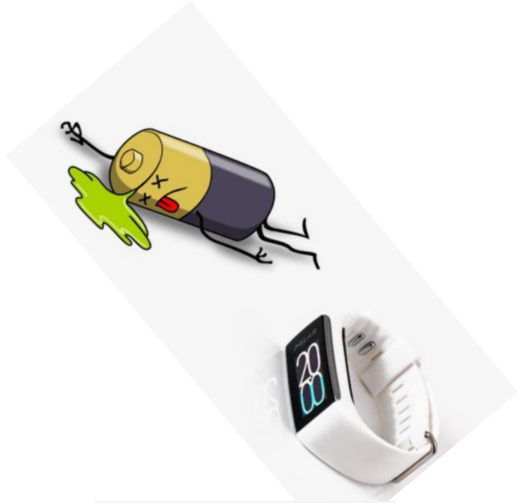

Low power medical devices, wearable electronics, and sensors

Proton conductivity enhanced

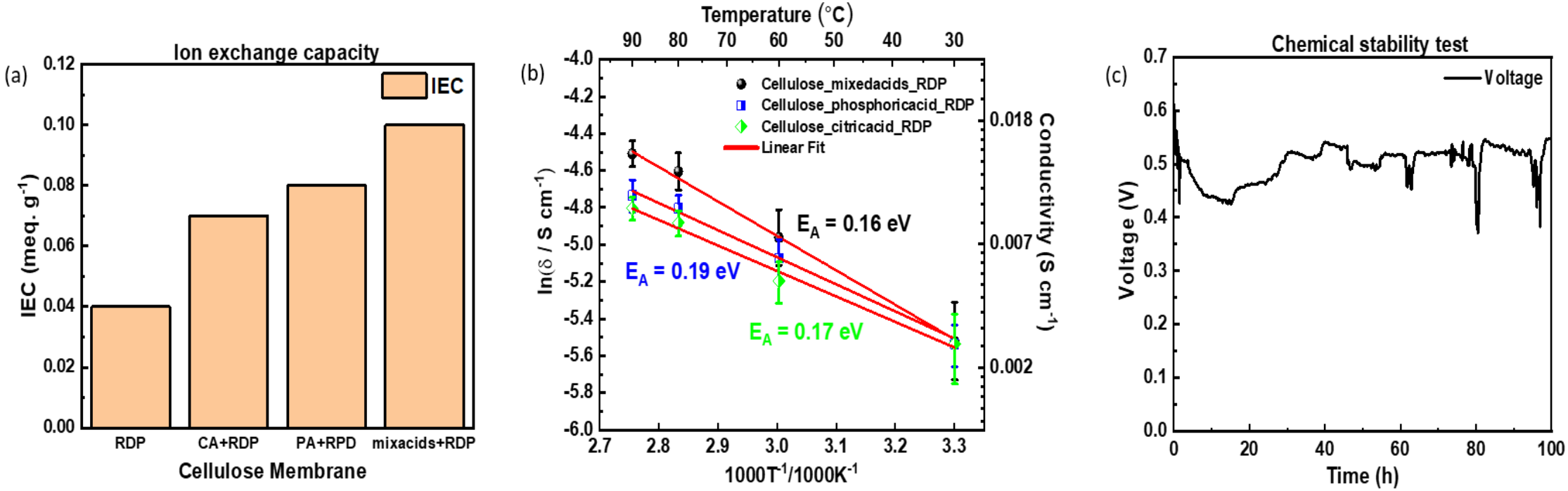

Fig. 28: (a) Ion exchange capacity of different membranes (b) Arrhenius plot of the conductivity of cellulose/RDP membrane and mixed acids with activation energy. The straight line is a linear fit to the Arrhenius model (error bars are for conductivity data points). (c) Voltage output of cellulose/RDP membrane treated with mixed acids under 60 mA constant current load at 60ºC for 100 hours continuous operation

Membranes	Cellulose/RDP	Cellulose/RDP/CA	Cellulose/RDP/PA	Cellulose/RDP/ mixed acids
Ion exchange capacity(meq. g^{-1})	0.04	0.07	0.08	0.10
Max power density (mW/cm^2)	4.9	11.8	10.8	16.1

SEM-EDX: RDP removes porosity

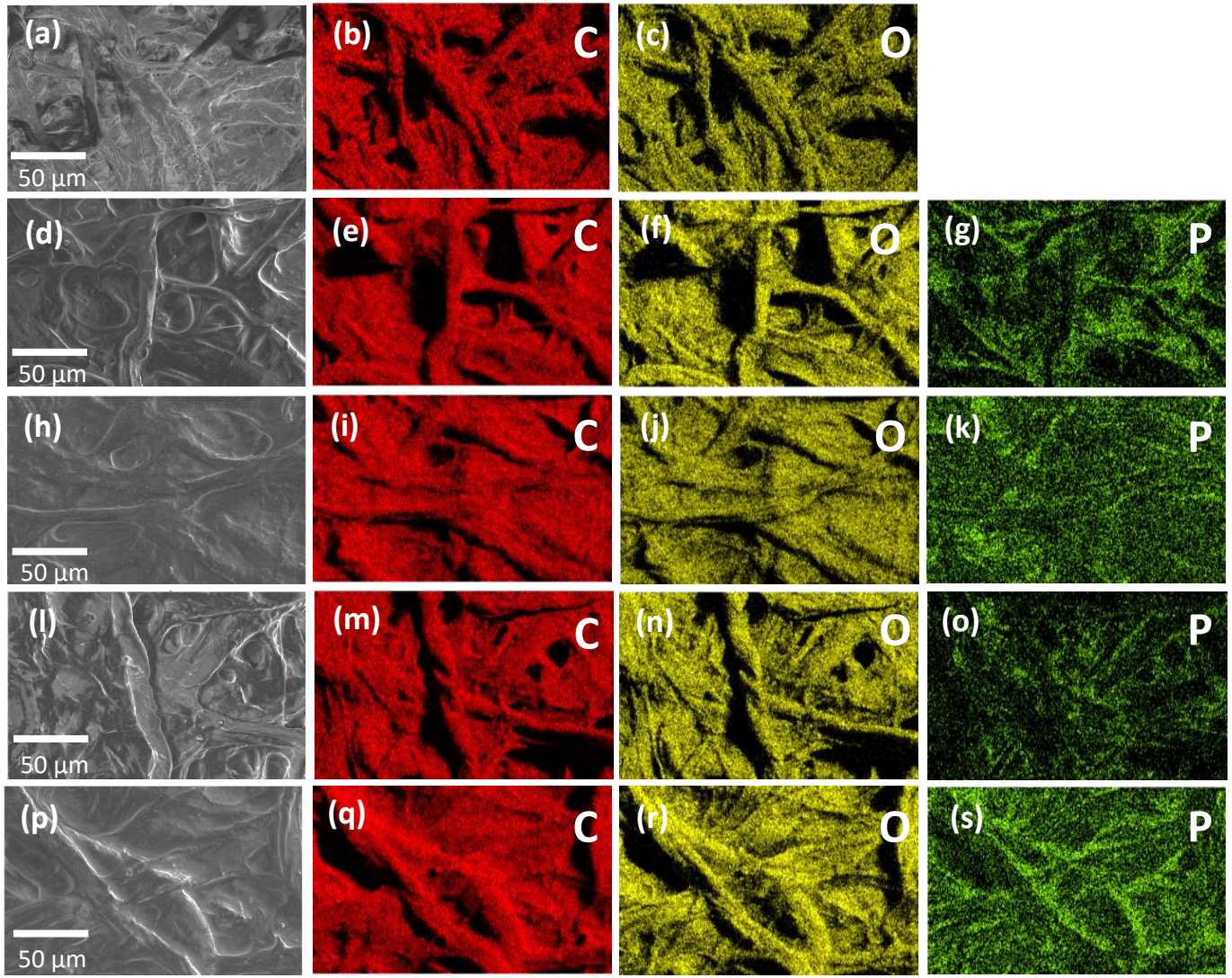

- The porosity is greatly decreased upon addition of RDP, where a membrane like film is observed to have formed.
- The uniformity of RDP distribution across the membrane was confirmed by the distinct Phosphorus signal originating from RDP.
- The Phosphorus signal was more prominent in the Cellulose/RDP membrane treated with phosphoric acid and mixed acids.

Fig. 29: SEM-EDX images of (a-c) a typical cellulose filter paper membrane (d-g) cellulose/RDP membrane (h-k) cellulose/RDP membrane treated with phosphoric acid (l-o) cellulose/RDP membrane treated with citric acid (p-s) cellulose/RDP membrane treated with mixed acids.

^{1}H MAS NMR

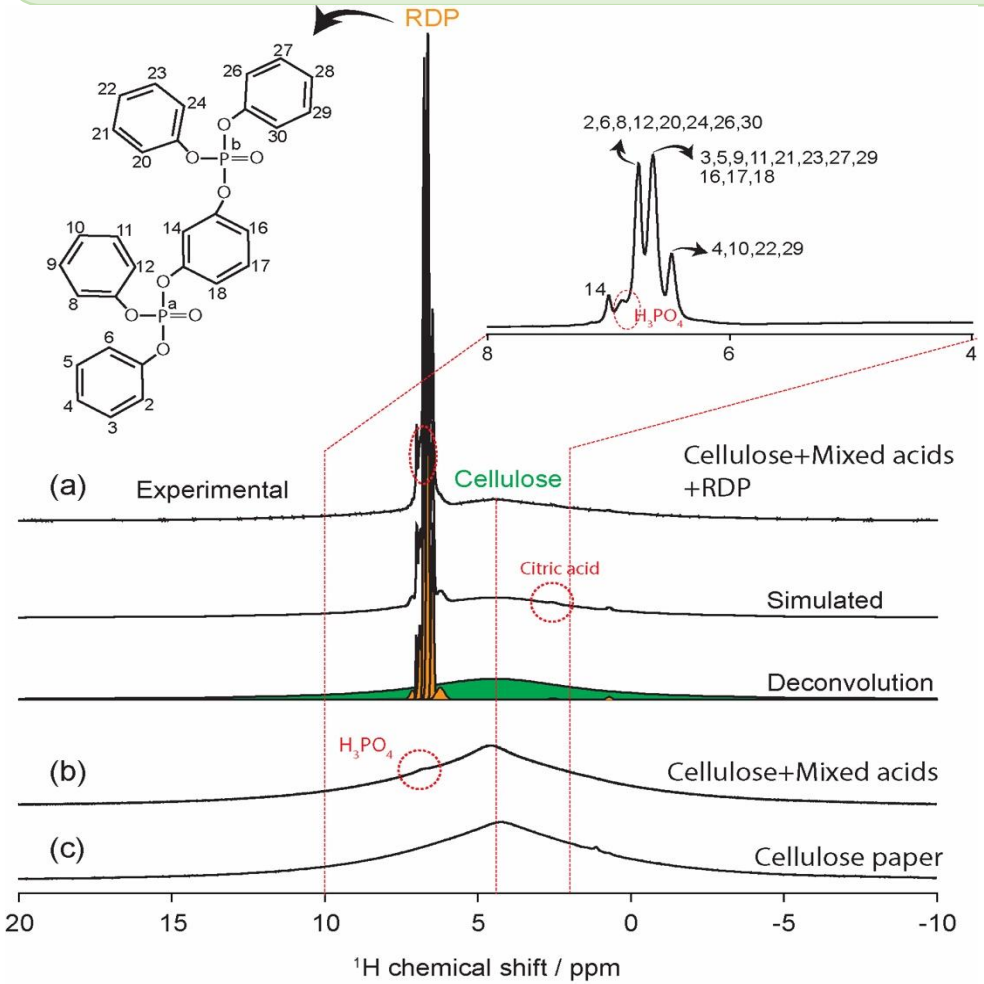

- The ^{1}H spectrum of cellulose paper that display a broad ^{1}H peak centered at 4.5 ppm could be assigned to the protons of cellulose structural units.
- A small peak at 6.8 ppm could be assigned to the H_3PO_4. A slight downfield shift of this ^{1}H peak as compared to 85% H_3PO_4 (5.7 ppm) suggests that the acid groups may form strong H-bonds with cellulose functional groups, consistent with the FTIR.
- In the case of cellulose with mixed acids and RDP, narrow ^{1}H peaks corresponding to H_3PO_4 (6.9 ppm) and citric acid (2.6 ppm) can be clearly distinguished from the broad cellulose ^{1}H peak centered at 4.5 ppm, in addition to four narrow ^{1}H peaks of RDP in the aromatic region.
- The ^{1}H peak at 6.9 ppm (H_3PO_4), which is small and broad for cellulose mixed acids without RDP, becomes narrow and intense for the one with RDP.

Fig. 31: (a, b, c)1D ^{1}H MAS NMR spectra of Cellulose filter paper (c), cellulose mixed acids without (b) and with RDP (a) collected on a 300 MHz spectrometer using 1.6 mm double resonance probe with 29 kHz MAS speed.

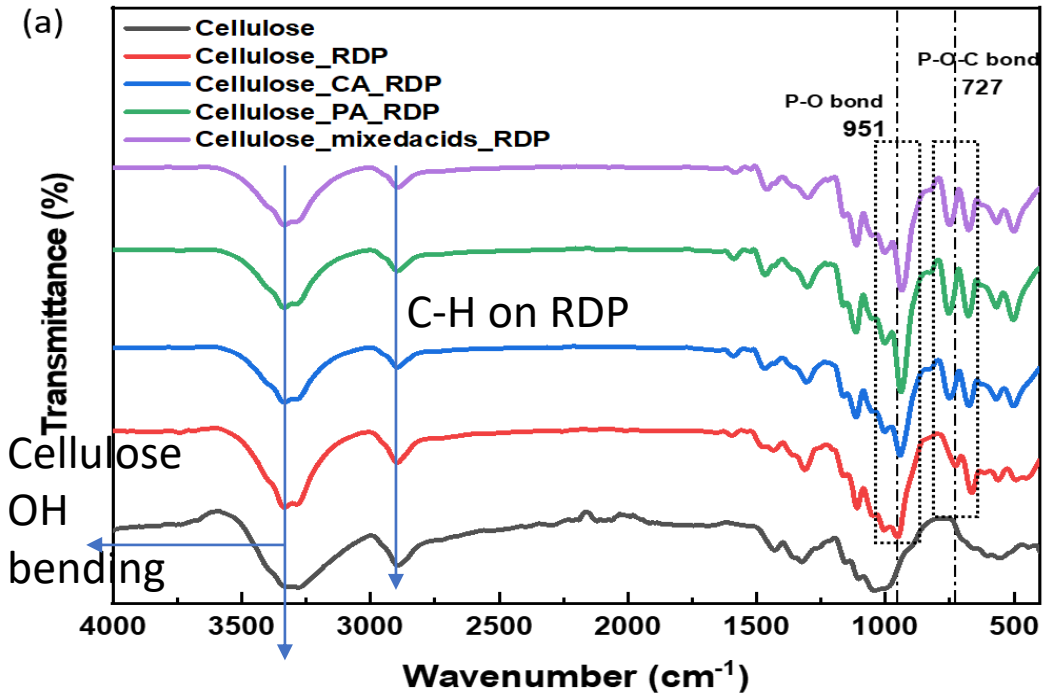

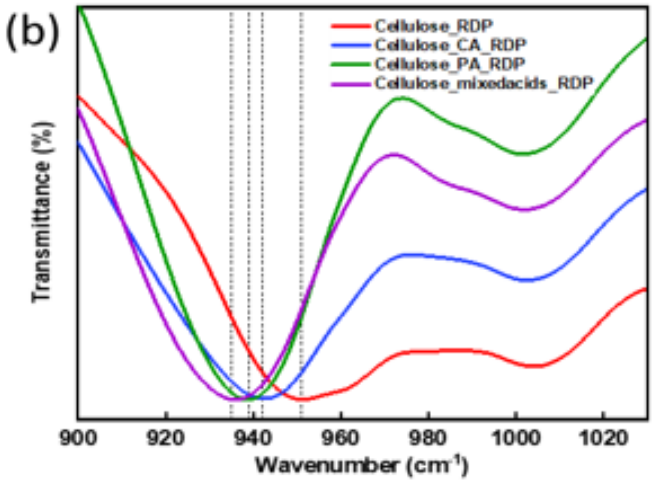

P-O vibration

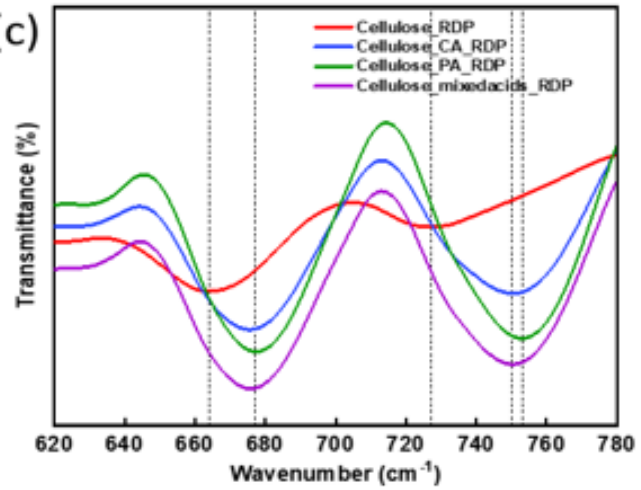

P-O-C bond

- RDP+ Cellulose: the benzene ring of the phenol groups in RDP interacts mostly with the OH groups of the cellulose ring, stretching the entire P-O-C bond.
- Acid+cellulose then RDP: Acid now binds to cellulose ring and blocks RDP binding in that site. The peak for C-H vibration in benzene ring and P-O-C stretching are back to the position in pure RDP.
- New Binding site: The largest shift now occurs at the P-O vibration, which shifted from 959 cm^{-1} to 942 cm^{-1} with citric acid, 939 cm^{-1} with phosphoric acid and to 935 cm^{-1} when a mixture of both acids is used. RDP binds to cellulose via the P-O oxygen binding site in acid modified cellulose.

Binding is weaker enhancing ion migration

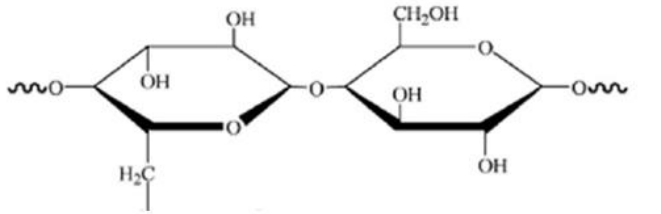

Active C-H binding site on cellulose: RDP or Acid binding site

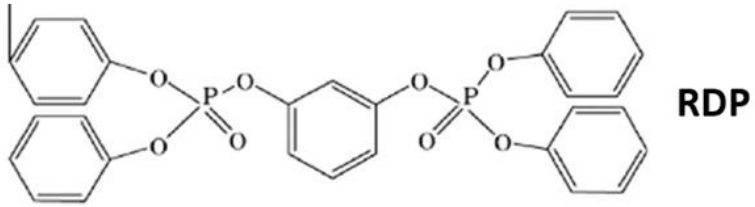

Cellulose (2021) 28:4455–4467

Conclusion

Proton and Anionic Fuel Cell technology is a nanoscale process.

Nanotechnology is the key to enabling improvements in gas exchange fuel cells.

Ensuring sustainability and affordability.

Conclusion

- Developed new membrane for PEMFCs using cellulose filter paper treated with weak acids and reinforced with RDP.
- Addition of RDP improved proton dynamics of acid groups and prevented gas crossover in the membrane.
- Combined treatment with citric and phosphoric acids and RDP resulted in 226% enhancement in power output, reaching 16 mW/cm^2 in air and 34.3 mW/cm^2 in an oxygen environment.
- Membrane demonstrated stability under a constant current of 60mA for at least 100 hours with only an 8% loss in voltage.
- Cellulose filter paper offers a cost-effective and sustainable alternative to Nafion membranes for low-power PEMFC applications.

RDP:

- The peak at 3066 cm^{-1} is attributed to the C-H stretching vibration of benzene ring
- The peaks at 1591 cm^{-1} and 1488 cm^{-1} correspond to the C=C stretching vibrations of aromatic ring.
- The absorptions at 1260 cm^{-1}, 1186 cm^{-1}, and 1120 cm^{-1} are due to the aromatic C-O vibrations.
- The peaks at 1300 cm^{-1} and 581 cm^{-1} are associated with the absorptions of double bonded P=O,
- The peak at 959 cm^{-1} is for P-O vibration.
- The characteristic C-H vibration of mono-substitution product of benzene ring appears at 687 cm^{-1}.

Cellulose:

- Absorption peaks; 3407 cm^{-1} due to O-H bending
- 2894 cm^{-1} related to C-H stretching, 1428 cm^{-1} and 1310 cm^{-1} contributed from C-H bending
- 1645 cm^{-1} due to C=O stretching, and 1124 cm^{-1} due to C-O bending

Graphic abstract

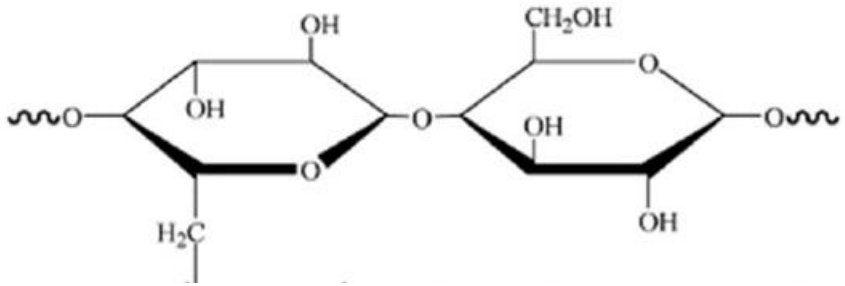

Cellulose

Active C-H binding site on cellulose: RDP or Acid binding site

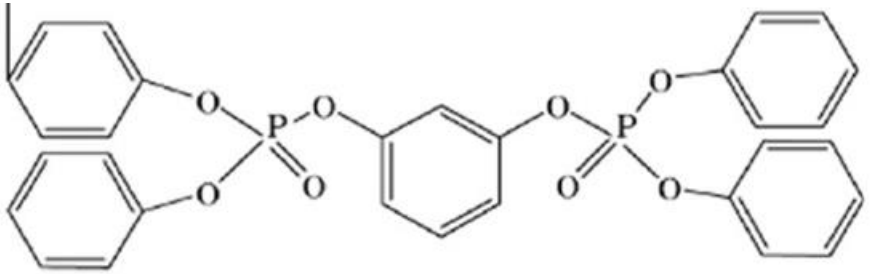

RDP

Cellulose (2021) 28:4455–4467

Acknowledgements

- Foremost, I would like to extend my profound gratitude to Professor Miriam H. Rafailovich, my advisor, for her exceptional guidance and support throughout my doctoral studies. As a professional materials scientist, her expertise and approach to research serve as a model for me to emulate. Her unwavering encouragement, persistent guidance, and continuous academic support have been invaluable, without which I would not have made any academic progress, let alone complete this dissertation.
- I would like to thank my dissertation committee members: Dr. David Sprouster, Dr. Jonathan Sokolov, Dr Tai-De Li and Dr. Ying Liu for their support, valuable suggestions and comments.
- I also appreciate all the Garcia MRSEC group members: Dr. Michael Cuiffo, Dr. Likun Wang, Dr. Kuan-Che Fang, Dr. Yuval Shmueli, Dr. Yuchen Zhou, Dr. Ya-Chen Chuang, Dr. Fan Yang, Dr. Kao Li, Yu-Chung Lin, Haoyan Fang, Yifan Yin, Yiwei Fang, Shi Fu, Md Farabi Rehman, Huiting Liu, Adam Hansen and Aaron Sloutski for their academic help and support.
- Last but not least, I would like to express my heartfelt gratitude to my family for their unwavering love and support throughout my PhD journey. Without their constant encouragement and understanding, I would not have been able to complete my studies and achieve this milestone in my academic career.

Thank You!

Questions?

Graphic abstract

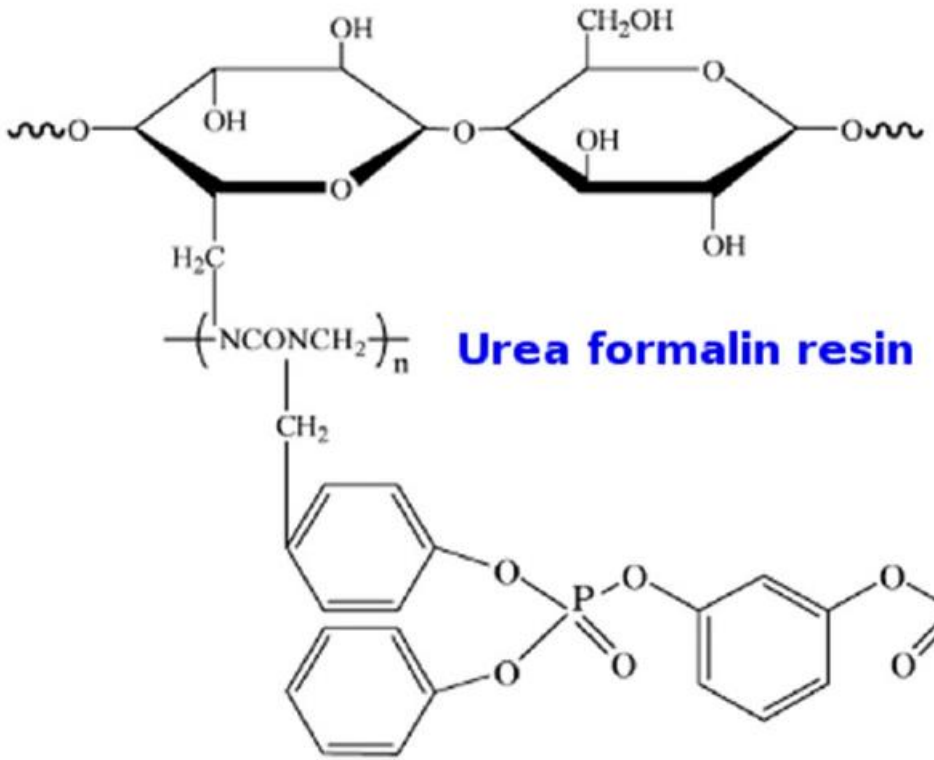

Cellulose (2021) 28:4455–4467

Solution

The correct option is **A**